AN INNOVATIVE AND ROBUST APPROACH TO STUDYING FATIGUE PROPERTIES OF ALUMINUM 7075 BAR UTILIZING MINIATURE I-BEAM GEOMETRY

A Thesis
Presented to
The Academic Faculty

by

Wendy M. Hynes

In Partial Fulfillment
of the Requirements for the Degree
Masters' in the
School of Aerospace Engineering

Georgia Institute of Technology
August 2006

AN INNOVATIVE AND ROBUST APPROACH TO STUDYING FATIGUE PROERTIES OF ALUMINUM 7075 BAR UTILIZING MINIATURE I-BEAM GEOMETRY

Approved by:

Dr. John W. Holmes, Advisor
School of Aerospace Engineering
Georgia Institute of Technology

Dr. Dr. David McDowell
School of Mechanical Engineering
Georgia Institute of Technology

Dr. Andrew Makeev
School of Aerospace Engineering
Georgia Institute of Technology

Date Approved: June 29, 2006

To my parents, John J. Hynes III and Ramona L. Mena
for their boundless support and love

ACKNOWLEDGEMENTS

I would like to extend my utmost gratitude to committee members, Dr. John W. Holmes, Dr. David McDowell, and Dr. Andrew Makeev for their time and guidance. The skills gained from their direction are invaluable; I have enjoyed completing this research with engineers of such high caliber. I present a special thanks to my advisor, Dr. John W. Holmes. I hope the respect and regard I have for him demonstrates my appreciation for all of his support. Advisor or not in the future, he is my friend.

Much appreciation is extended to my colleagues at LM Aero – Marietta. Without the boundless patience and encouragement of such an exemplary team of people, this endeavor would have been all but impossible. Particular thanks to my lead, Pete Caruso, and my managers, Skip Ellsworth and Ralph Sykes, for their insight, as well as their tolerance of a student's unpredictable schedule.

Thanks are due to the members of the MAST Research Lab at Georgia Tech. My lab mates were continuously optimistic, knowledgeable, and generous. Much thanks to Terry Williams for all of his insight into initial testing preparation.

I would like to acknowledge the patience and support of my family and friends throughout the four years I attended graduate school. Although I will forever appreciate my graduate student experience, I regret the time I spent away from them.

There are no words to express my admiration for the person who was a foundation throughout this learning experience; there is no measure large enough to define the size of his character. I will spend many years striving to be as remarkable of a friend to Rich Stover as he has been over the past few years.

Finally, to all who have tolerated my magnified 'Jersey' attitude with the utmost cheerfulness throughout this undertaking, I sincerely thank you.

TABLE OF CONTENTS

LIST OF TABLES

LIST OF FIGURES

Page

Page

Page

Page

LIST OF ABBREVIATIONS

ACPD	Alternating Current Potential Drop
AFGROW	Air Force Fracture Mechanics Crack Growth Software
ASM	American Society of Metals
ASTM	American Society of Test and Measurement
C(T)	Compact Tension
DOD	Department of Defense
EDM	Electrical Discharge Machining
ESDU	European Standard Data Unit
FAA	Federal Aviation Administration
FEA	Finite Element Analysis
FELIX	Loading Standard for Fixed- or Semi-Rigid Rotorcrafts
FEM	Finite Element Model
LEFM	Linear Elastic Fracture Mechanics
LHS	Left-Hand Side
M(T)	Middle Tension
MTS	Material Test Systems
NASA	National Aeronautics and Space Administration
NASGRO	NASA Fatigue Crack Growth Software
NASM	National Aerospace Standards
PC	Personal Computer
RHS	Right-Hand Side
SAE	Society of Automotive Engineers
SENT	Single Edge Notch Tension

SIF	Stress Intensity Factor
SSE	Sum of the Squares of the Error
SST	Sum of the Squares of the Total

LIST OF SYMBOLS

a	Crack Size
a_i	Initial Flaw Size
a_{cr}	Critical Crack Length
a_L	Left-Hand Side Crack Length
a_R	Right-Hand Side Crack Length
β	Beta Correction Factor
b	Elastic Strain-Life Slope
β_{cr}	Critical Beta Correction Factor
c	Plastic Strain-Life Slope
C	Crack Growth Rate Coefficient
da/dN	Cyclic Crack Growth Rate
ΔK	Stress Intensity Range
ΔK_{th}	Threshold Stress Intensity Range
ΔK_{theff}	Effective Threshold Stress Intensity Range
ε	Strain
$\varepsilon_{applied}$	Applied Strain
E	Young's Modulus
E'_f	True Fracture Ductility
F_{tu}	Ultimate Strength
H	Helicopter
Hz	Hertz
K	Stress Intensity Factor
K	Strength Coefficient

K’	Cyclic Strength Coefficient
K_c	Fracture Toughness
K_{Ic}	Mode I Critical Stress Intensity Factor
L	Length
L-T	Long-Transverse
L_s	Crack Tip Shielding Length
μ	micron
m	meter
m	Crack Growth Rate Exponent
mm	millimeter
MPa	Mega-Pascal
MPa√m	Mega-Pascal per Square Root Meter
n	cycles
n	Data Point Location
n	Strain Hardening Exponent
ν	Poisson Ratio
N’	Cyclic Strain Hardening Exponent
N	Newton
N_f	Flight-Hours
N/sec	Newton per second
π	Pi
$P_{applied}$	Applied Load
r	Radius

R	Load Ratio
ρ	Grain Size
r_o	Plastic Zone Size
R-L	Radial-Longitudinal
R^2	Coefficient of Determination
r_y	Plastic Zone Size
σ	Stress
SiC	Silicon-Carbide
σ_{linear}	Linear Standard Deviations
σ_{log}	Lognormal Standard Deviation
σ_{max}	Maximum Applied Stress
σ_{min}	Minimum Applied Stress
$\sigma_{applied}$	Applied Stress
σ'_f	True Fracture Strength
σ_e	Endurance Limit
σ_u	Ultimate Strength
σ_y	Yield Strength
T-L	Transverse-Longitudinal
t	Thickness
W	Width
x	Horizontal Axis
y	Vertical Axis

Y	Stress Intensity Range Data Point
Y’	(Stress Intensity Range Data Point)+1
Y-hat	(Stress Intensity Range Data Point)+1
Z	Out-of-the-Page Axis

SUMMARY

Aerospace structures are optimally designed and analyzed to specifically-defined engineering parameters. Thus, there is a strong drive to understand fatigue properties of materials, enabling an engineer determine their influence on these constraints. Space structures are usually designed to minimize weight and volume; hence thin designs utilizing strong, lightweight materials are ultimately desired. The goal of this research is to address an innovative testing technique of material properties not readily obtained from current test methods. The properties studied in this research include crack growth rates of small diameter rods in both the radial and transverse grain directions under a constant-amplitude tensile load at room temperature. This approach is illustrated on I-beam specimen manufactured from Aluminum 7075-T7351 Bar. The crack growth rates from the experimental data are then compared with literature results for plates, sheets, and extrusions of the same material. The research completed reveals the test results have comparable [Paris relationship] exponential m-values. The significance of quantifying small diameter metallic material properties have potential for great impact on the future of space structures, but are not limited to one part of the industry.

CHAPTER 1

BACKGROUND

1.1 Introduction

Aerospace structures are known for their demanding light-weight and high-strength requirements. Due to the nature of their complex applications, an engineer contributes a large part of the initial design to selecting a material and geometry that ensures structural optimization. The broader and better our understanding of a material's characteristics, the more effective we can be as engineers.

Fatigue crack growth is an important property in the long-term reliability of a structure; the study of fatigue in metallic materials has been on-going for over a half a century. To best understand the fatigue behavior of aluminum alloys, we have to continuously re-assess our current knowledge. This includes challenging established limitations of the material as well as our engineering techniques that validate them. Materials are manufactured to certain minimum criteria, usually outlined by ASTM and SAE standards here in the United States. Experimental testing is a key criterion in defining these standards.

The goal of this research work was to focus on utilizing a unique specimen design to gain a better understanding of crack growth rates for small-diameter aluminum bar material. Specifically, experimental cyclic fatigue data was accumulated and compared to previously published work to determine the accuracy of the design for experimental testing. With a new design comes many challenges and potential rewards in a well-established engineering discipline. This requires a sound understanding of the current knowledge in this area and a strong motivation to improve conventional methods.

This dissertation documents the work performed for this research. General fatigue theory was reviewed, as well as published crack growth rates for the material studied. Similar experimental test techniques were summarized, as well as the procedures implemented in this research. Finally, the results will be presented and discussed, with

the hope that the lessons learned and recommended will contribute an improvement in the engineering field of structural analysis.

1.2 Metallic Fatigue Crack Growth

Crack growth can generally be characterized into three stages: initiation, propagation, and fast fracture. Crack propagation was focused on in this research. Once the experimental data was collected, crack growth rates were calculated. A statistical review of the resulting fatigue crack growth rates was also completed. This was primarily to observe the amount of scatter in the results. The measurement of both the coefficient of determination and the standard deviation were employed. These calculations will be summarized in this section, along with a review of previously-published crack growth rates for the specimen material, Aluminum 7075.

1.2.1 Fatigue Theory

The crack growth parameters in this study included the maximum applied stress level, σ_{max}, cycle count, n, crack length, a, crack growth rate, da/dN, and the Stress Intensity Range, ΔK. The maximum applied stress value, the crack length, and the number of cycles were those observed during experimental cycling. From these values, the crack growth rate and stress intensity ranges were determined. Several material characteristics and parameter relationships were revealed from these results.

The fracture mechanics approach applied to fatigue cycling was the method applied to calculate crack growth rates for this research with the secant (or point-to-point) data regression method[1]. The crack growth rate relationship describes change in crack length over a period of cycles

$$\left(\frac{da_i}{dN_i}\right) = \frac{(a_i - a_{i-1})}{(N_i - N_{i-1})}$$

and the applied stress intensity range relationship is a function of the far-field stress and crack length

$$\Delta K = \beta\left(\frac{\sigma_i - \sigma_{i-1}}{2}\right)\sqrt{\pi\left(\frac{a_i - a_{i-1}}{2}\right)}$$

where β is a dimensionless function based on LEFM and defined by the geometry and loading configuration. Also known as the Geometric Correction Factor or Beta Factor, the geometric function[2] representing the specimen design in this research is a generic SENT specimen illustrated in Figure 1.1 and defined by

$$\beta = \sqrt{\frac{1}{\pi}}\left(1.99 - 0.41\left[\frac{a_i}{W}\right] + 18.7\left[\frac{a_i}{W}\right]^2 - 38.48\left[\frac{a_i}{W}\right]^3 + 53.85\left[\frac{a_i}{W}\right]^4\right)$$

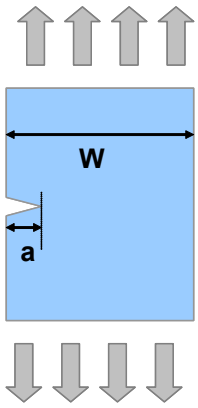

Figure 1.1

Single Edge Notch Tension (SENT) Geometry[2]

For metallic materials, there is a relationship between the values of da/dN and ΔK for a data set on a log-log plot that forms a straight line in the center region of the data, illustrated in Figure 1.2.

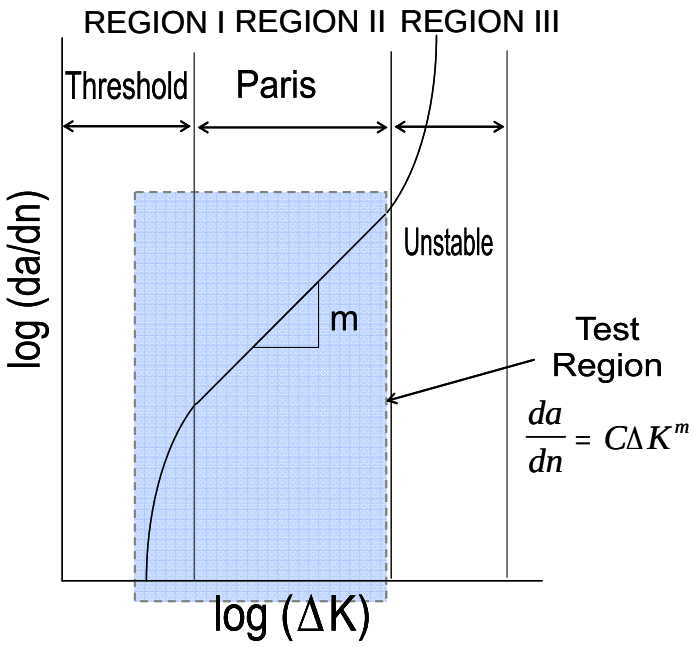

Figure 1.2

Crack Growth Rate Characterization[3]

This relationship can be defined by the equation[1]

$$\left(\frac{da}{dN}\right)_n = C(\Delta K_n)^m$$

where C is a coefficient constant and m is the slope of the middle section of data on the log-log plot. This range is called Region II of crack growth rate plots or the Paris law region. For the experimental data sets in this research, the fatigue parameters, C and m, were determined using a least squares fit regression of a power curve-format equation for each specimens set of experimental data points.

At low growth rates, the data slopes steeper to a vertical asymptote at a value below which cracks generally do not grow. This value is defined as the fatigue crack growth threshold and was utilized in establishing the cyclic stress level for this research. The data again slopes steeper during fast fracture in Region III to the right of the Paris region on the plot. The critical stress intensity factor was calculated from the experimental data in this region.

1.2.2 Statistical Analysis

As mentioned above, the fatigue parameters are based on a power curve function that can be calculated by regression to best fit the data to a straight line on a log-log plot. The suitability of the calculated parameters to the data set can be reviewed with statistical analysis. For this research, both the parameters and the data set they were created from will be reviewed. The coefficient of determination will analyze the fatigue parameters and the 3-σ standard deviation range will be defined for each data set.

The coefficient of determination is an indicator from 0 to 1 describing how well the estimated values for the trend line correspond to the experimental data.[4] The closer the value is to one, the better the equation fits the data. The equations[5] used to calculate this value is

$$R^2 = 1 - \frac{SSE}{SST}$$

where SSE[5] is the sum of the squares of the error

$$SSE = \sum \left(Y_i - \hat{Y}_i \right)^2$$

and SST[5] is the sum of the squares of the total

$$SST = \left(\sum Y_i^{\,2} \right) - \frac{\left(\sum Y_i^{\,2} \right)}{n}$$

The standard deviation measures the range of values from the average value (or the mean), and can be calculated for the log-normal values with the relationship[4]

$$\sigma_{\log} = \sqrt{\frac{\sum_{i=1}^{n} \left(\log(y_n) - \log\left(y_n^{'}\right) \right)^2}{n}}$$

and this is related to the linear values with the equation[4]

$$\sigma_{linear} = 10^{\sigma_{\log}}$$

1.2.3 Previously Published Studies

We are familiar with aluminum alloys as high strength materials used in a wide range of industries, including aerospace, marine, electric utility, robotics, rail transportation, and building construction. As a result, it is a well-studied material with a variety of publications examining every structural characteristic in great detail. Differences in the experimental conditions used in those studies will be reviewed in this section. These crack growth trends will be compared with experimental data in the Results section of this document. All studies reviewed included tests completed with Aluminum 7075 coupons at room temperature on a constant-amplitude spectrum. Table 1.1 summarizes the list of test conditions from these reports. Variations of the Paris Law relationship were used in these studies. These equations are defined in this section.

A number of these publications on material properties are developed by national and international societies. Several of these sources were reviewed for this research. Data from the MMPDS document, FAA Fatigue Crack Growth Database, ASM Materials Handbook, and ESDU standards were compared with the experimental results from this research.

The MMPDS-01[6] and ASM[7] fatigue crack growth curves were reviewed to determine how well the research data correlated. The published data in these references fits a Paris Law relationship that will be superimposed over the experimental data for comparison.

The FAA Fatigue Crack Growth Database fits experimental data to multiple variations of the Paris Law. The equation format[8] used by the NASGRO curve fit software is

$$\frac{da}{dn} = C\left(\frac{(1-f)}{1-R}\Delta K\right)^n \frac{\left(1-\frac{\Delta K_{th}}{\Delta K}\right)^p}{\left(1-\frac{K_{\max}}{K_c}\right)^q}$$

The Walker equation curve fit format[8] from the FAA Fatigue Crack Growth Database is

$$\frac{da}{dn} = C\left(\frac{\Delta K}{(1-R)^{1-m}}\right)^n$$

The data for the ESDU fatigue parameters was fit to the same power curve relationship as the experimental data[9], defined in Section 1.2.1.

Standards such as these are augmented by industry and educational research that complement and expand on the scope of material handbooks and standards. Other published technical documents vary the parameters used by standard publications and expanded our knowledge bank for understanding these materials under a wider variety of conditions. These works are extremely useful in understand the range in properties of materials.

The crack growth rates of S. C. Forth, J. C. Newman Jr. et al., and J. K. Kim et al. were compared against the experimental results of this research. The Region II relationship[10] from Forth, Newman et al. research fit the format

$$\left(\frac{da}{dN}\right)_{M(T)} = \frac{\Delta P}{\beta\sqrt{W}} \frac{\left(2+\frac{2a}{W}\right)}{\left(1-\frac{2a}{W}\right)^{\frac{3}{2}}} \left(0.886 + 4.64\left(\frac{2a}{W}\right) - 13.32\left(\frac{2a}{W}\right)^2 + 14.72\left(\frac{2a}{W}\right)^3 - 5.64\left(\frac{2a}{W}\right)^4\right)$$

$$\left(\frac{da}{dN}\right)_{C(T)} = \frac{\Delta P}{\beta}\sqrt{\frac{a\pi}{W^2}\sec\left(\frac{a\pi}{W}\right)}$$

The experimental results from Kim et al. research were fit to the same Paris Law relationship[11] as the experimental data, defined in Section 1.2.1.

Table 1.1

Test Conditions for Published Data [6-11]

Source	Temper	Crack Direction	Specime Type	Load Ratio	thickness [mm]	Kic [MPavm]
Kim, Shim Int'l Journal Fatigue 2000	T6 Plate	L-T	CT	0	1.6 - 9.8	21 - 29
ASM Atlas of Fatigue Curves 1986	T7351	--	--	0.1	--	--
FAA Fatigue CG Database NASGRO Equation 2005	T73 Plate	L-T	--	-1	4.6 - 12.7	29
FAA Fatigue CG Database Walker Equation 2005	T73 Plate	L-T	--	0.1 - 0.8	4.6 - 12.7	29
Forth, Newman, Jr. Int'l Journal Fatigue 2003	T73 Plate	L-T	C(T) & M(T)	0.1	12.7	--
ESDU 81083B 1998	T7351 Bar	L-T & T-L	C(T)	0.11	19 - 25	24 - 47
MMPDS-01 2003	T7351 Plate	L-T	M(T)	0.1 - 0.51	6.35	--
AFGROW 2004	T73 Forging	L-T	--	0	--	--

1.3 Specimen Design

One of the most significant components of this research is the unique design of the specimen in Figure 1.3. This design allows for testing of a wide variety of functional usages on edge-notch tension specimens, potentially offering more efficient testing.

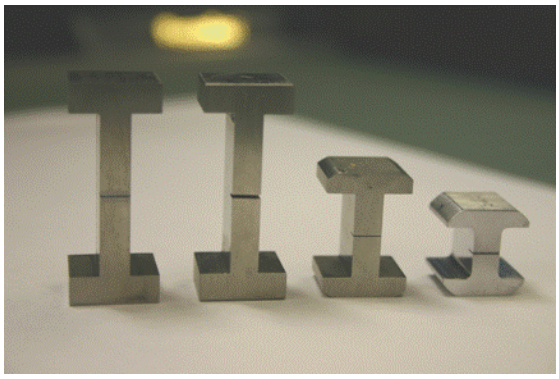

Figure 1.3

Miniature I-Beam Test Specimen

1.3.1 Experimental Testing Coupon Types

There is a variety of standard test specimen geometry used in axial tension testing, as shown in Figure 1.4. Figure 1.5 illustrates how standard specimens use different test stand attachment methods from simple to complex. Each design offers its own benefits to various test situations. The miniature I-beam specimens used in this study offers a simple design easy to machine or extrude with simple mechanical attach locations. It is readily scalable in design, with previous testing showing no effects of center web height on cyclic fatigue test results. The design of the grip ends allows the specimen to be utilized in a variety of tests, including fatigue, fracture toughness, tension or compression, and creep, to name a few.

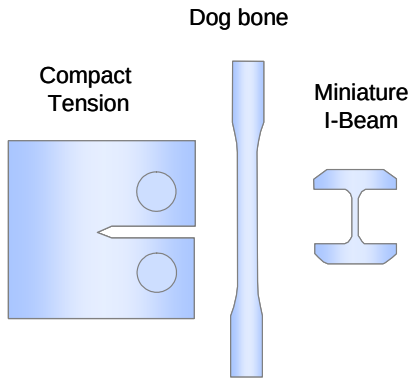

Figure 1.4

Comparison of Test Specimen Geometries[13, 14]

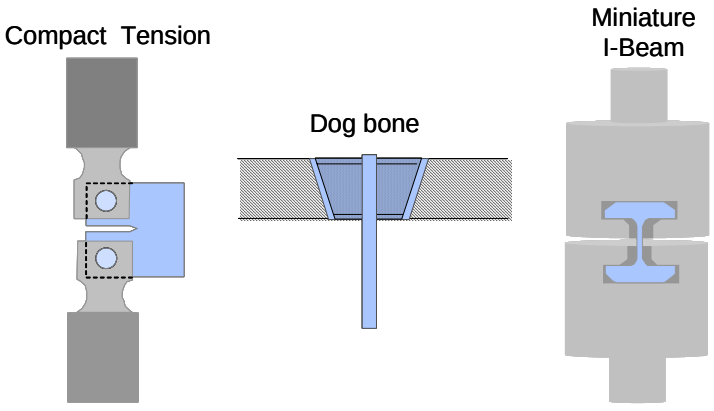

Figure 1.5

Comparison of Test Specimen Installations[13, 14]

Table 1.2

Coupon Geometry Comparison

Type	Pros	Cons
Compact Tension	Most common configuration well understood	Minimum geometry limited by pin diameter -- High Temperature limitations
Dog Bone	Simplest Geometry	For pinned grips, minimum width limited by pin diameter -- For clamped grips, potential slippage during loading
Miniature I-Beam	Simple Geometry -- L-T Plate grain direction -- No size or high temperature limitations -- Use for several test types -- Simple grip installation	New grip manufacturing for large scale specimen -- Lack of data

1.3.2 Test Environment

The environment of aerospace applications varies widely throughout the life of a structure. These designs are certain to be subject to high- or low-temperature environments, whether these thermal changes are cyclic or interim. It is important that testing standards are extremely robust in all environments to accrue valid test data. This specimen design would not have any mechanical variations in extreme temperature environments and could offer potential benefits over current standard geometries. For example, a high temperature test environment could affect the results of test using a C(T) specimen, as illustrated in Figure 1.6. This environment would affect the modulus and strength of the pins during the test. The I-beam specimen in this extreme environment, shown in Figure 1.7, would not be susceptible to this issue.

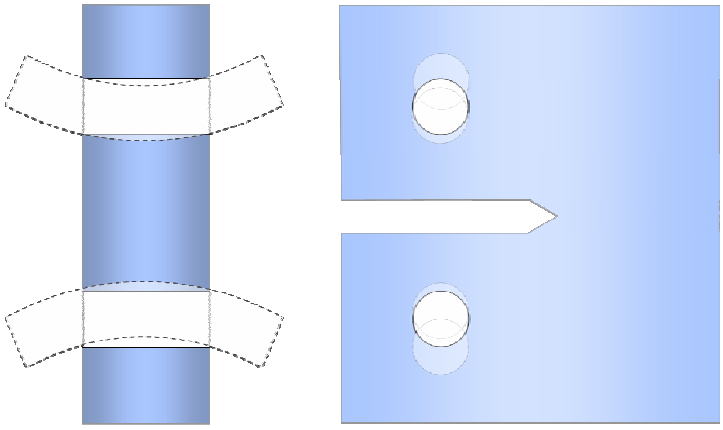

Figure 1.6

High-Temperature Testing of CT Geometry

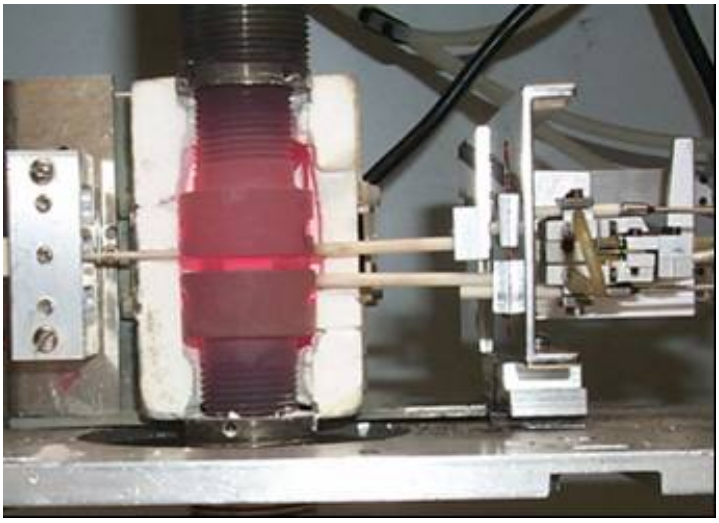

Figure 1.7

High-Temperature Testing of Miniature I-Beam

1.3.3 Material Direction

With the miniature I-beam geometry, there is an opportunity to study metallic materials in grain directions not regularly utilized for structural applications. Metallic core composites are already successfully used in an enormous variety of applications within most structural designs. Examples[15] include automobile brake drums, performance boat bulkheads/floors, and robotic arms, where its high-stiffness properties can reduce the vibrations resulting from movement. Rail transportation utilizes pre-

crushed metallic honeycomb assemblies as energy absorbers and driver protection. It is also used in satellite solar panels, satellite rocket fairings, and Acoustic Lining Panels in aircraft engines. This specimen geometry can be manufactured from plate material in the L-T grain direction, which can be used in both the core and skin materials of composites, as shown in Figures 1.8 & 1.9.

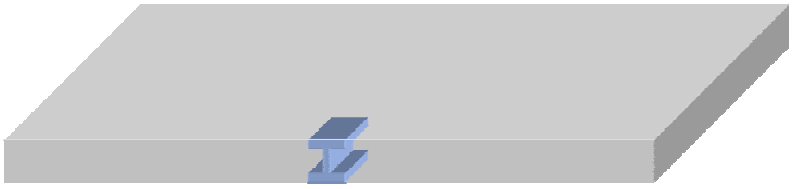

Figure 1.8

Transverse Plate Specimen Direction

Figure 1.9

Composite Core

Companies like Cellular Materials, Inc. manufacture a wide range of distinctive core designs, such as a periodic open cell tetrahedral truss core, that are specially-glue (transient liquid phase approach) or welded between aluminum face sheets[16], illustrated in Figure 1.10. This specimen design is representative of this type of core as well as the face sheet. These designs are produced for applications such as jet blast deflection on aircraft carriers, blast and ballistic protection on armored vehicles, heat management for electronics storage, impact defense for vehicle bumpers, and flow separation control in scramjets. These cores can have relative densities less than 2% and allow fluid to pass through, making them less susceptible to corrosion & depressurization[16].

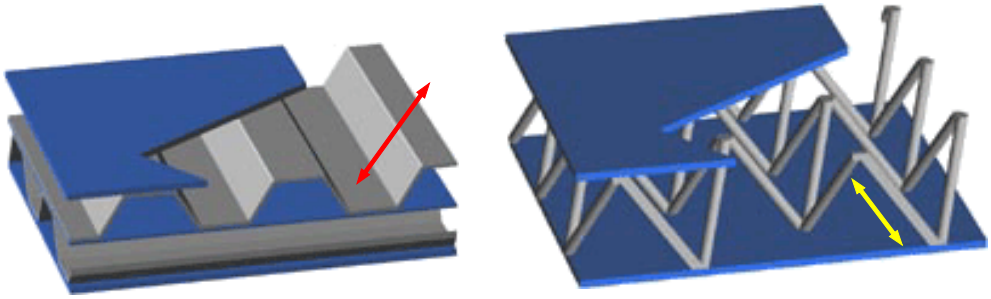

Figure 1.10

Metallic Composites[16]

The specimen geometry is also representative of fasteners tests performed throughout the industry. Fasteners are tested several direction for standardization requirements, as shown in Figures 1.11, including the axial direction. This is potentially representative of this specimen design.

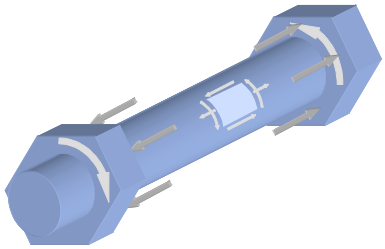

Figure 1.11

Fastener Loads

Figure 1.12 illustrates the variation in fastener test fixtures defined by several organizations[17-19]. This miniature I-beam design would potentially be a more cost effective method for initially testing fastener materials.

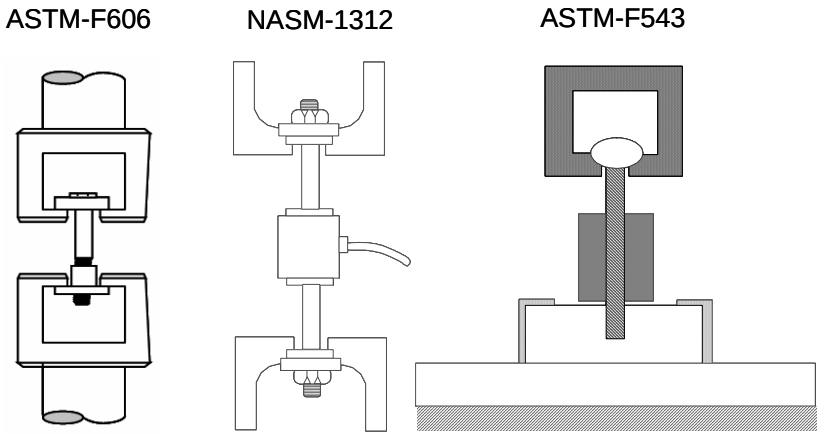

Figure 1.12

Fastener Testing Installations[17-19]

1.3.4 Small Crack Effects

The severity of the spectra in structural applications can vary greatly and sometimes result in much smaller critical flaw sizes. Rotorcraft spectra have historically seen more severe loading conditions and smaller critical crack sizes than commercial aircraft spectra[20], as shown in Figure 1.13. In this example, we see there are very few flight-hours left in a material subject to this loading with an initial flaw at any value above 0.05 mm prior to failure of the material.

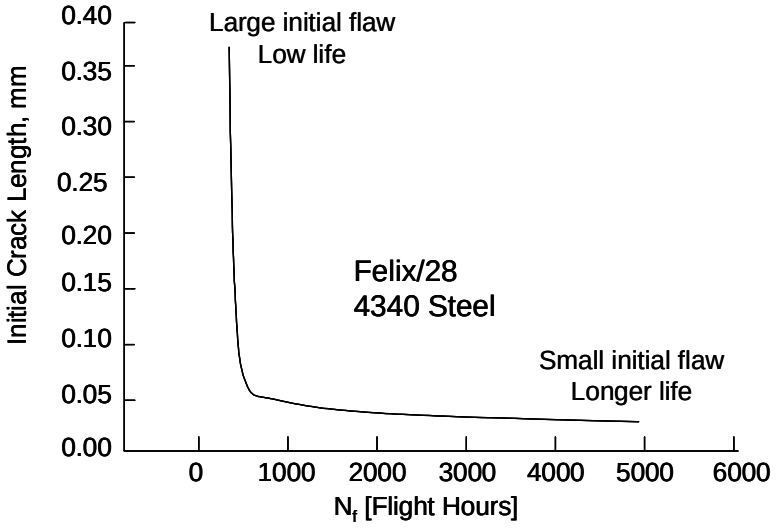

Figure 1.13

Spectra Severity[20]

A specific occurrence of this severity can be seen in the inspection findings of an H-60 Jayhawk helicopter in 2002. An 8-inch crack was discovered during routine inspection on the 7075 fuel tank pylon support. The crack initiated from corrosion pitting, growing at a rapid rate of 1.5 mm per 1000 loading cycles[21]. It is important to understand crack growth rates in cases such as this.

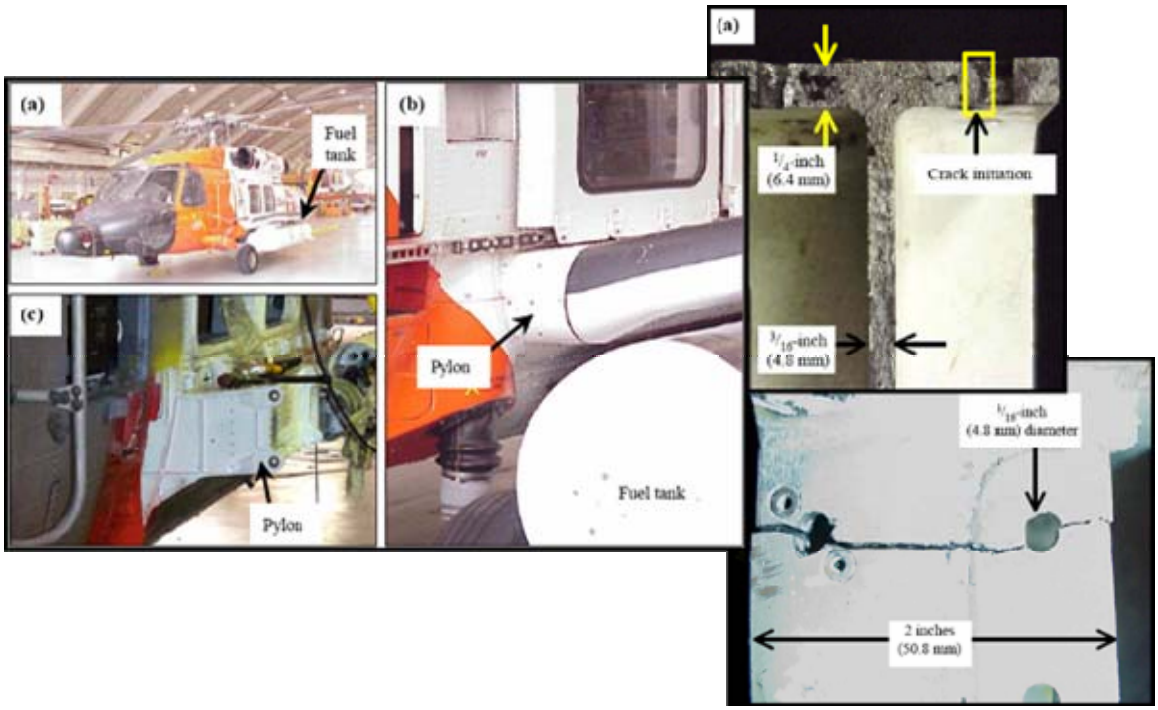

Figure 1.14

Rotorcraft Inspection Results[21]

The scale of the initial flaw size in a situation such as this can be categorized into the small crack regime, where crack behavior can vary from that of LEFM. The differences for the crack growth lengths vary depending on the material property influenced[22], as illustrated in Figure 1.15.

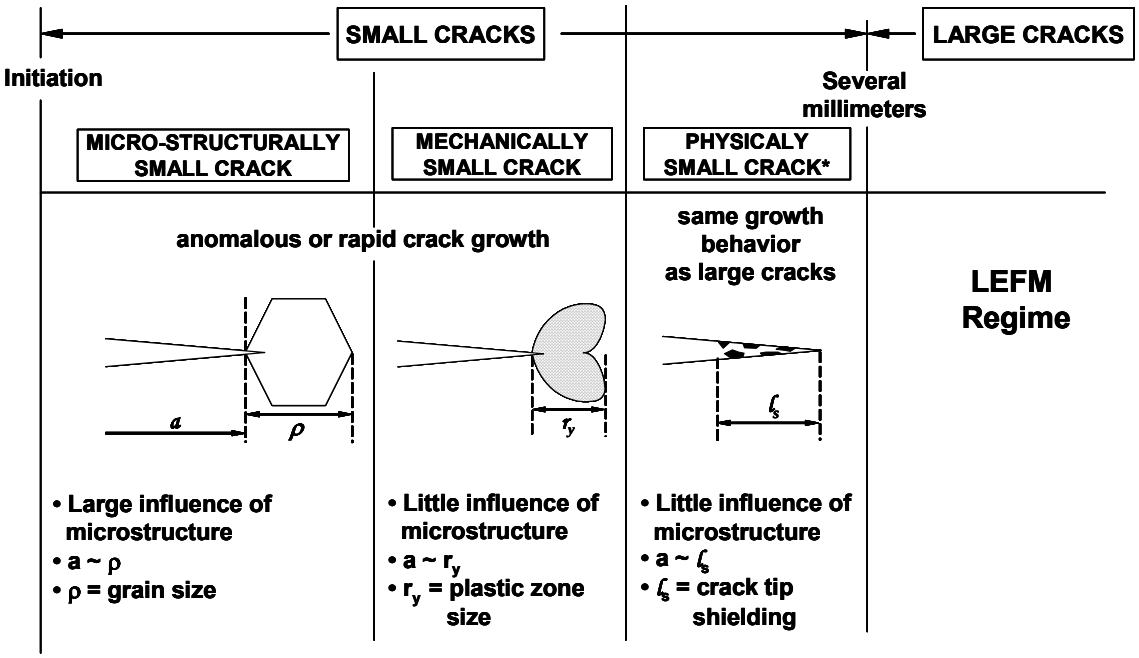

Figure 1.15

Small Crack Regimes[22]

These small cracks can result in different crack growth rates for a given material[23], as illustrated in Figure 1.16. The I-beam specimen geometry is an ideal design to study crack growth rates in smaller cross-sections of materials.

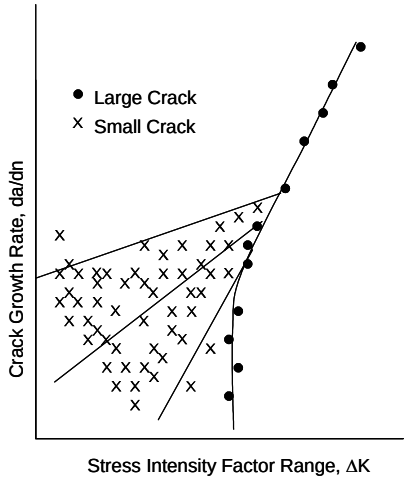

Figure 1.16

Small Crack Fatigue Characteristics[23]

ASTM currently recommends a variety of small crack geometries in standard E647[1], illustrated below in Figure 1.17. Each of these geometries could be applied to the miniature I-beam geometry.

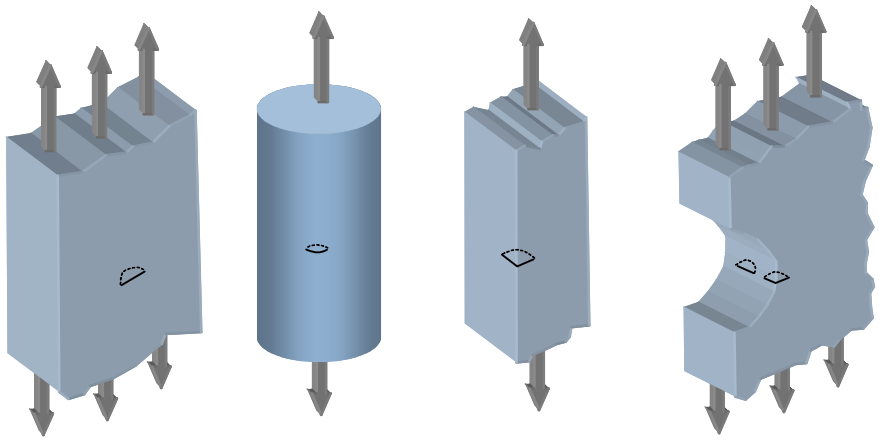

Figure 1.17

Small Crack Coupon Geometries[1]

1.3.5 Stress State

ASTM currently does not have a published method to test and analyze fatigue crack growth experiments in the plane stress state. The ability to test specimen of a miniature scale offers the potential to study this plane stress condition of materials in greater detail.

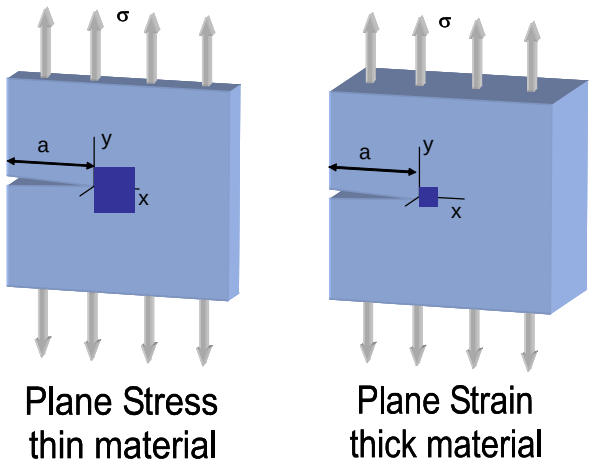

Figure 1.18

Axial Stress States[24]

The change in characteristics of the stress state affect the local crack tip plastic zone, influencing the fracture & fatigue properties of a material for different thickness.

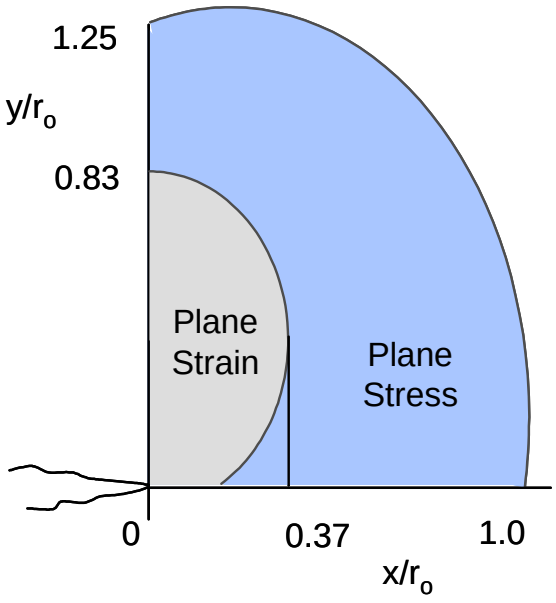

Figure 1.19

Stress-State Plastic Zone Shapes[25]

CHAPTER 2

EXPERIMENTAL DETAILS

2.1 Specimen

The specimens were designed in the shape of an I-beam, as shown in Figure 2.1. The overall size was limited within the diameter of the rod material purchased. Therefore, the width and height were defined by the diameter of the rod, but the overall depth of the design was not restricted. The specimens have a height of 16.26 mm, a depth of 12.7 mm, and an overall flange width (used to clamp the specimen) of 15.24 mm. The thickness of the center web varies among the specimen with three values: 1.524 mm, 3.048 mm, and 5.080 mm. The specimen design drawings were generated in CATIA v4 and can be found in Appendix A. Effects of the varying center web thicknesses will discussed in the Results section.

Figure 2.1
Specimen Design Examples

The specimens are manufactured from a 0.75”-diameter Aluminum 7075 rolled rod material. The inspection report for the stock material is displayed in Appendix B. The specimens were machined in the R-L load-crack direction illustrated in Figures 2.2, in accordance with ASTM-E399[26]. All specimens were machined by Holan Inc. and heat-

treated to T7351 temper from the rod in Figure 2.3. The monotonic[27] and cyclic[7] structural properties of this material are listed in Tables B.1 & B.2 of Appendix B.

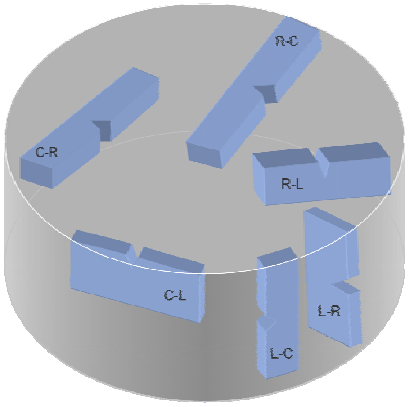

Figure 2.2
Load-Crack Direction Definition[26]

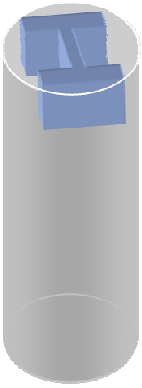

Figure 2.3
Specimen Orientation

The initial flaw size for this research was 1 mm past the edge of the notch, with the purpose of generating a sharp flaw tip. The initial manufactured notch was intended to create an initial stress concentration at the center of the web and the added pre-crack was generated to remove any influences of the initial notch from the crack growth data. No plastic zone length was assumed, calculated, or incorporated into the flaw size value at any point in these calculations. The notch was 2.54 mm long, 0.127mm high, and thru-thickness. The stress concentrations were manufactured using two different techniques.

Seven of the specimens were EDM-notched and the remaining four specimens were saw-cut to a square-notch. All notches were manufactured by either Sherer Machining Inc or Holan Inc. The EDM notch has a semi-circular tip diameter of 0.127 mm and the square notch has tip corner radii of 0.04 mm. The notch geometries are shown in Figures 2.4 & 2.5. The potential effects of the different specimen notches will be discussed in the Results section.

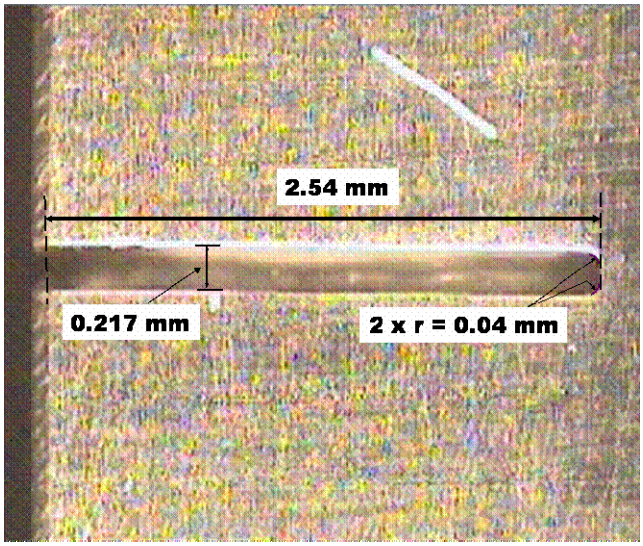

Figure 2.4

Square Notch Geometry

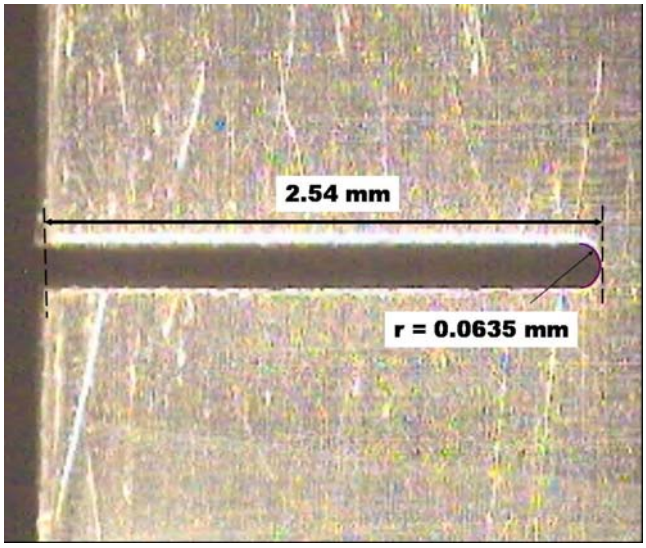

Figure 2.5

EDM Semi-circular Notch Geometry

The test matrix consisting of eleven specimens is shown in Table 2.1 below.

Table 2.1

Specimen Test Matrix

Specimen	t [mm]	Count
AL0664	1.524	2
AL1264	3.048	4
AL2064	5.08	5

Throughout this document, the specimen axis system will be defined as x-direction horizontal, y-direction vertical, and z-direction out of the page, illustrated in Figure 2.6.

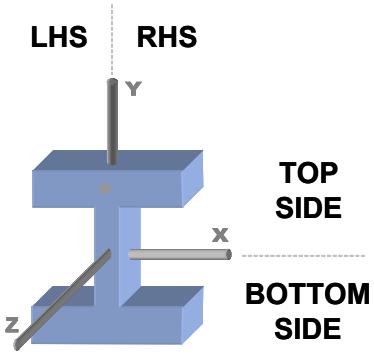

Figure 2.6

Specimen Axes

2.2 Test Equipment

A complete description listing of the equipment used throughout this research is located in Appendix C.

2.2.1 Calibration

For calibrations, two CEA-05-062UW-350 strain gages were attached to a steel miniature I-beam specimen as shown in Figure 2.7. The gages have a gage factor of 2.11 ± 0.5%. A strain gage soldering unit was used to attach the wires to the specimens, and a voltmeter was used to verify the strain gage readings. After installing the specimen into the test fixture, strain indicator unit and a switch & balance unit were used to record the strains on the center web during loading.

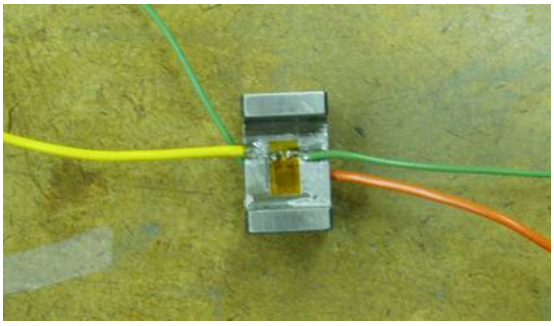

Figure 2.7

Calibration Strain Gage Attached to Specimen

2.2.2 Specimen Preparation

Preparation of the specimen prior to fatigue cycling included polishing, cleaning, and pre-cracking. The polishing required sandpaper, emery paper, olive oil, and diamond paste. An ultrasonic cleaner was used to clean the specimen and an MTS810 Test Stand and optical microscope were used to pre-crack the specimens and track the pre-crack length.

2.2.3 Fatigue Cycling

All fatigue crack growth experiments were performed on an MTS servo-hydraulic load frame equipped with mechanical grips designed to accommodate the miniature I-specimens. The specially-designed Inconel 718 grips manufactured by the Nickel Company are displayed in Figure 2.8. The MTS 810 servo-hydraulic test stand was outfitted with a 250 kN force transducer, an MTS Teststar IIs controller, MTS hydraulic power unit, and a Compaq desktop PC with Windows NT 4.0 OS.

The MTS Station Manager software commanded the actuator after the spectrum was defined in the Multi-Purpose Testware software. Optical crack growth measurements were recorded manually into a Microsoft Excel spreadsheet. The data was then regressed in the same file. The data was measured with a Nikon optical microscope using the 10sc (0.1) lens and a WF10X eyepiece. All digital photos of the specimen were taken with either an Olympus digital camera or a National digital microscope, attached to a Gateway PC with Windows XP OS. Motic Images Plus 2.0 OML software was used to store the digital files captured with the microscope.

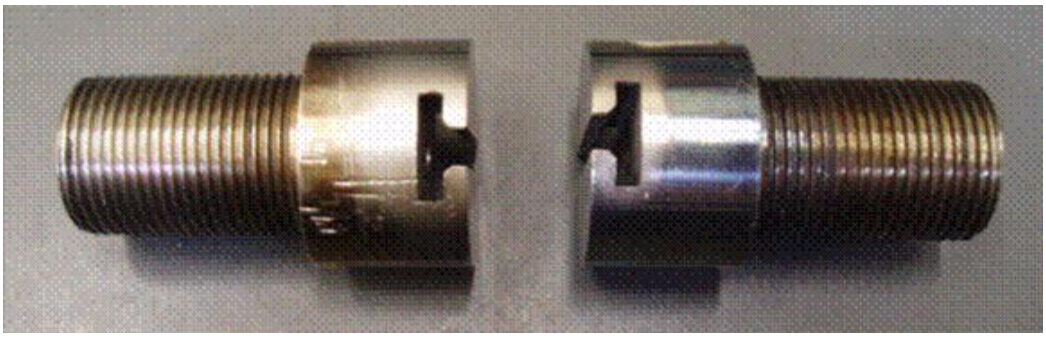

Figure 2.8

Nickel-base Super Alloy Grips

2.3 Test Procedures

2.3.1 Calibration

For the specimen calibration, axial strain gages and wires were attached to both sides of the center web of a steel specimen utilizing a strain gage installation procedure[28] defined by Vishay Measurements Group. The gages were connected to an amplifier during specimen loading, as illustrated in Figure 2.9. To replicate the testing environment, both the grips and the threaded rods used to attach the specimen to the fixture were left un-tightened by 2-3 threads to help alleviate fixture rigidity, which could cause additional load due to bending. From there, the strain gage factor was set on the strain indicator unit and then the gages were zeroed with the switch and balance unit. The specimen was loaded from zero to 3000 N at a loading rate of 600 N/sec, where the load level was held for one minute while the strains were read for both gages. The specimen was unloaded at the same rate, and strain readings were recorded again to verify there was no resulting deformation due to loading. The procedure was repeated several times for verification purposes. The specimen was rotated 180 degrees about the y-axis for half the calibration readings, but not about the x- or z-axis, duplicating the fatigue cycling environment.

Figure 2.9
Calibration Set Up

2.3.2 Specimen Preparation

Prior to testing, the specimens were prepared for visual inspections and pre-cracked to a pre-defined length. A crack is easier to locate on a clean, smooth surface, so both faces of the center web of the specimens were polished using 600-grit SiC emery paper. Then they were polished with emery paper coated in olive oil and diamond paste. Three grades of diamond paste, 18-, 6-, and 1-μ paste were applied separately during multiple polishing iterations. The specimens were then washed in a water & liquid dish soap solution for 20 minutes in a Cole Palmer ultrasonic cleaner. This preparation is outlined in greater detail on pages 2-5 of the procedure in Appendix D.

Fatigue pre-cracking guidelines are not clearly defined by ASTM standards[1]. It is suggested that the minimum length of the fatigue pre-crack should be 10 percent of the width or height of the specimens or about 1 mm, whichever is greater. With this in mind, the pre-crack length was chosen to be 1 mm, and specimens were cycled at their testing stress levels and inspected at 5000 cycle intervals.

2.3.3 Fatigue Cycling

Fatigue cycling tests were performed under load control using a constant-amplitude sinusoidal waveform with a loading frequency of 15 Hz. All tests were operated at room temperature ambient and a load ratio of 0.1. The general test spectrum block profile is shown in Figure 2.10. As mentioned previously, both the grips and the threaded rods are left un-tightened by 2-3 threads during cycling. The specimens were tested using the MTS operating procedures outlined in Appendices E & F. A detail view of the specimen installed in the test fixture is shown in Figure 2.11.

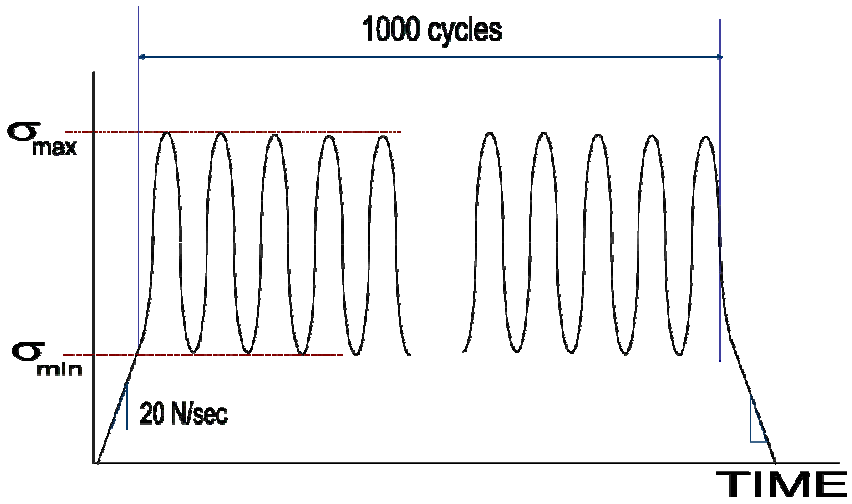

Figure 2.10

Test Spectrum Load Profile

Figure 2.11

Specimen Testing Installation

After each loading block, the specimen was removed from the fixture and crack growth along the front face was measured with the optical microscope. The specimens were rotated 180° about y-axis, as shown in Figure 2.12, every 1000 cycles to ensure even loading across the crack during cycling. An inspection of one side of a specimen is illustrated in Figure 2.13.

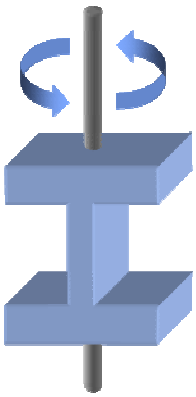

Figure 2.12

Specimen Rotation

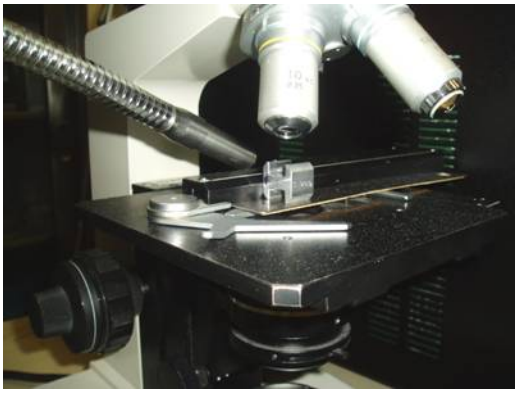

Figure 2.13

Specimen Inspections

The maximum stress levels applied to the specimen are shown in Table 2.2. The maximum stress levels for each thickness value were determined through initial cycling.

Table 2.2

Maximum Applied Stress Levels

Specimen	t [mm]	σ_{max} [MPa]
AL0664-02	1.524	68.20
AL0664-03	1.524	68.20
AL1264-03	3.048	54.25
AL1264-06	3.048	54.25
AL1264-08	3.048	59.42
AL1264-10	3.048	58.13
AL2064-01	5.08	32.55
AL2064-02	5.08	46.50
AL2064-03	5.08	46.50
AL2064-04	5.08	46.50
AL2064-06	5.08	46.50

CHAPTER 3

RESULTS AND DISCUSSION

3.1 Results

This section will document the results from the calibrations and experimental testing, along with the results of the crack growth rate calculations.

3.1.1 Calibrations

Calibrations were performed on a miniature 4340 steel I-beam specimen to determine if any bending loads were being applied to the specimen through the grip configuration. A 3000N load applied to the specimen during calibrations generating a stress of 155.5 MPa on the 1.524 mm center web. Assuming there are no load components or moments other than the y-direction load to induce additional stresses on the specimen center web, the resulting expected strain from the applied load can be determined with the Young's Modulus.

$$\varepsilon_{applied} = \frac{\sigma_{applied}}{E} = \frac{P_{applied}}{EWt} = \frac{3000}{205 \times 10^{9} \times 0.0127 \times 0.001524} = 756 \mu strain$$

Readings were recorded from strain gages applied to both sides of the center web. The raw data results can be found in Appendix L. The plotted data and theoretical value is shown in Figure 3.1 below. The strains from the applied loads are slightly lower than the theoretical value calculated and appear to differ by up to 150 μstrains form experimental scatter.

During the unloaded periods between calibrations, it was observed the strain readings fluctuated up to 50 μstrains (of equal & opposite values) on the gages. During the periods the specimen was held at constant load, the strain readings remained within a range of 4 μstrains.

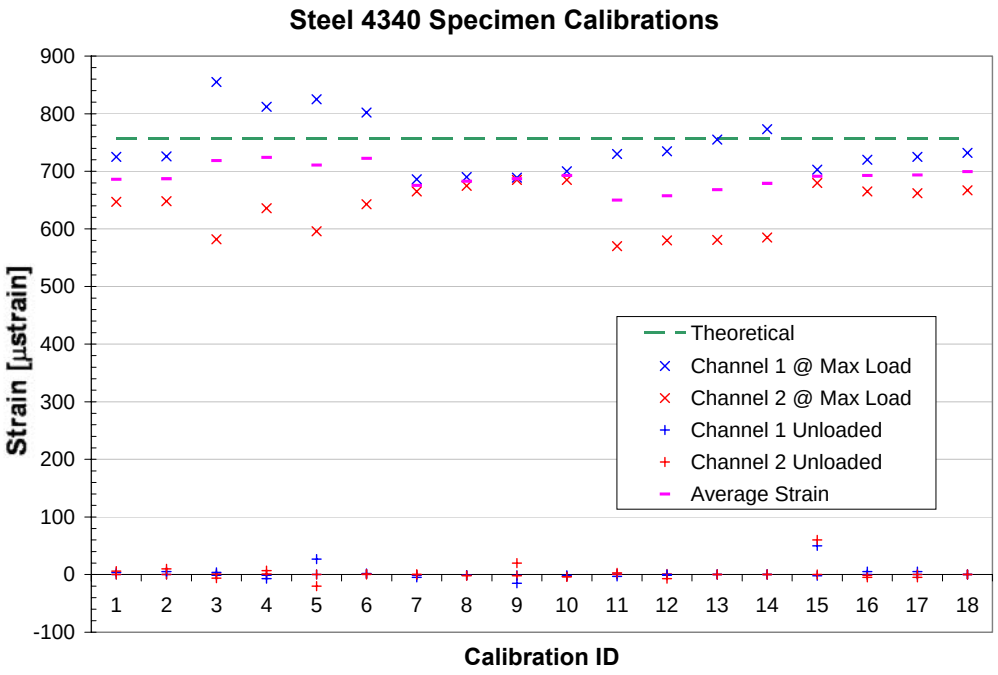

Figure 3.1

Calibration Results

3.1.2 Experimental Results and Calculations

All the specimens were cycled from their initial pre-crack to failure under a constant stress level. The total cycle count is shown in Table 3.1.

Table 3.1

Total Cycles to Failure

Specimen	t [mm]	σ_{max} [MPa]	Cycles - Fail
AL0664-02	1.524	68.20	101000
AL0664-03	1.524	68.20	113493
AL1264-03	3.048	54.25	83525
AL1264-06	3.048	54.25	104428
AL1264-08	3.048	59.42	146406
AL1264-10	3.048	58.13	117887
AL2064-01	5.08	32.55	304605
AL2064-02	5.08	46.50	228607
AL2064-03	5.08	46.50	123637
AL2064-04	5.08	46.50	223022
AL2064-06	5.08	46.50	126732

All individual specimen figures displayed in this chapter will use the results from specimen AL1264-10. All results corresponding to the other 10 specimen will be found in appendices specified. The failed fracture surface for specimen AL1264-10 is in Figure 3.2. The other fracture surface figures are located in Appendix G. The crack growth plot for this specimen is in Figure 3.3 and the plotted crack growth rate is shown in Figure 3.4. The other specimens crack growth curves are in Appendix I.

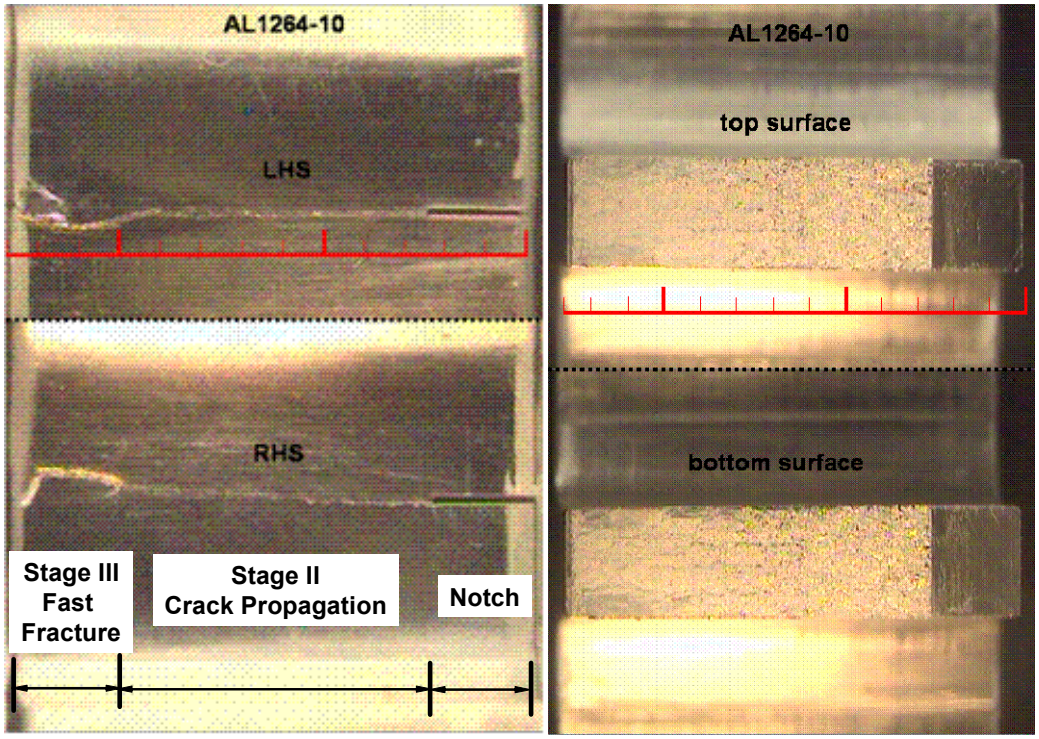

Figure 3.2

Specimen AL1264-10 Fracture Surfaces

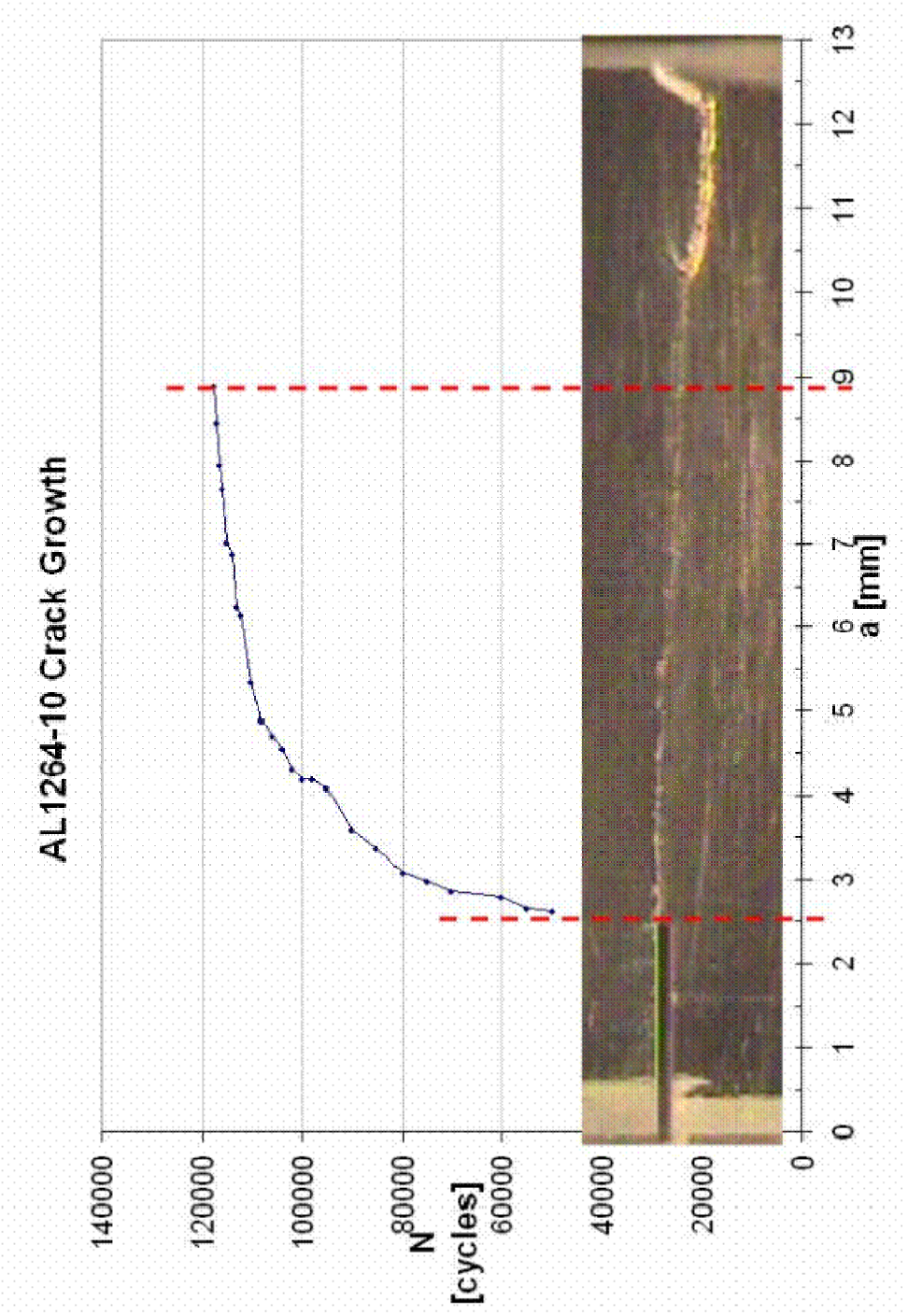

Figure 3.3
Specimen AL1264-10 Crack Growth Plot

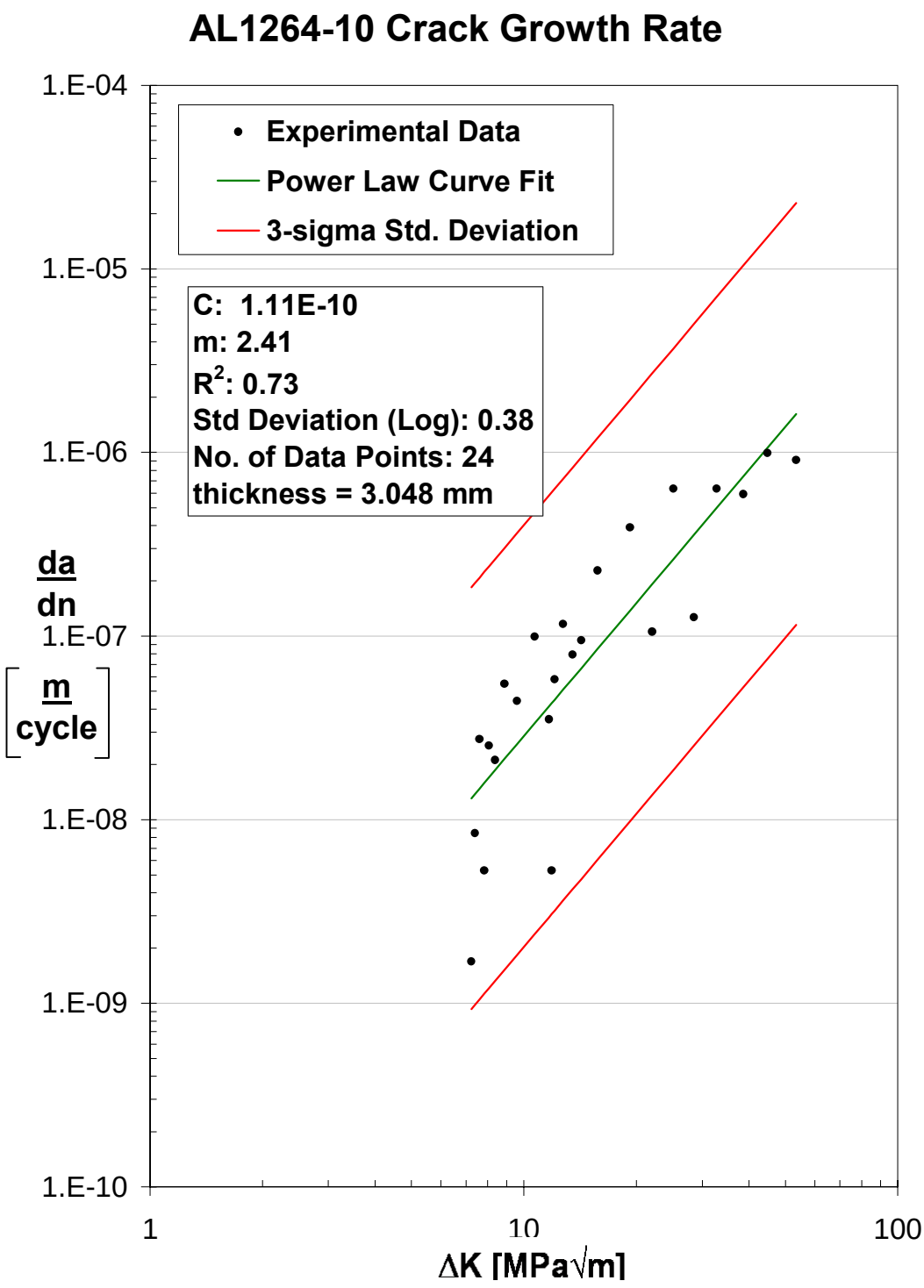

Figure 3.4

Specimen AL1264-10 Crack Growth Rate Plot

The fatigue parameters determined from the experimental data for the complete test matrix are summarized in Table 3.2.

Table 3.2

Crack Growth Rate Parameters

Specimen	t [mm]	C	m
AL0664-02	1.524	1.74E-10	2.09
AL0664-03	1.524	1.96E-10	2.09
AL1264-03	3.048	3.13E-10	2.09
AL1264-06	3.048	1.89E-10	2.23
AL1264-08	3.048	1.24E-10	2.46
AL1264-10	3.048	1.11E-10	2.41
AL2064-01	5.08	1.51E-10	2.37
AL2064-02	5.08	3.28E-10	2.07
AL2064-03	5.08	3.76E-10	2.03
AL2064-04	5.08	2.33E-10	2.26
AL2064-06	5.08	1.69E-10	2.38

Several statistical parameters representing the 'goodness' of the data fit are summarized in Table 3.3.

Table 3.3

Statistical Evaluation

Specimen	t [mm]	R^2	Std Dev Log	Std Dev Linear
AL0664-02	1.524	0.52	0.45	2.79
AL0664-03	1.524	0.63	0.46	2.88
AL1264-03	3.048	0.64	0.50	3.13
AL1264-06	3.048	0.80	0.29	1.56
AL1264-08	3.048	0.78	0.31	2.04
AL1264-10	3.048	0.73	0.38	2.41
AL2064-01	5.08	0.71	0.44	2.78
AL2064-02	5.08	0.63	0.44	2.75
AL2064-03	5.08	0.66	0.36	2.31
AL2064-04	5.08	0.76	0.32	2.10
AL2064-06	5.08	0.71	0.32	2.09

3.2 Discussion

This section will discuss the experimental results and calculations presented in the previous section. The data will be compared to those from the published sources discussed previously.

3.2.1 Calibrations

The values seen in the calibration results plot suggest a small moment is applied to the specimen in the fixture. This difference in strain could be due to the placement of strain gages, as shown in Figure 3.5, but the difference in strain gage angles is not large and the range in readings suggest the moment is very small.

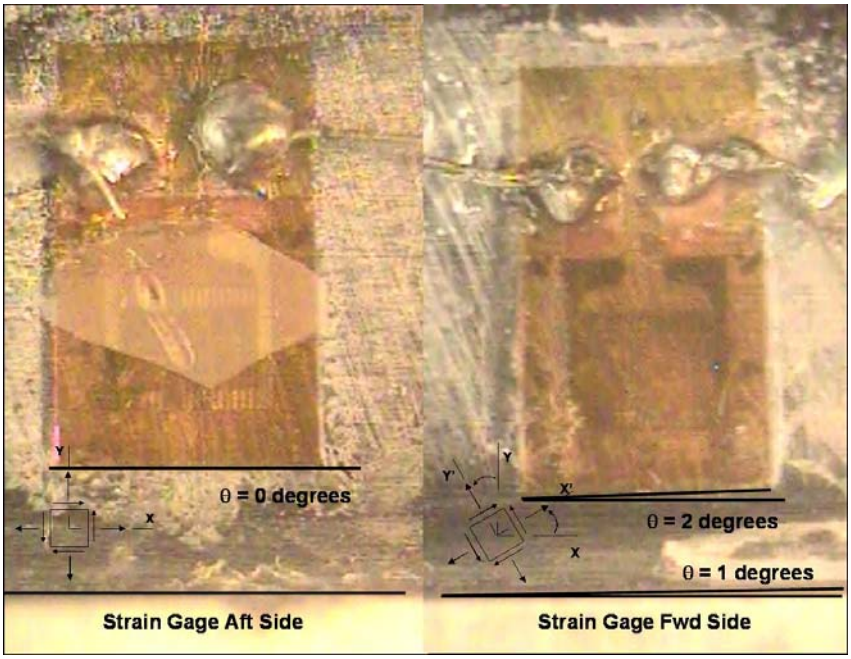

Figure 3.5

Calibration Strain Gage Angles

It was assumed in Section 3.1.1 there is no x- or z- direction loads on the center web during specimen loading. The material will naturally react to axial displacement with

the Poisson effect on the center web. This will result in the shape shown in Figure 3.6 and can decrease the strain due to an additional strain component. If the difference in values was large, the stress and strain components could be measured in each direction and the experimental values could be determined using Mohr's circle.

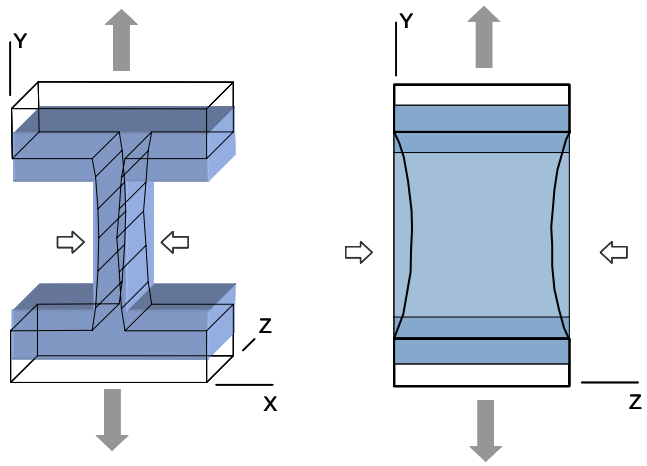

Figure 3.6

Poisson Effect on Center Web

3.2.2 Experimental Test Data and Calculations

Crack initiation trends were not analyzed since multiple load levels were applied to part of the test matrix. All initial flaws were 3.54 mm in length. The ΔK range for the determination of the fatigue parameters was between 10^6 and 10^8. The data was reviewed by specimen thickness, as shown in Figures 3.7 through 3.9.

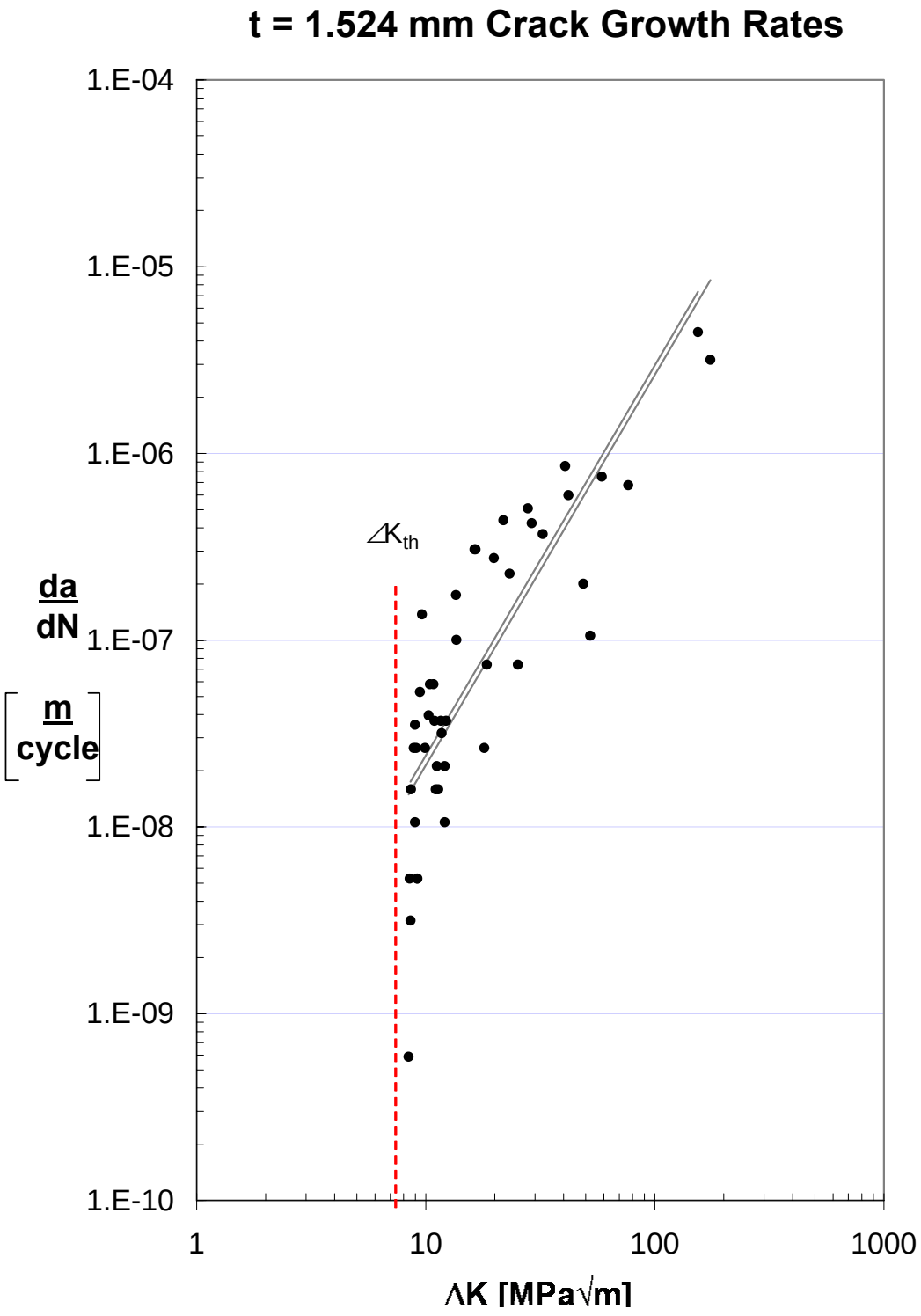

Figure 3.7

Crack Growth Rate Plot for (2) 1.254 mm specimens

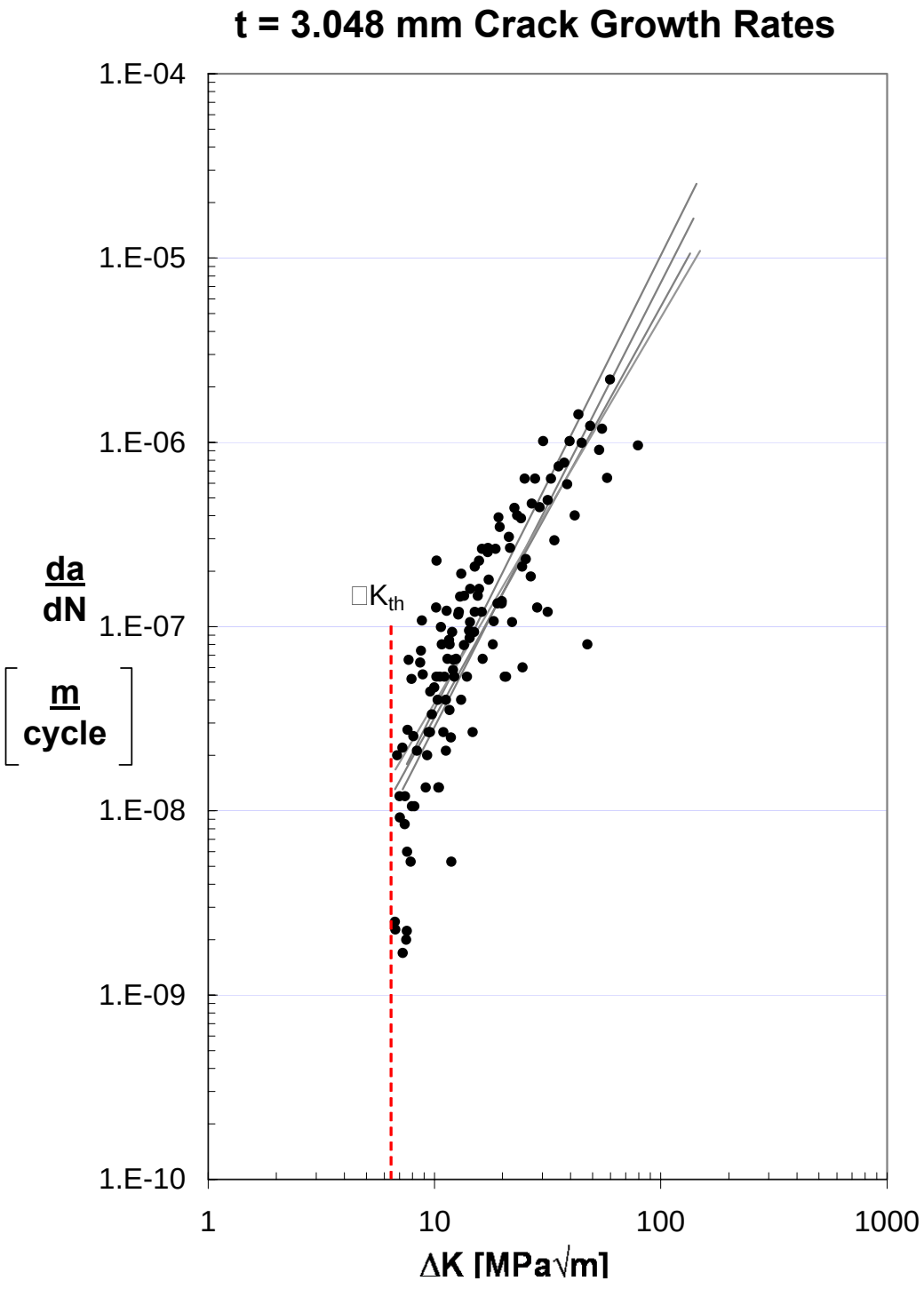

Figure 3.8

Crack Growth Rate Plot for (4) 3.048 mm specimens

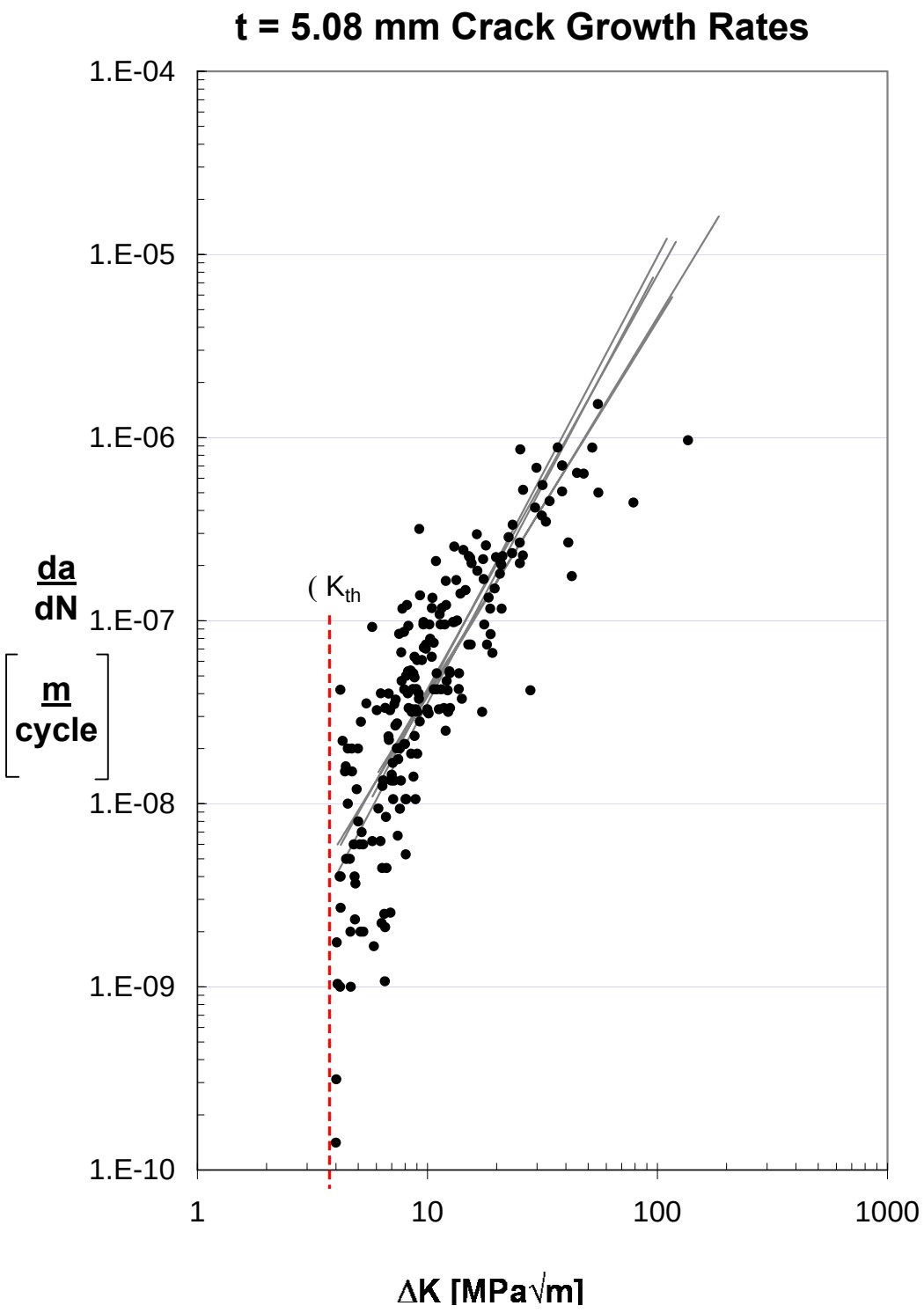

Figure 3.9

Crack Growth Rate Plot for (5) 5.08 mm specimens

The coefficient of determination between the experimental data and the fitness of the regression for the fatigue parameters varied from 0.5 to 0.8. The standard deviation ranges were compared for each thickness, as shown in Appendix H.

The minimum SIF calculated from the experimental data range between 3.5 and 8.5 MPa√m and the maximum SIF range from 45 to 85 MPa√m. The ΔK_{th} values increased as the thickness of the specimen decreases as seen in Figure 3.10 and agrees with thickness effects of a material on the fracture toughness value[29], as illustrated in Figure 3.11.

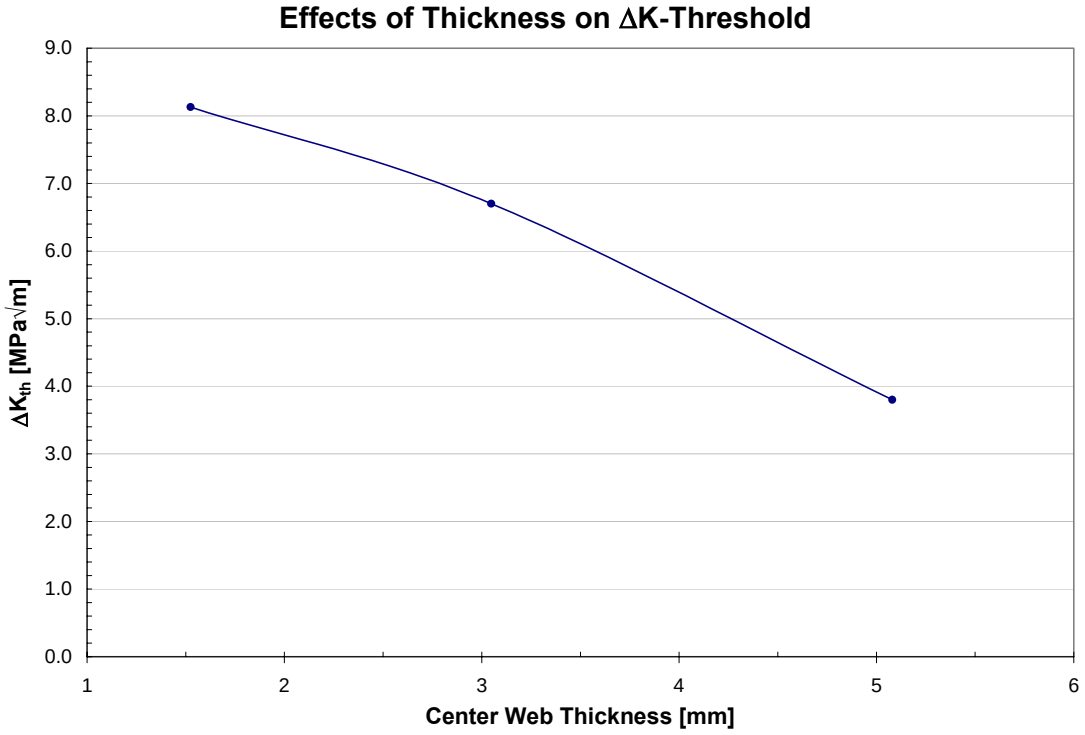

Figure 3.10

Thickness Effects on Threshold Stress Intensity Range

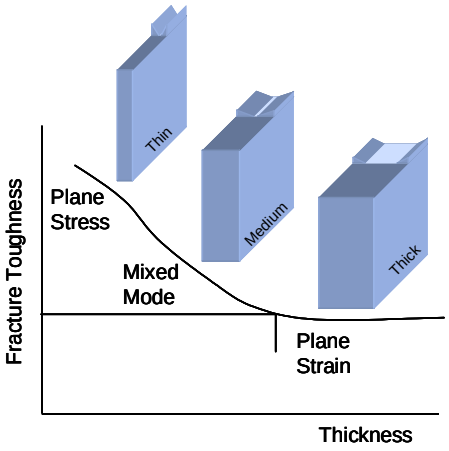

Figure 3.11

Relation between Stress Intensity and Thickness[29]

3.2.3 Data Comparison

The results were compared to published data for Aluminum 7075. The crack growth rates for the other sources of data correlate satisfactorily with the initial test data collected. The Stress Intensity Range of the experimental crack growth data correlated well with the data from ASM, showing a larger range of scatter at the lower end, as seen Figure 3.12, and the crack growth rate calculated is the same as the ASM data.

Figure 3.13 compares the experimental results of this research with the crack growth data from the MMPDS-01. Both have the same slope and over lap in their crack growth rate ranges. Differences in where the ranges fall on the plots could be due to the differences in specimen material direction o load ratios. The data from the MMPDS-01 was derived from tests on Plate material for a variety of load ratios ranging from 0.1 to 0.51. The experimental data is for bar material for a single load ration of 0.1.

Figure 3.14 and Figure 3.15 compares the experimental result with data from technical journals, both comparisons suggesting good correlation. The correlation with the Newman et al. data suggests the miniature I-beam specimen results in the same data as the C(T) and M(T) geometry. The correlation with the Kim et al. data suggests that the range of thicknesses in this study, as well as theirs, do not have a large affect on the crack growth rates.

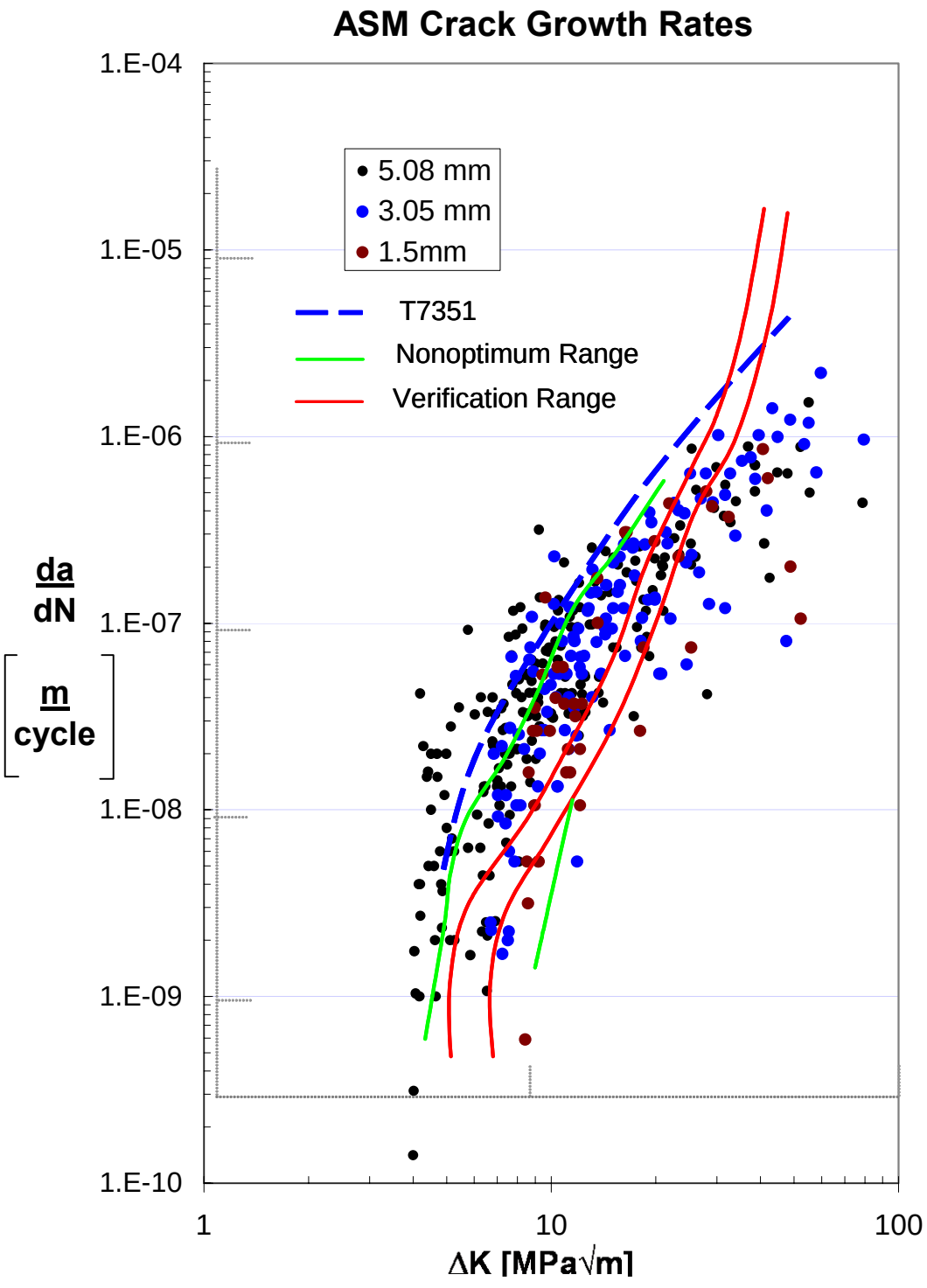

Figure 3.12

Comparison with ASM Crack Growth Rates[7]

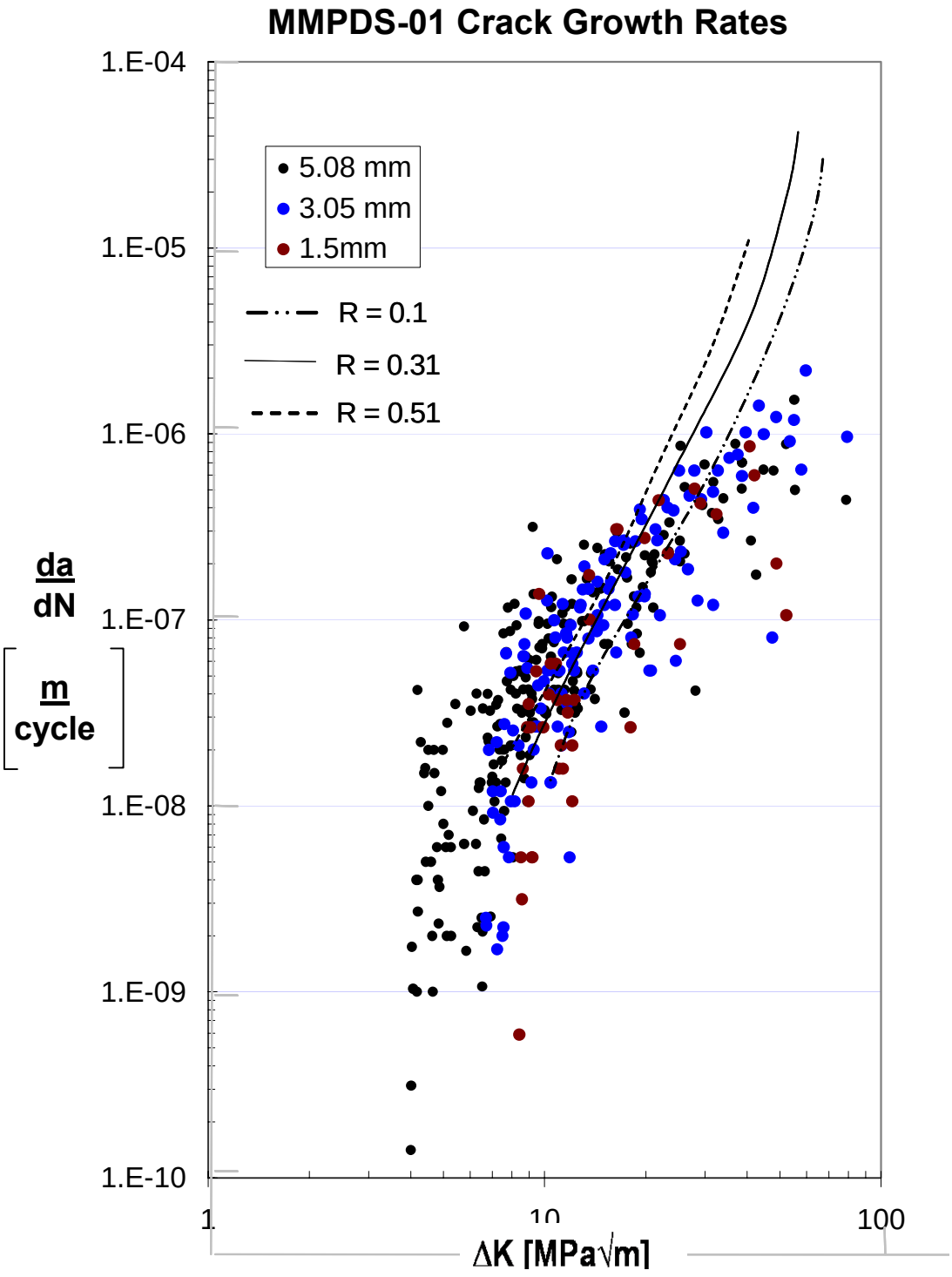

Figure 3.13

Comparison with MMPDS-01 Crack Growth Rates[6]

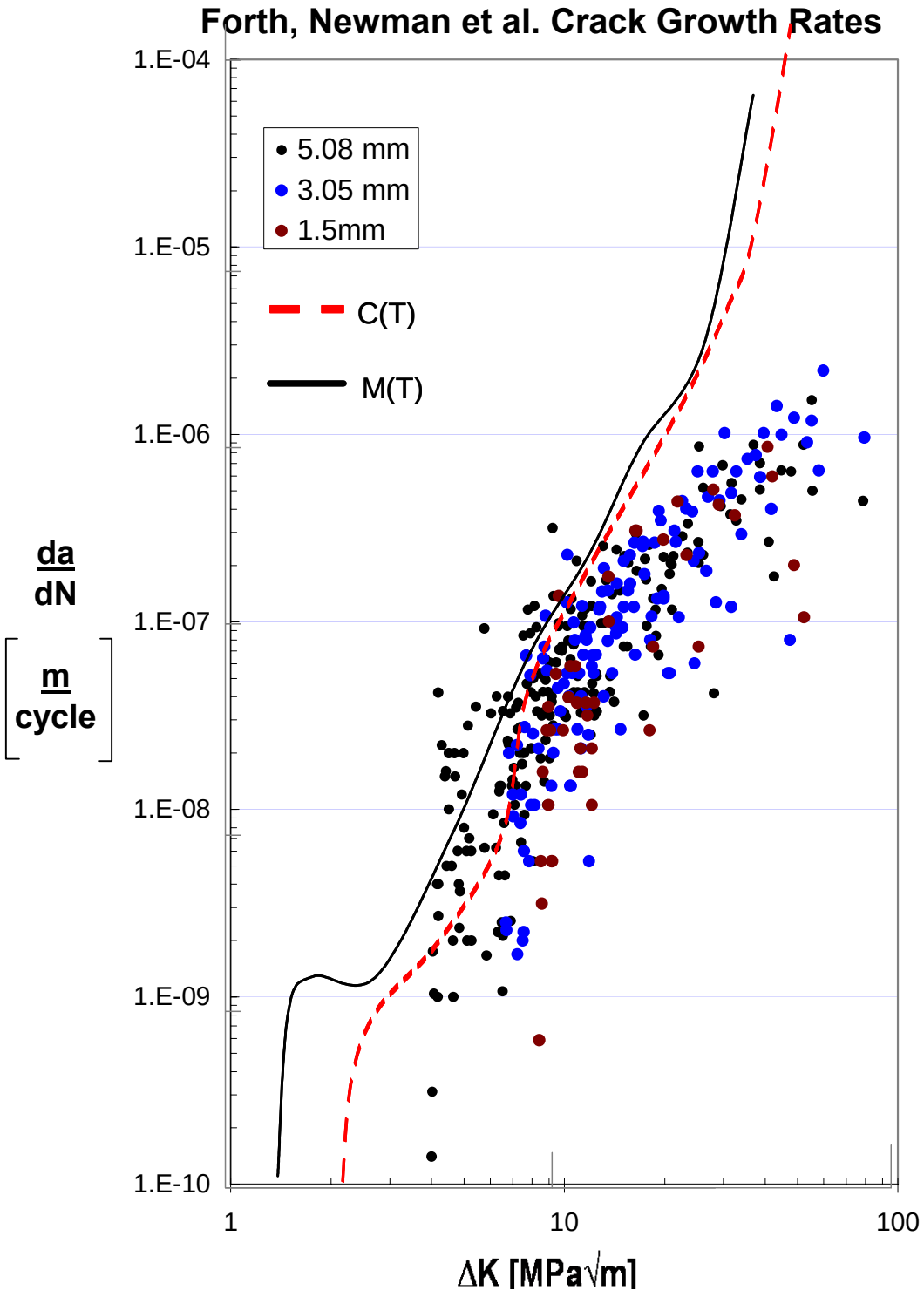

Figure 3.14

Comparison with Forth, Newman et al. Crack Growth Rates[10]

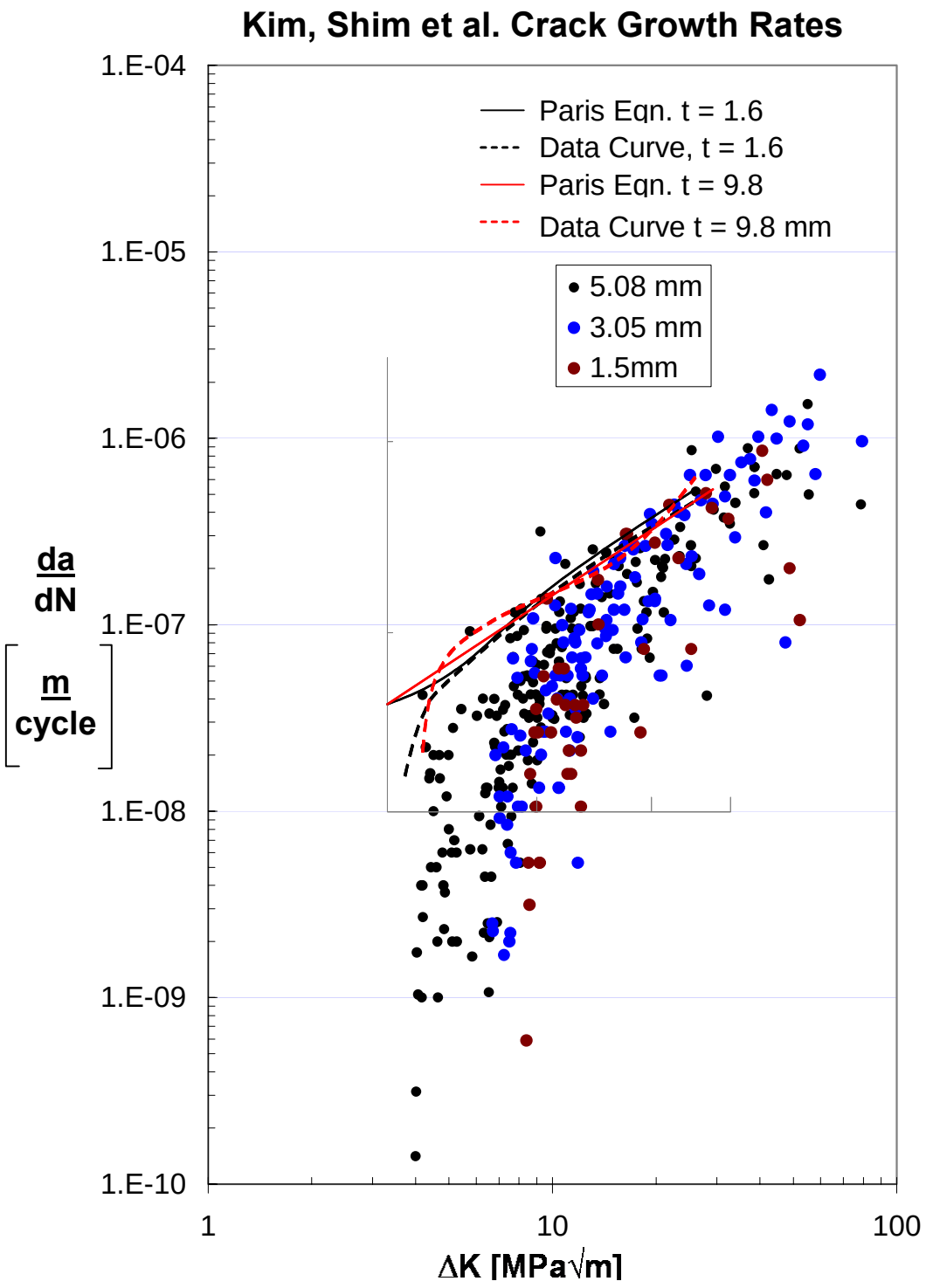

Figure 3.15

Comparison with Kim, Shim, et al. Crack Growth Rates[11]

The experimental crack growth results were also compared to the crack growth data used by the Air Force crack growth software tool, AFGROW. Three different sets of crack growth rate data are available for use with the program. They all represent 7075-T73 material tested at room temperature at a load ratio of zero. The experimental results of this research fall in the range of the experimental data in Figure 3.16.

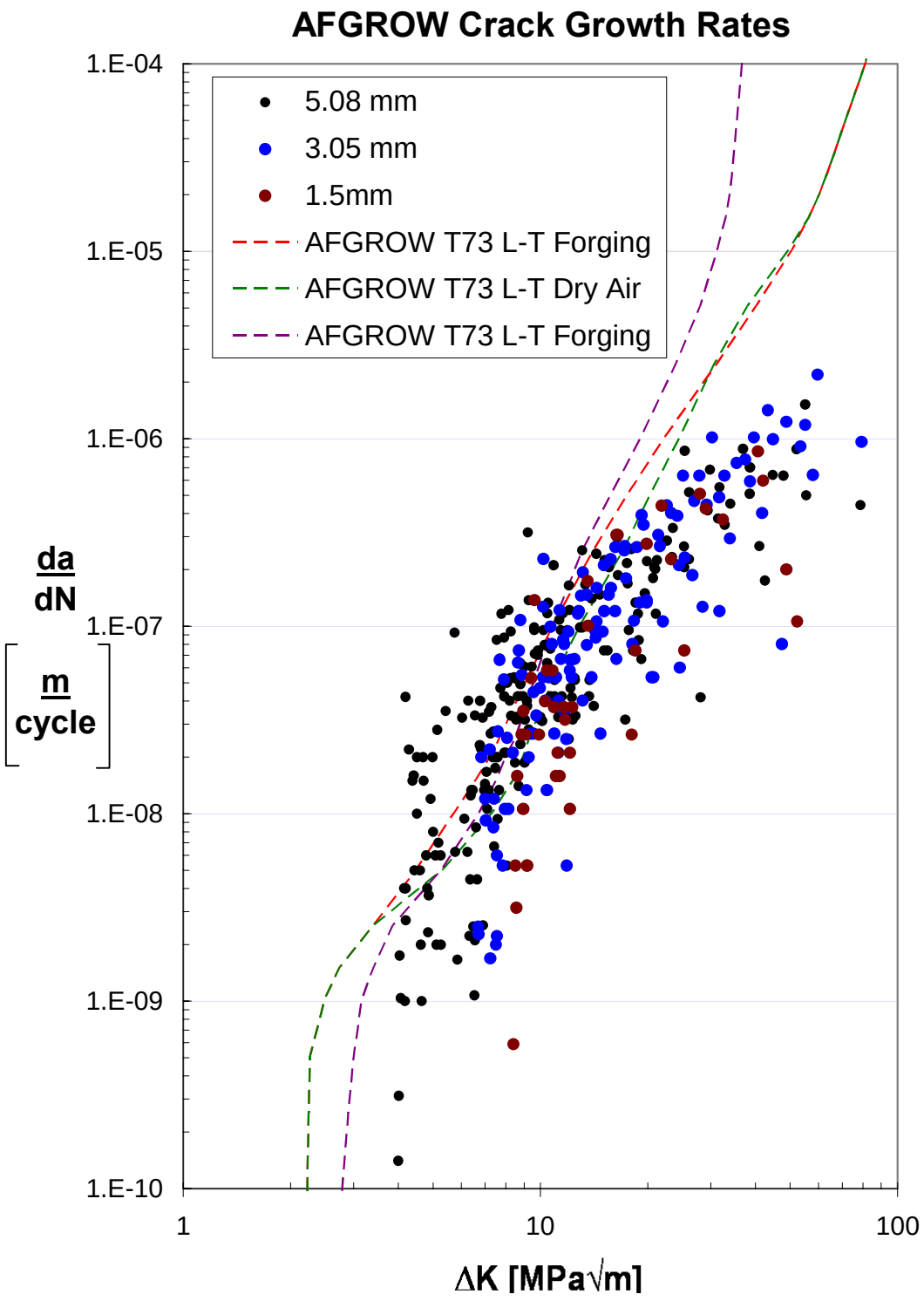

Figure 3.16

Comparison with AFGROW Crack Growth Rates

The fatigue parameters calculated from a number of published works and experimental data were compared in Table 3.4. The standard deviation of the experimental parameters is displayed in Table 3.5. Plots of the compared fatigue parameters can be found in Appendix H. The plots compare the experimental data with the fatigue parameters from the published work. This was completed by inputting the experimental ΔK values into the relationships defined by the published fatigue parameters.

Table 3.4

Comparison of Fatigue Parameters[8, 9, 11]

Source	Thickness Range [mm]	da/dn Range	C	m
ESDU Higher CGR	19 - 25	10^{-5} - 10^{-6}	3.10E-09	2.00
ESDU Lower CGR	19 - 25	10^{-6} - 10^{-7}	2.91E-11	3.60
FAA Equation Fit	4.5 - 12.7	Unknown	8.10E-11	2.90
FAA Walker Eqn	4.5 - 12.7	Unknown	1.66E-11	3.16
Int'l Jnl Fatigue	1.60	Unknown	3.96E-10	2.54
Kim/Shim	3.20	Unknown	4.52E-10	2.66
February 2000	4.80	Unknown	2.16E-10	2.85
	9.80	Unknown	5.36E-10	2.43
AL0664-02	1.524	10^{-6} - 10^{-9}	1.74E-10	2.09
AL0664-03	1.524	10^{-6} - 10^{-9}	1.96E-10	2.09
AL1264-03	3.048	10^{-6} - 10^{-9}	3.13E-10	2.09
AL1264-06	3.048	10^{-6} - 10^{-9}	1.89E-10	2.23
AL1264-08	3.048	10^{-6} - 10^{-9}	1.24E-10	2.46
AL1264-10	3.048	10^{-6} - 10^{-9}	1.11E-10	2.41
AL2064-01	5.08	10^{-6} - 10^{-9}	1.51E-10	2.37
AL2064-02	5.08	10^{-6} - 10^{-9}	3.28E-10	2.07
AL2064-03	5.08	10^{-6} - 10^{-9}	3.76E-10	2.03
AL2064-04	5.08	10^{-6} - 10^{-9}	2.33E-10	2.26
AL2064-06	5.08	10^{-6} - 10^{-9}	1.69E-10	2.38

Table 3.5

Statistical Analysis of Fatigue Parameters

Parameter	Mean	Standard Deviation
m	2.22	0.1591248
C	2.15E-10	8.758E-11

3.2.4 Parameters Affecting Data

A number of parameters can have significant effect on the experimentally measured crack growth rate, although such variables are not incorporated into ΔK.

Different notch geometries could affect the initiation of a crack. A review of the notch geometry reviewed the values were too small to determine the stress concentration for both geometries from standard published data shown in Appendix figure J.1. Mechanica FEA models were generated for the two notch geometries, as shown in Appendix figure J.2. Gross stress concentration values of 14.50 and 16.19 were calculated for the EDM and square notch, respectively. The difference in these values is small and should not affect the initiation of the flaw.

Published notch sensitivity plots for aluminum suggest the smaller a notch radius, the small the notch sensitivity factor, which would decrease the fatigue stress concentration factor. Other sources for the effects of the notch could come from the grain shape of the material or the notch manufacturing process.

The beta equation used in the stress intensity factor calculations is valid for specimens where the length is at least two times smaller than the unclamped height. This is not the case for the specimen geometry utilized in this research. The length is longer than the unclamped height. The possible effects of the too short specimens would need to be studied further.

The magnification of the optical equipment used for crack growth measurements could affect the accuracy of the readings. Although measurements are recorded for both sides of the notch, the crack path in the center of the material is not recorded. Other inspection methods or a more powerful microscope could increase the accuracy of the measurements.

The specimens are thin enough to begin to act in the plane stress condition. This could have some effect on the results.

CHAPTER 4

CONCLUSIONS

Eleven miniature I-beam specimens varying in 3 web thicknesses were successfully utilized in fatigue crack growth testing of aluminum specimen. Crack growth data was gathered and fit with the Region II Paris Law relationship. The results were compared with data from existing literature. The fatigue parameters and life predictions suggest correlation with published analysis methods. The C-coefficient remained within a range of 1E-10 m^{-1} and 4E-10 m^{-1}; the m-exponent ranged between 2 and 3. The data also suggests that ΔK_{th} decreases as the specimen thickness increases.

CHAPTER 5

RECOMMENDATIONS

The first recommendation of future work would be additional testing of the current specimen and parameters. This research is a solid foundation for utilizing this design geometry in a variety tests and further investigation would generate a more robust set of data and results for material properties. There would also be an increase in the confidence of the data for each individual set of specimen thicknesses. Data form crack growth rates in other material directions would contribute to a better understand of the material properties overall. A micro-structural investigation into the grain size would contribute to a better understanding of the crack growth rates, as well. Frictionless spherical bearings could be used during testing to alleviate any potential bending introduced into the specimen during cycling.

Confidence in the experimental data could be complemented by additional analytical studies of the test set up and data. A finite element analysis of loads applied to a specimen geometry with varying crack lengths or grip stiffness could offer better insight to the stress distribution effects on the assembly as well as the experimental results.

In addition to accruing crack growth data, it is suggested that further testing of this specimen geometry include a variety of test types, such as monotonic ultimate and fracture toughness to validate the usefulness of the geometric design. This should also lead to the study of environmental effects on the geometric and loading parameters.

Other significant areas of study would include variations in the testing parameters and material geometry. The study of load ratio effects would also complement the initial work completed on this material.

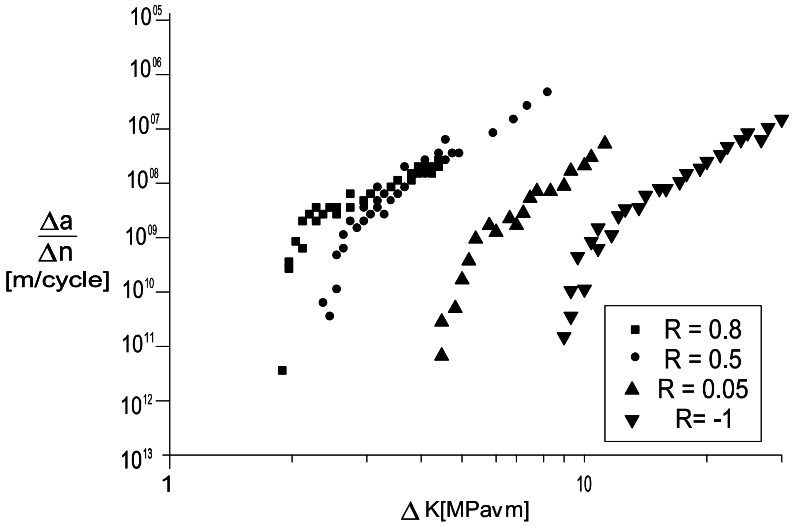

Figure 5.1

Load Ratio Effects on Crack Growth Rates[30]

Other materials in similar applications, such as steel or titanium could be tested in this manner, as well. Steel has as many applications as aluminum in the aerospace industry. Prior research by sources such as ASM has shown the difference in crack growth rates for aluminum and steel can vary greatly. It also has been observed that the small crack effect is not as prominent in steel.

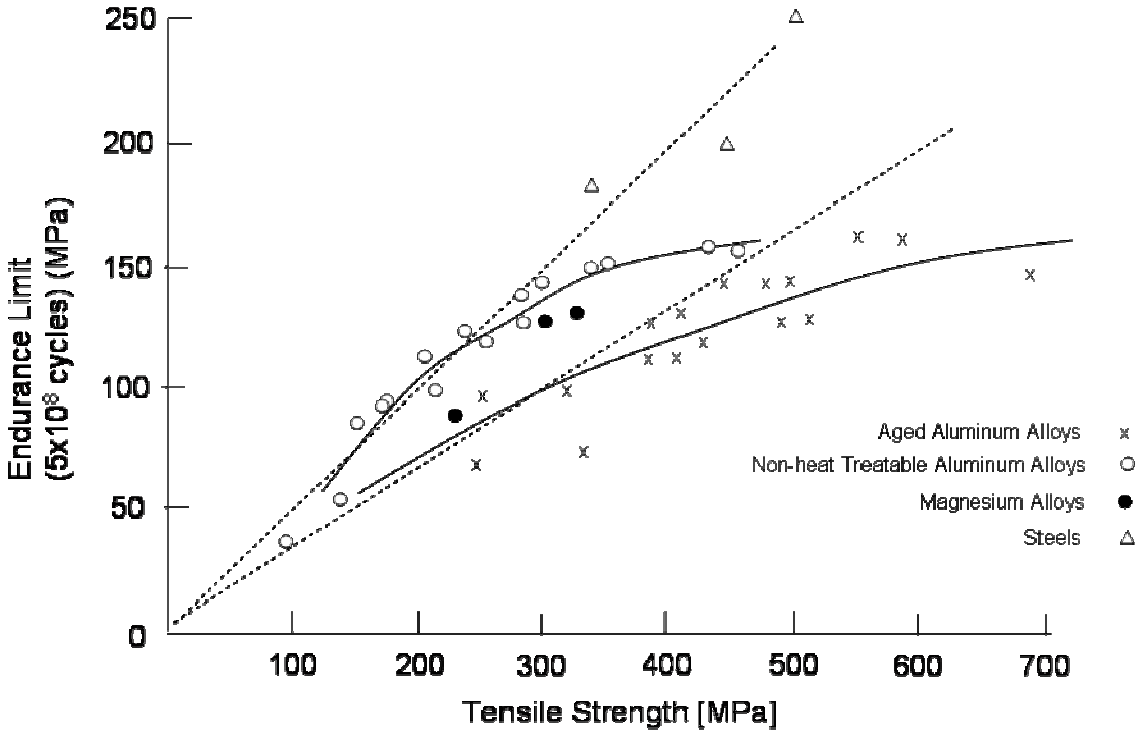

Figure 5.2

Crack Growth Rates of Various Materials[7]

This then offers another opportunity to study cracks on a much smaller scale with state-of-the-art health monitoring instrumentation, such as ACPD. This would allow for greater precision in crack growth measurements at much smaller crack sizes. The materials are good conductors and the flat surfaces allow for easy attachment of the probe wires. Aluminum wires have successfully been ultrasonically-welded to the narrow faces of this specimen geometry, which should make the opportunity to utilize this inspection option even more appealing. This then also creates an opportunity to study small cracks and their fatigue characteristics, such as crack closure.

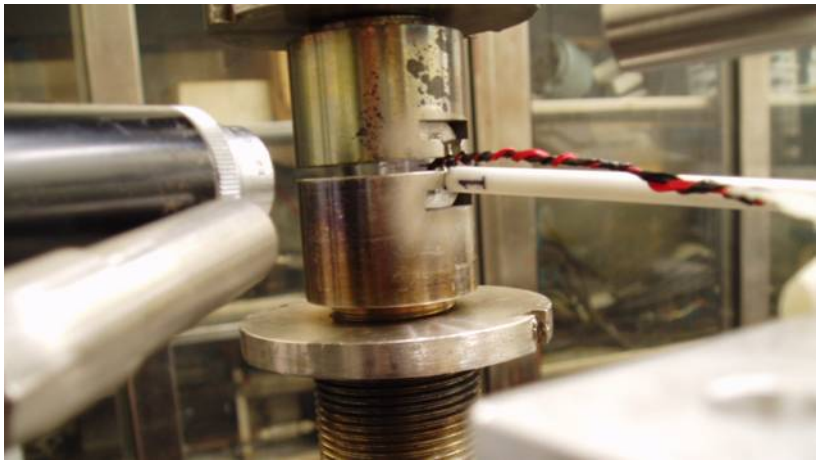

Figure 5.3

AC Potential Drop Crack Growth Monitoring

Overall, the research has validated the material's crack growth properties and demonstrated the effectiveness of the design.

APPENDIX A

SPECIMEN DRAWINGS

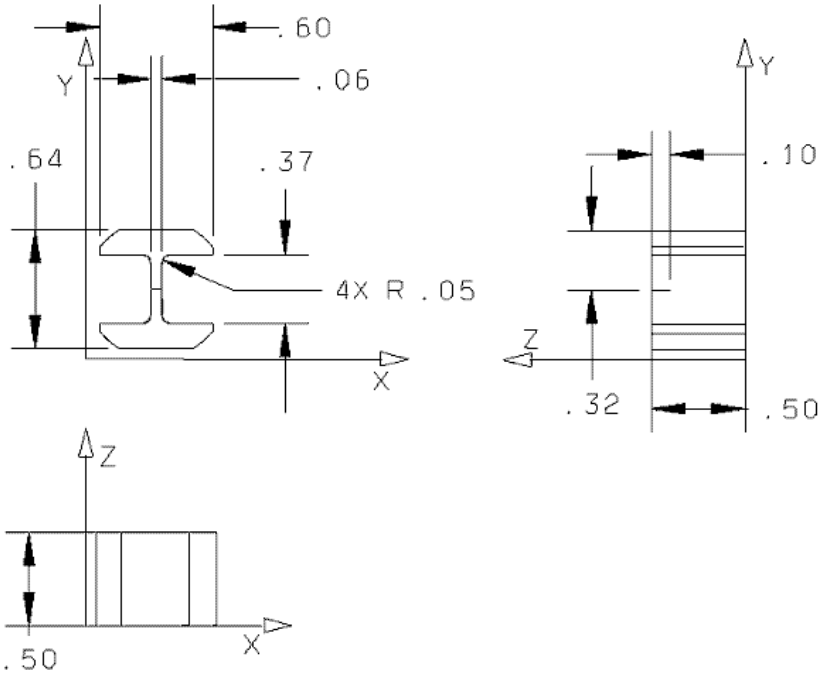

Figure A.1
Three-View Drawing of Specimen (in Inches) (Center Web t = 1.524mm)

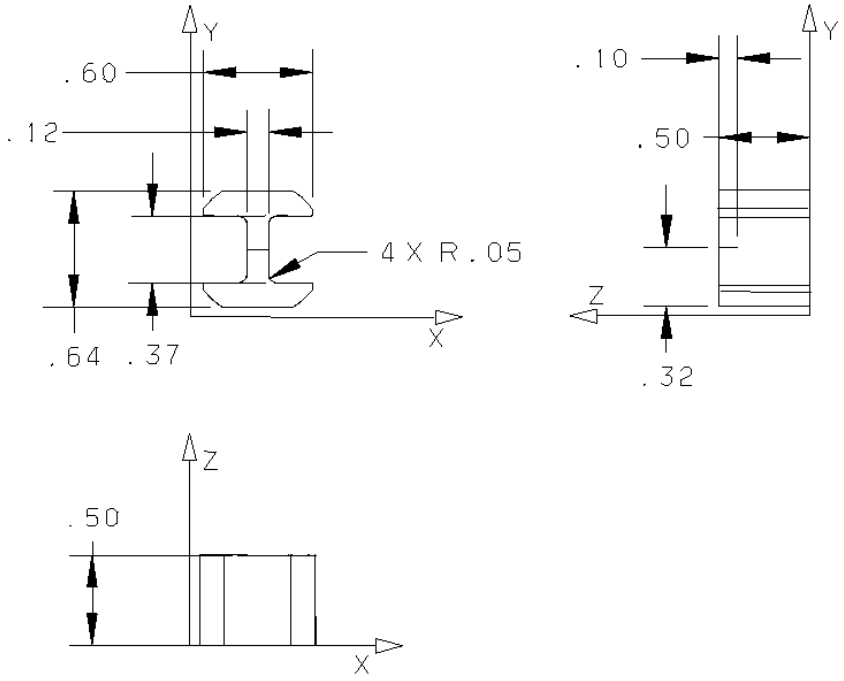

Figure A.2
Three-View Drawing of Specimen (in Inches) (Center Web t = 3.048 mm)

APPENDIX A

SPECIMEN DRAWINGS

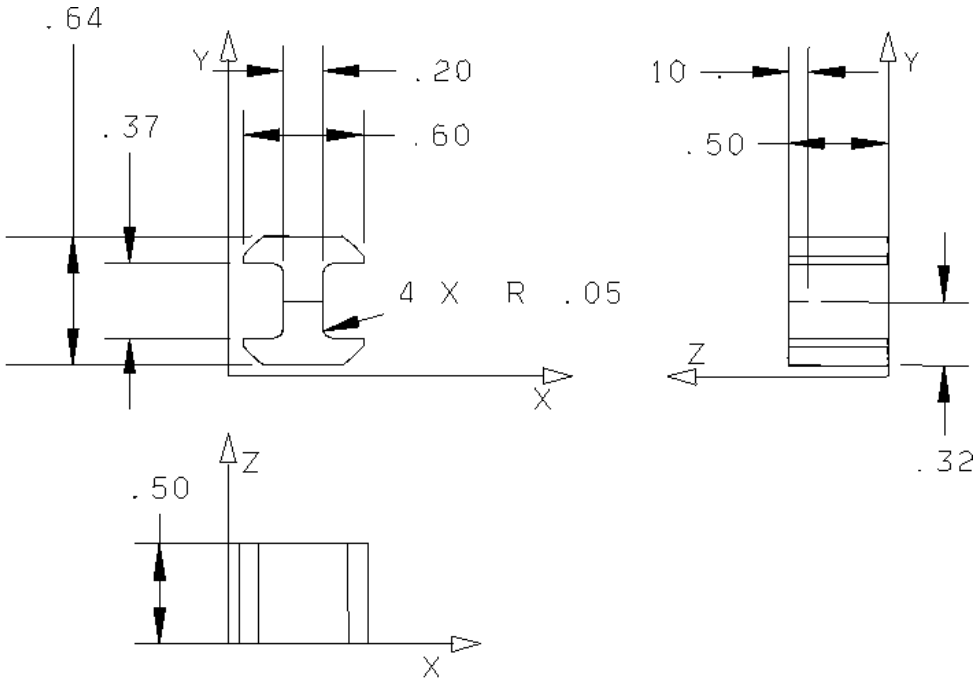

Figure A.3
Three-View Drawing of Specimen (in Inches) (Center Web t = 5.04mm)

APPENDIX B

MATERIAL PROPERTIES

Table B.1
Monotonic Material Properties[27]

Cyclic Strength Coefficient	K'	695	MPa
True Fracture Strength	s_f'	989	MPa
True Fracture Ductility	e_f'	6.812	
Cyclic Strain Hardening Exponent	n'	0.094	
Elastic Strain-Life Slope	b	-0.14	
Plastic Strain Life Slope	c	-1.198	

Table B.2
Cyclic Material Properties[7]

Young's Modulus	E	71	MPa
Yield Strength	s_y	435	MPa
Ultimate Strength	s_u	505	MPa
Endurance Limit	S_e	150	MPa
Fracture Toughness	K_c	18 - 32	MPa
Strength Coefficient	K	633	MPa
Strain Hardening Exponent	n	0.055	
Poisson Ratio	ν	0.33	

APPENDIX B

MATERIAL PROPERTIES

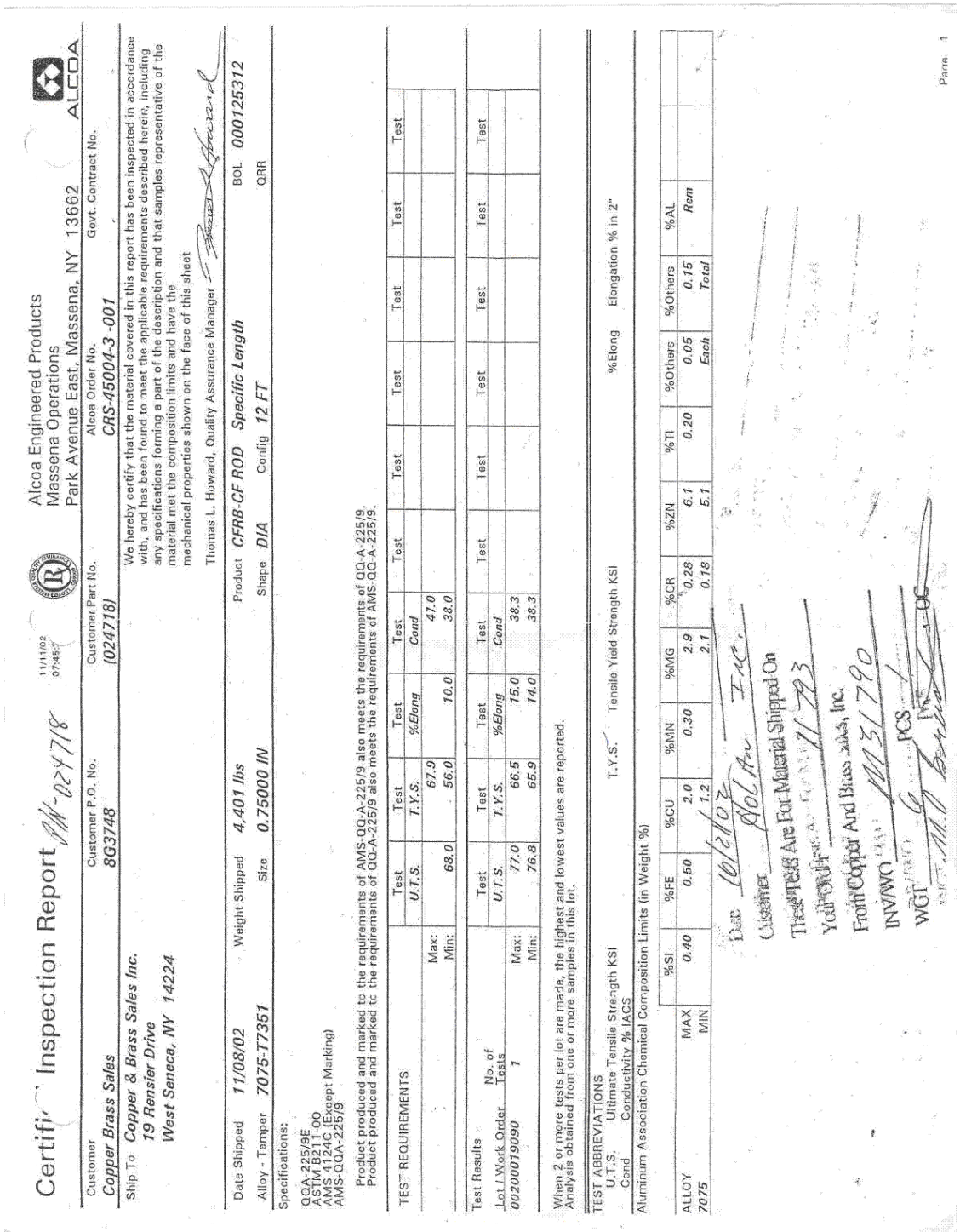

Certifi Inspection Report MM-02-7718

11/11/02
07:45

Alcoa Engineered Products
Massena Operations
Park Avenue East, Massena, NY 13662

ALCOA

Customer	Customer P.O. No.	Customer Part No.	Alcoa Order No.	Govt. Contract No.
Copper Brass Sales	8G3748	(024718)	CRS-45004-3 -001	

Ship To Copper & Brass Sales Inc.
19 Rensier Drive
West Seneca, NY 14224

We hereby certify that the material covered in this report has been inspected in accordance with, and has been found to meet the applicable requirements described herein, including any specifications forming a part of the description and that samples representative of the material met the composition limits and have the mechanical properties shown on the face of this sheet

Thomas L. Howard, Quality Assurance Manager

Date Shipped	11/08/02	Weight Shipped	4,401 lbs	Product	CFRB-CF ROD	Specific Length	BOL	000125312
Alloy - Temper	7075-T7351	Size	0.75000 IN	Shape	DIA	Config 12 FT	QRR	

Specifications:

QQA-225/9E
ASTM B211-00
AMS 4124C (Except Marking)
AMS-QQA-225/9

Product produced and marked to the requirements of AMS-QQ-A-225/9 also meets the requirements of QQ-A-225/9.
Product produced and marked to the requirements of QQ-A-225/9 also meets the requirements of AMS-QQ-A-225/9.

TEST REQUIREMENTS		Test U.T.S.	Test T.Y.S.	Test %Elong	Test Cond	Test	Test	Test	Test	Test	Test	Test
	Max:		67.9		41.0							
	Min:	68.0	56.0	10.0	38.0							

Test Results	No. of	Test	Test	Test	Test	Test	Test	Test	Test	Test	Test	Test
Lot / Work Order	Tests	U.T.S.	T.Y.S.	%Elong	Cond							
00200019090	1 Max:	77.0	66.5	15.0	38.3							
	Min:	76.8	65.9	14.0	38.3							

When 2 or more tests per lot are made, the highest and lowest values are reported.
Analysis obtained from one or more samples in this lot.

TEST ABBREVIATIONS
U.T.S. Ultimate Tensile Strength KSI T.Y.S. Tensile Yield Strength KSI %Elong Elongation % in 2"
Cond Conductivity % IACS

Aluminum Association Chemical Composition Limits (in Weight %)

		%SI	%FE	%CU	%MN	%MG	%CR	%ZN	%TI	%Others	%Others	%AL		
ALLOY	MAX	0.40	0.50	2.0	0.30	2.9	0.28	6.1	0.20	0.05	0.15	Rem		
7075	MIN			1.2		2.1	0.18	5.1		Each	Total			

Date 10/28/02 Per Mel Fac
Customer
These Tests Are For Material Shipped On
Your Order # 11283
From Copper And Brass Sales, Inc.
INV/WO 1131790
WGT PCS
PS

Page 1

Figure B.1
Material Inspection Sheet

APPENDIX C

EQUIPMENT LIST

Table C.1
Experimental Equipment

Equipment	Manufacturer	Model	Serial Number
Servo-Hydraulic Test Stand	MTS	Load Unit 318.25 Actuator 318.25	Load Unit 1043559 Actuator 1018649
Hydraulic Power Unit	MTS	505.11	1046944
Controller	MTS	493.01	1021899
Force Transducer	MTS	661.22c-01	1042541
Personal Computer	Compaq	Desk Pro P400/6.4/64/NTC US	6930BW431149
Microscope	Nikon	--	124165/110891
Ultrasonic Cleaner	Cole Palmer	18895-16	RTF110393167
Fiber Optic Light	Dolan-Jenner Industries	Fiber-Lite 3100	--
Strain Gage Soldering Unit	Vishay	Mark VIII	--
Switch & Balance Unit	Measurements Group	SB-10	GT-003782
Strain Indicator Unit	Measurements Group	P3500	GT-0080286
Digital Voltmeter	Sperry	DM-350A	--
Strain Gages	M&M Measurements Group	CEA-05-062UW-350	--
Microscope	National	DC3-4207	--
Personal Computer	Gateway	838GM	XAB5A I10 07176
Digital Camera	Olympus	Stylus 400	--

APPENDIX D

SPECIMEN PREPARATION PROCEDURE

Introduction

This procedure reviews the process of polishing, cleaning, and instrumentation welding of aluminum "I-beam" test specimen for FAA-sponsored Small Crack Research.

Specimen - Description

The specimens are manufactured by Holan, Inc. The specimens have an "I-beam" cross-section and a notch in the center of one side of the cross-section. The specimens are machined aluminum and steel. Examples of test specimen are shown in Figure 1. The specimens are polished and cleaned prior to the attachment of the instrumentation wires.

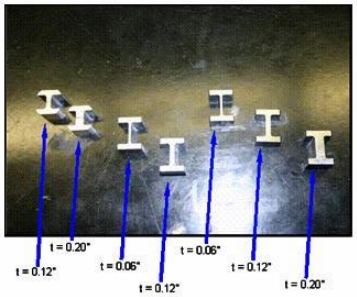

Figure 1.
I-beam Specimen

Specimen - Product Support

Product and procedure support is available through the specimen manufacturer. The contact information is as follows:

Attn: John Holba
Holan, Inc.
724-774-1660
724-744-1444 (Fax)
1048 Sandy Hill Road, Irwin, PA 15642

Georgia Institute of Technology
Daniel Guggenheim School of Aerospace Engineering
Materials & Advanced Structural Testing Lab

FAA-P-05C | SPECIMEN PREPARATION PROCEDURE | 01-13-06

Specimen – Preparation Procedure

1. Polish specimen webs. Polishing supplies are shown in Figure 2.
   a. Cut eight half-inch by one-and-a-half-inch rectangles of Mager paper.
   b. Attach a piece of Mager paper around one edge of metal plate.
   c. Apply a dab of olive oil to Mager paper. (Figure 3)
   d. Apply a dab of 14 micron diamond paste to Mager paper. Apply the smallest amount possible. (Figure 3)
   e. Polish web of specimen in direction perpendicular to notch direction for 30 seconds. (Figure 4)
   f. Repeat steps 1-b through 1-e seven more times. Overall, polish both webs of specimen with 14 micron twice and then 1 micron twice. The finished specimen can be seen in Figure 5)

Figure 2.
Polishing Materials

APPENDIX D

SPECIMEN PREPARATION PROCEDURE

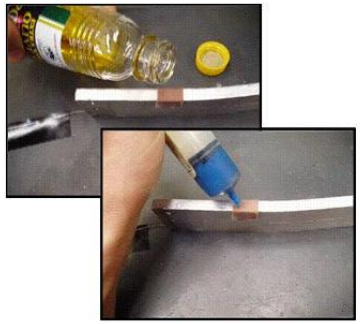

Figure 3.
Applying Oil and Diamond Paste to Mager Paper

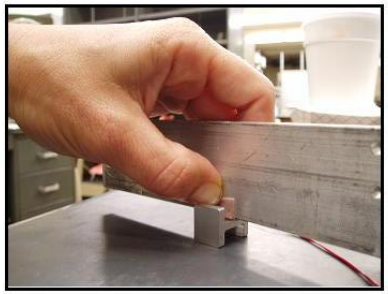

Figure 4.
Polishing Specimen

Georgia Institute of Technology
Daniel Guggenheim School of Aerospace Engineering
Materials & Advanced Structural Testing Lab

FAA-P-05C | SPECIMEN PREPARATION PROCEDURE | 01-13-06

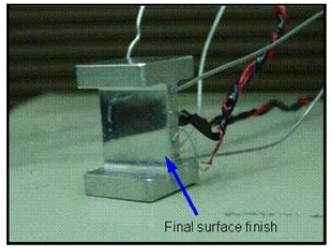

Figure 5.
Polished Specimen

2. Clean specimen with ultrasonic cleaner (Cole Parmer Pat No. CPN-214-153). The Ultrasonic Cleaner is shown in Figure 6.
a. Power on cleaner.
b. Add cleaning solution and enough water to within an inch of the top of the tank. Put beaker in tank. (Figure 7)
c. Set degas for 5 to 10 minutes and start. (Figure 8)
d. When complete, set cleaning time 30 minutes, set tank temperature no higher than 80 degrees. (Figure 8)
e. Turn sonics on to clean specimen. (Figure 8)
f. Take specimen out when complete and dry on a towel.
g. Power off, unplug, empty, and let ultrasonic cleaner dry.

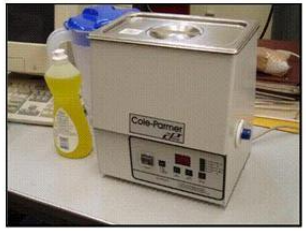

Figure 6.
Cole Parmer Ultrasonic Cleaner Model DTH

Figure 7.
Ultrasonic Cleaner Ready to Power On

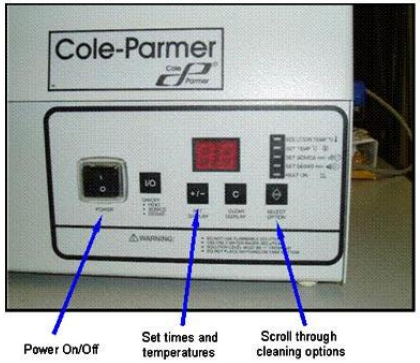

Figure 8.
Ultrasonic Cleaner Control Panel Steps

Georgia Institute of Technology
Daniel Guggenheim School of Aerospace Engineering
Materials & Advanced Structural Testing Lab

FAA-P-05C | SPECIMEN PREPARATION PROCEDURE | 01-13-06

Welder – Background

Ultrasonic welding uses a combination of static forces (pressure) and oscillating shear forces (horizontal vibrations) to bond two metallic pieces together. Ultrasonic welding is used on aluminum specimen to avoid material properties changes due to local specimen heating, a negative effect of other attachment methods, such as spot welding or soldering. A slight temperature increase occurs at the weld location, but it does not affect the material properties. Further information on ultrasonic welding can be found on-line through the vendor listed under the "Welder – Product Support" of this document.

Welder - Description

The ultrasonic welder is a STAPLA model D-6092 Keisterbach Albatross, manufactured in West Germany. The welder assembly consists of several pieces including the power converter, generator unit, foot pedal, and contact horn, as seen in Figure 9. Although contact horns with varying geometry are available through the vendor, this procedure will review and demonstrate the operation of the single prong horn used in GT-FAA Small Crack Research.

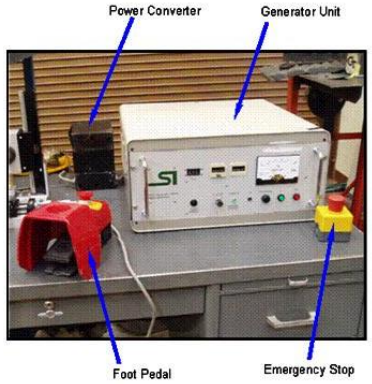

Figure 9.
Stapla Ultrasonic Welder Model D-6092 Keisterbach Albatross & Specimen Weld Fixture

Welder - Product Support

Product and procedure support is available through the vendor. The contact information is as follows:

Attn: Kevin Gordon
Stapla Ultrasonics
http://www.staplaultrasonics.com/
(978) 658-9400
(978) 658-6550 (Fax)
375 Ballardvale Street, Wilmington, MA 01887

Fixture - Hardware

The location and weld quality of the instrumentation wire attachment points need to be accurate and consistent for each specimen tested. A fixture was manufactured and assembled to allow for this requirement. The fixture grips the horn/booster assembly, as well as the specimen, while the weight of the fixture and booster act as the static mechanical load during the welding. The assembled fixture consists of a base plate, two displaceable platforms, two L-shaped grips, two upright tracks, and a machined block containing a weld horn/booster cut-out and a ball-bearing path on either side. The assembly is secured together with fasteners. The assembly is shown in Figure 10. Set-up of the fixture assembly will be explained in further detail under the "Weld - Procedure" section of this document.

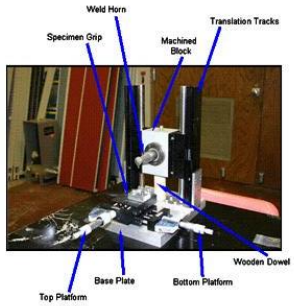

Figure 10.
Specimen Fixture for Welding

Georgia Institute of Technology
Daniel Guggenheim School of Aerospace Engineering
Materials & Advanced Structural Testing Lab

FAA-P-05C | SPECIMEN PREPARATION PROCEDURE | 01-13-06

Wire – Description

The wire welded to the specimen in this procedure is made of aluminum 1100 alloy. Aluminum alloy wire is used to avoid additional resistance in the instrumentation readings due to bonding of dissimilar metals. The current supply wires have a diameter of 0.0250" = 0.650 mm. The voltage probe wires have a diameter of 0.0125" (0.316 mm) and should not exceed 0.350 mm. The wires need to be prepared prior to welding.

Wire – Preparation Procedure

Current Supply Wire

1. For a single-sided specimen, cut two pieces of 0.0250" aluminum wire. One length should be 5.4" long and the other should be 5.1" long. Thread both wires through one of the two alumina tubes (3.90" in length) available. For a double-sided specimen, cut two more wires, 6.1" long and 6.4" long.
2. Be sure alumina tubes are clean and dry. Water or oil can vary the instrumentation reading. If necessary, clean the alumina tube in the ultrasonic welder, and dry THOROUGHLY prior to this step. Step 3 in the "Specimen – Preparation Procedure" can be used, with a (decreased) 15 minute cleaning cycle.

Voltage Probe Wire

1. Cut two pieces of 0.0125" aluminum wire. The length of both should be 5.6". For a double-sided specimen, cut two more wires, 6.6" long.
2. Tape off 0.2" of either end of one wire with masking tape.
3. Stir the Plasti-Dip material thoroughly with a wooden skewer.
4. Holding both taped-ends together dip the wire into the Plasti-Dip and slowly remove it from the container. Hang the wire by one end with one of the plastic clothes pins available. Let dry as instructed on the Plasti-Dip container. (Figure 11)
5. Cut a length of electrical tape 5.2". Wrap along length of second wire, leaving 0.2" un-taped at either end. Cut away any excess tape along the length of the wire.
6. When both wires are covered and dry, tightly twist then around each other, leaving as little wire untwisted as possible.

APPENDIX D

SPECIMEN PREPARATION PROCEDURE

Figure 11.
Wire Preparation Materials

Weld - Procedure

1. Assemble Specimen Fixture. (View of Platform set-up in Figures 12 and 13.)
a. Install first displacement platform onto base plate in horizontal direction with two fasteners within platform. Use the displacement platform with the non-reading digital measurement screen.
b. Install the second displacement platform on top of and perpendicular to the first in the same manner.
c. Lift machined block and slip wooden dowel underneath to hold block up.
d. Install weld horn through machined block and tighten screw on top to secure booster.
2. Install Specimen by into grips, also shown in Figure 14. Use the elongated fastener holes in the grips to securely hold the specimen. Fit the grip to the specimen snugly.
3. Position overhead magnifying glass above welder and switch on light.
4. Plug welder assembly in to power source and turn on by pressing "on" green button located in the lower RH corner on the front of the generator unit.
5. Verify weld settings for aluminum: (View of control panel seen in Figure 15.)
a. Time = 20
b. Amplitude knob set at 3rd notch above "-" sign.
6. Move platforms to offset specimen from the weld head for weld. Weld the instrumentation wires in the following locations:
a. Voltage (inner) wires installed 2mm from either side of notch. Red-coated wires attaches above crack.
b. Current (outer) wires installed 5mm from either side of notch. Longer current wire attaches above crack.
7. Lower Weld head assembly to specimen. (View of assembly seen in Figure 16.)
8. Attach wires at predetermined locations shown in Figure 14, using foot pedal to apply weld.

9. Lift weld head and support with wooden dowel.
10. Cover leads in super glue to protect wires and weld surfaces on specimen. Be sure not to let glue run onto webs of specimen. (Figure 17)
11. Remove specimen.
12. If flaws exist on both sides of specimen, turn over to opposite face.
13. Reinstall specimen, placing washers between platform and specimen, to hold specimen off platform surface. This will keep the existing wires already welded to the lower side are not damaged.
14. Attach reference wires as in step 6.
15. Cover leads with glue as in step 10.
16. Remove specimen.
17. Turn off welder by pressing red "-" off" button located in the lower RH corner on the front of the generator unit and disconnect power converter from power source.
18. Disassemble weld fixture and return everything to its original location.
19. Cover both ends of specimen with scotch tape. Cut off excess tape. (Figure 18)
20. Specimen can be installed into loading fixture for testing. (Figure 19)

Figure 12
Plan View of Base Plate Assembly

Figure 13
Plan View of Base Plate Assembly

APPENDIX D

SPECIMEN PREPARATION PROCEDURE

Figure 14.
Plan View of Platform Configuration

Figure 15.
Ultrasonic Welder Control Panel

Figure 16.
Weld Application on I-Beam Specimen

Figure 17.
Coating Weld Location

APPENDIX D

SPECIMEN PREPARATION PROCEDURE

Figure 18.
Insulation Specimen

Figure 19.
Final Specimen Assembly

APPENDIX E

MTS OPERATING PROCEDURE

FAA-P-06B	MTS 810 EMERGENCY STARTUP	01-13-06

1.Located the grey electric switchbox on the wall above the pump. Reset the switchbox by cycling the handle, down and then back up again.
2.Hit the rest button on the pump to turn off all the error lights. If your standing at the MTS machine and facing the pump, the rest button and status lights are located on the adjacent left-side of the pump.
3.Turn the black MTS Teststar IIs controller box off, wait 10 seconds, and turn it back on.
4. Within a few minutes, the orange "Service" light on the front of the controller should turn off. (The green light should stay on.)
5.Turn the MTS PC power button off and then on. Let it boot up and log I with the following user id and password:
User id: Administrator
Password: admin
On the MTS PC, click on
"Start > Programs > MTS Teststar > System Loader"
(At this point a program will initialize, but a temporary screen will appear and then disappear.)
6. On the MTS PC, click on
"Start > Programs > MTS Teststar > Station Manager"
7. When the program starts, Open the file named "liuliu.cfg" and choose parameter "liuliu" to restart machine.
8. On the Control panel, located to the left of the load fixture, clear the interlock, if necessary.
9. On the Control panel, located to the left of the load fixture, start the pump: (also described in the MTS 810 start up procedure)
10. Click on "HPS1 Low" and wait for green indicator to stop blinking
11. Click on "HMS1 Low" and wait for green indicator to stop blinking
12. Click on "HPS1 High" and wait for green indicator to stop blinking
13. Click on "HMS1 High" and wait for green indicator to stop blinking
14. Remove load on specimen with displacement control until Control Panel display reads zero load on specimen.
15. On the MTS PC, click on
"Start > Programs > MTS Teststar > Multi-Purpose Testware"
16. Open file "C:\\faa/faa-cycle-1" and choose specimen ID from list in active window. At this point, you will be ready to modify the procedure or click on "Reset" and "Run" to cycle.

FAA-P-01C	MTS 810 OPERATIONS MANUAL	01-13-06

Be sure the load on the fixture does not exceed ±10 LB. CAUTION: Do not rotate the specimen out of the lower grip.
12. For I-beam specimen:
a. Install the I-beam grips into the test fixture assembly, if they are not already in place.
b. Using the control dial, raise the lower grip to within an inch of the upper grip. Continue to raise the lower grip VERY SLOWLY until the I-beam specimen can be installed into the grips. (Figure 3) WARNING: At NO point should the MTS machine see more than 10 LB. of compression load. This could cause the grips to buckle and damage them.
c. Disable manual control on test fixture control panel.
d. Press F4 on the control panel until "Load" appears on the control panel screen in the center box. The MTS machine will maintain (approximately) zero load on the specimen now. CAUTION: Manual control must be disabled to start test.
13.Connects specimen wires to ACPD machine using wire attach platform. Verify wires are attached securely below tightened screws and not along side them for best signal. (Final setup shown in Figure 5.)
14. Upper white current wire attaches to red/blue coaxial cable wires on wire attach platform.
15. Lower white current wire (in alumina tube) attaches to white wire in coaxial cable on wire attach platform.
16. Upper voltage (red) wire attaches to red wire on wire attach platform.
17. Lower voltage (black) wire attaches to black wire on wire attach platform.
18. Input test loading parameters into the "Procedure" window on the MTS PC. For the I-beam specimen, a generic procedure, C:\faa\test bar.000" is available. (Windows shown in Figure 3.)
19. Input ACPD instrumentation parameters into the "Setup" window on the ACPD PC. (Windows shown in Figure 4.)
20. Start test by clicking on the green "Run" button in the "MPT Control Panel" window on the MTS PC.
21. To rerun after procedure is complete, click on the "reset" button and then "Run" button in the "MPT Control Panel" window in the MTS PC.
22. Save loads and instrumentation data files to new name prior to beginning another test. 23. Log file is located under the filename, C:\tsiis\config\liuliu and C:\tsiis\mpt\Specimens\spec01\specimen. The load file is located under the filename C:\ tsiis\mpt\Specimens/spec01. The location/title of this file is prescribed in the "Destination" section of the "Timed Acquisition Parameter" window within the "Procedure" window on the MTS PC. MTS support documentation can be found in multiple .pdf files on the MTS PC in the directory: C:\TEMP\mts

APPENDIX E

MTS OPERATING PROCEDURE

End – Procedure

1. To remove specimen from fixture, first disconnect wires from ACPD.
2. For bar specimen:
   a. Keeping the fixture in load control and manually disabled, rotate the lower grip clockwise until the specimen threads are removed from upper grip.
   b. Enable manual control and apply a slight tension load to fixture to move specimen away from upper grip.
   c. Disable manual control, change to "Displacement" control, and re-enable manual control to move specimen away from upper grip until lower grip bottoms out. When lower grip at bottom, remove specimen from lower grip.
3. For bar specimen:
   a. Put fixture into displacement control and manually enabled.
   b. Put specimen out of grips.
   c. Lower bottom grip away form top grip.
4. To turn off pump, (in the "Control Panel" window on the MTS PC or on test fixture remote control panel):
   5. Click on "HMS1 Low" and wait for green indicator to stop blinking
   6. Click on "HPS1 Low" and wait for green indicator to stop blinking
   7. Click on "HMS1 Off" and wait for green indicator to stop blinking
   8. Click on "HPS1 Off" and wait for green indicator to stop blinking
9. Turn off monitor but leave MTS PC on. WARNING: Do not ever turn off or reboot MTS PC. Establishing communications between the load fixture and the PC is extremely difficult.

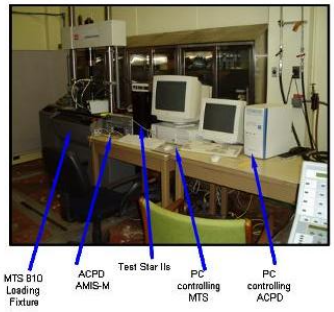

Figure 1.
MTS 810 Loading Fixture, located M-K Building Room 108

Georgia Institute of Technology
Daniel Guggenheim School of Aerospace Engineering
Materials & Advanced Structural Testing Lab

FAA-P-01C | MTS 810 OPERATIONS MANUAL | 01-13-06

Figure 2.
MTS 810 Control Panel

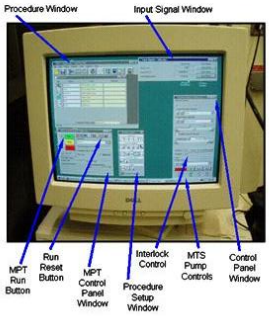

Figure 3.
MTS MPT Setup Windows

APPENDIX E

MTS OPERATING PROCEDURE

APPENDIX F

MTS EMERGENCY REBOOT PROCEDURE

FAA-P-06A	MTS 810 EMERGENCY STARTUP	01-13-06

Introduction

This procedure reviews the process of running constant amplitude fatigue cycling on an "I-beam" specimen for the MTS 810 Load Fixture located in Montgomery-Knight Building, Room 108. This procedure supports FAA-sponsored Small Crack Growth Research.

Start Up – Procedure

1. Start up or confirm PC and MTS MPT software is on. (PC shown in Figure 1.)
2. Disable manual control on test fixture control panel. (Figure 2.)
3. To turn on pump, (in the "Control Panel" window in the MTS PC or on test fixture remote control panel):
4. Click on "HPS1 Low" and wait for green indicator to stop blinking
5. Click on "HMS1 Low" and wait for green indicator to stop blinking
6. Click on "HPS1 High" and wait for green indicator to stop blinking
7. Click on "HMS1 High" and wait for green indicator to stop blinking
8. Verify on the remote control panel that the test fixture is in "Displacement" control. If it is not, use F4 to change to "Displacement" control.
9. Enable manual control on test fixture control panel.
10. Verify on PC monitor that the load hovers around zero. If not, reset it with "Auto Offset" button in the "Input Signal" window in the MTS PC. (Window shown in Figure 3.) Keep in mind the system only allows a 5 inch displacement from where ever the bottom grip was last zeroed, so an interlock (system lock out) will occur if you raise or lower the bottom grip more than 5 inches. If this occurs anytime during use, reset the displacement in the "Input Signal" window with the "Auto Offset" button and then reset the "Interlock 1" in the "Control Panel" window on the MTS PC.
11. For bar specimen:
    a. Install specimen into lower test fixture/grips until bottomed out on lowest threads.
    b. Manually turn control dial to move specimen up until the top of specimen is ½" from top grip. The control dial turns counter-clockwise to move the lower grip up (compression load), and clockwise to move the lower grip down (tension load).
    c. Disable manual control.
    d. Change to "Load" control on test fixture control panel.
    e. Enable manual control.
    f. Specimen should slowly rise toward the top grip. If it does not, barely turn the control dial until it begins to creep toward the upper grip. WARNING: At NO point should the MTS machine see more than 10 LB. of compression load. This could cause the grips to buckle and damage them.
g. When the specimen just barely touches the top grip, begin to rotate by hand the LOWER grip counter-clockwise to thread the specimen into the upper grip. Continue until the specimen threads bottom out in the upper grip.

Georgia Institute of Technology
Daniel Guggenheim School of Aerospace Engineering
Materials & Advanced Structural Testing Lab

FAA-P-06B	MTS 810 EMERGENCY STARTUP	01-13-06

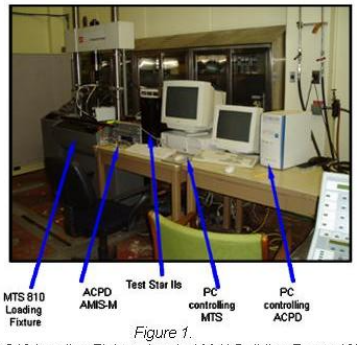

Figure 1.
MTS 810 Loading Fixture, located M-K Building Room 108

Figure 2.
MTS 810 Control Panel

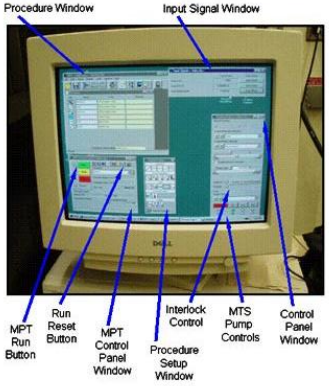

Figure 3.
MTS MPT Setup Windows

APPENDIX G

FRACTURE SURFACES

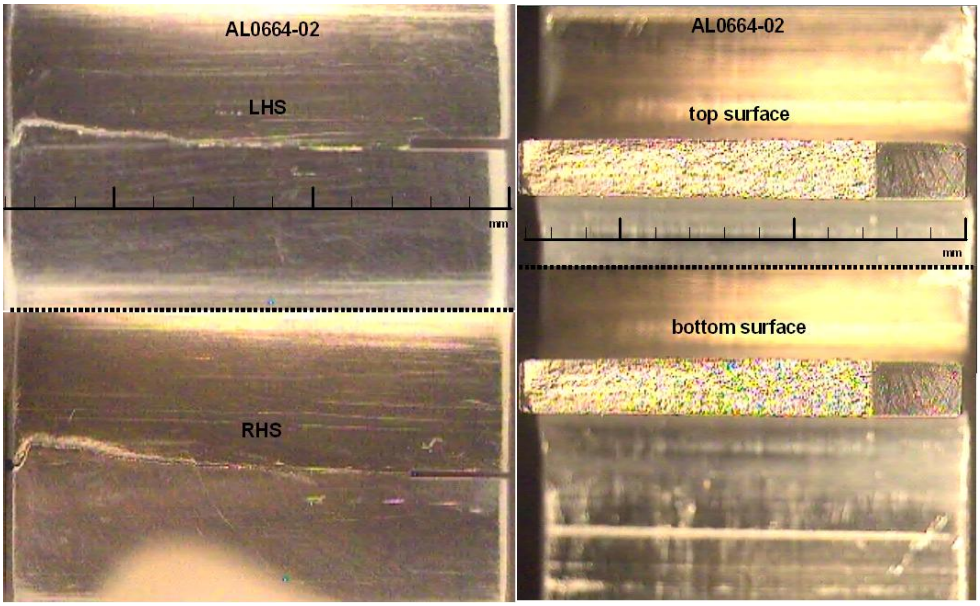

Figure G.1
AL0664-02 Crack Surfaces

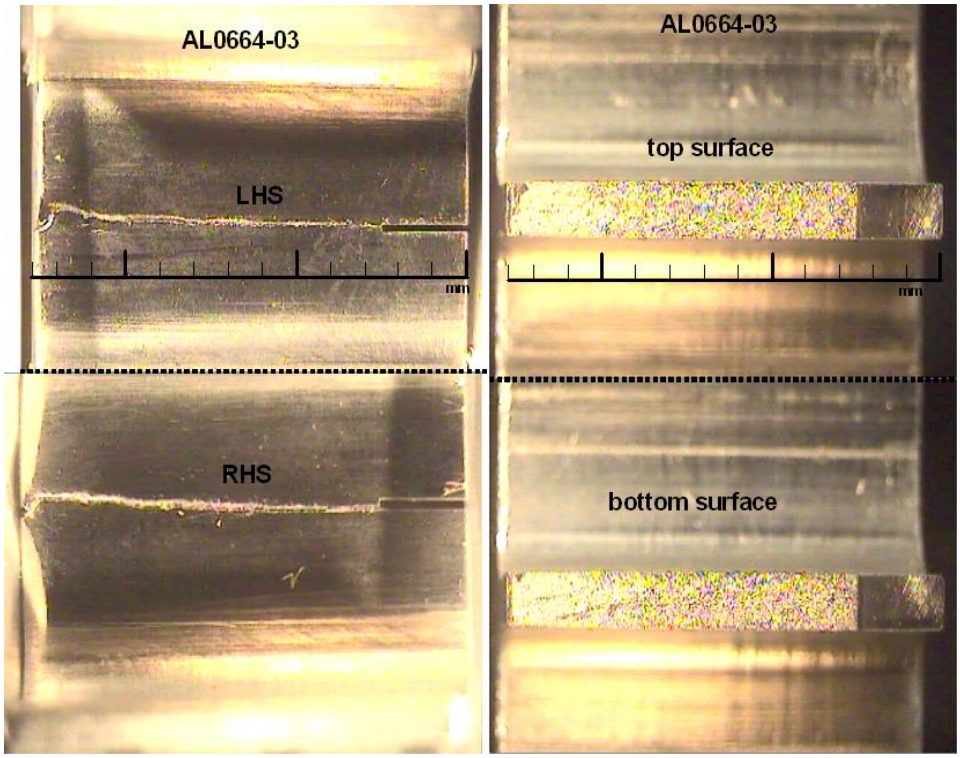

Figure G.2
AL0664-03 Crack Surfaces

APPENDIX G

FRACTURE SURFACES

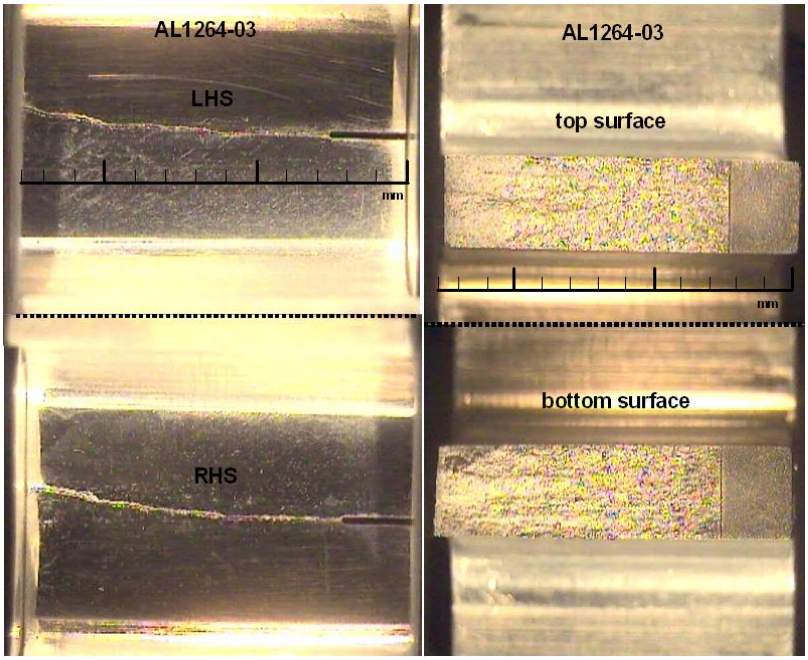

Figure G.3
AL1264-03 Fracture Surfaces

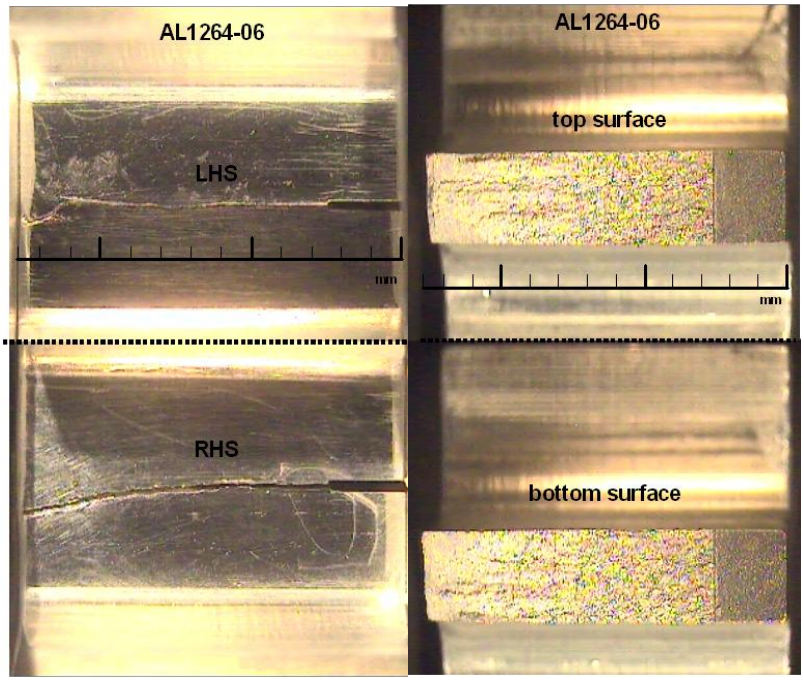

Figure G.4

AL1264-06 Fracture Surfaces

APPENDIX G

FRACTURE SURFACES

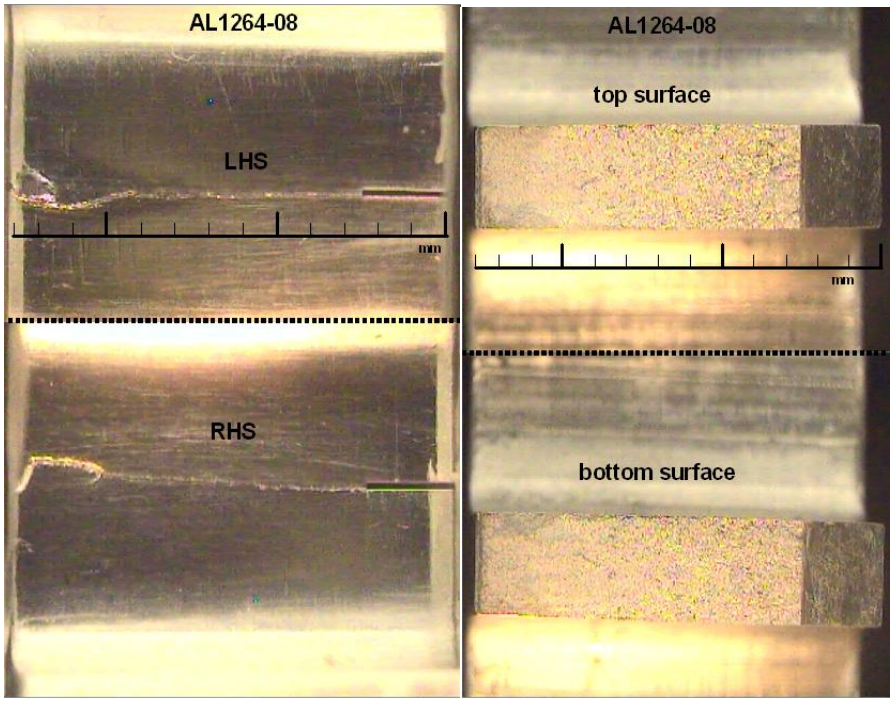

Figure G.5
AL1264-08 Fracture Surfaces

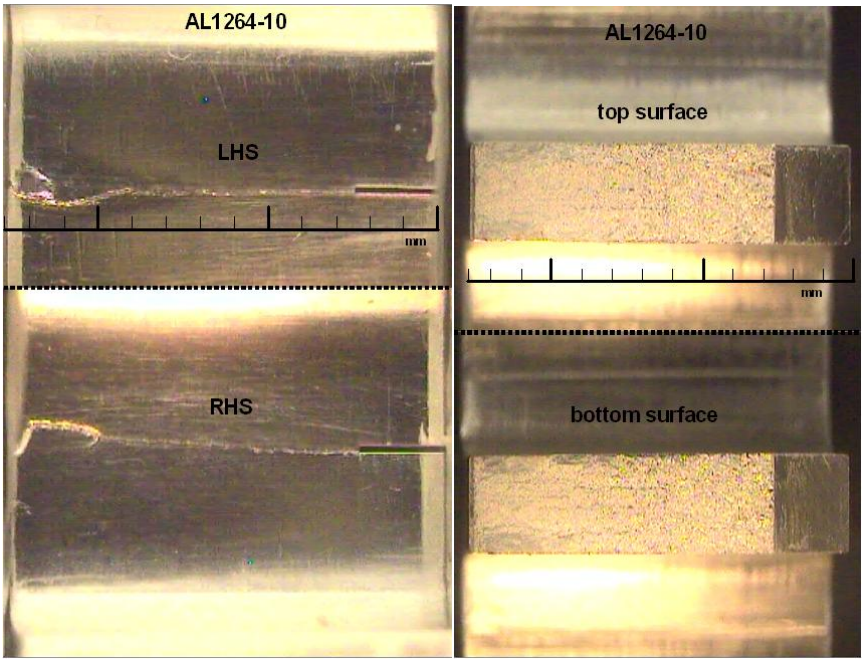

Figure G.6
AL1264-10 Fracture Surfaces

APPENDIX G

FRACTURE SURFACES

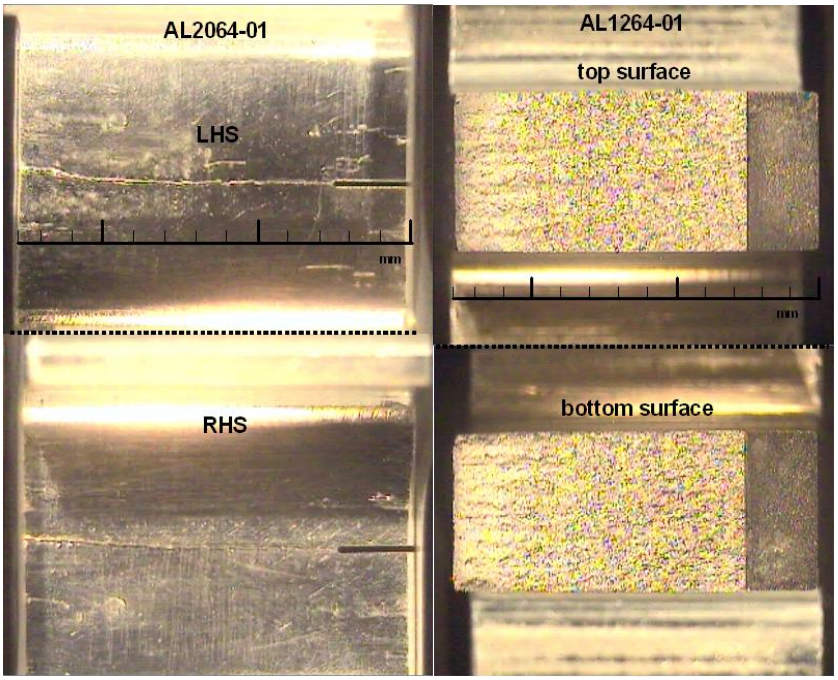

Figure G.7
AL2064-01 Fracture Surfaces

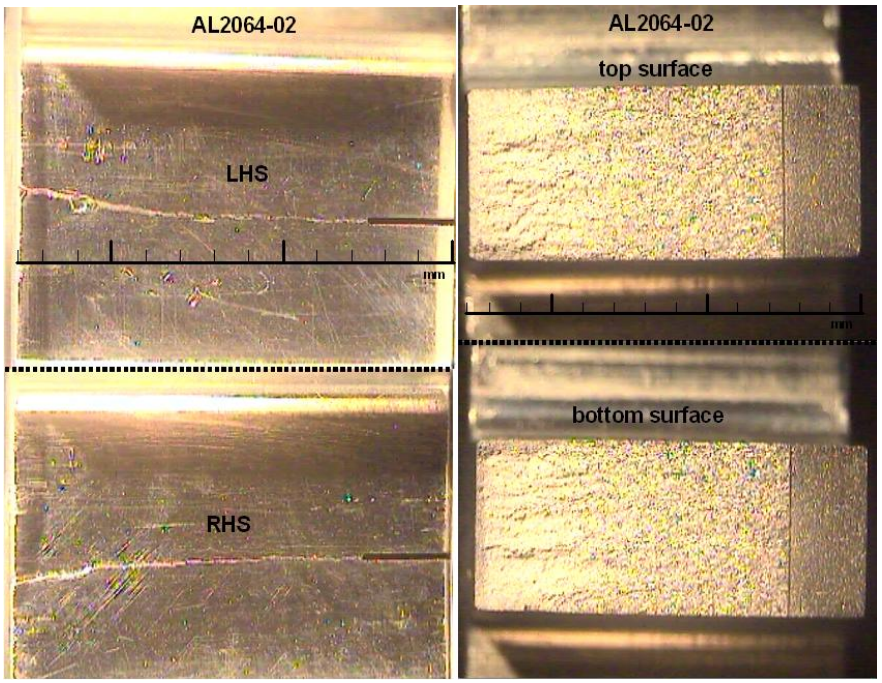

Figure G.8
AL2064-02 Fracture Surfaces

APPENDIX G

FRACTURE SURFACES

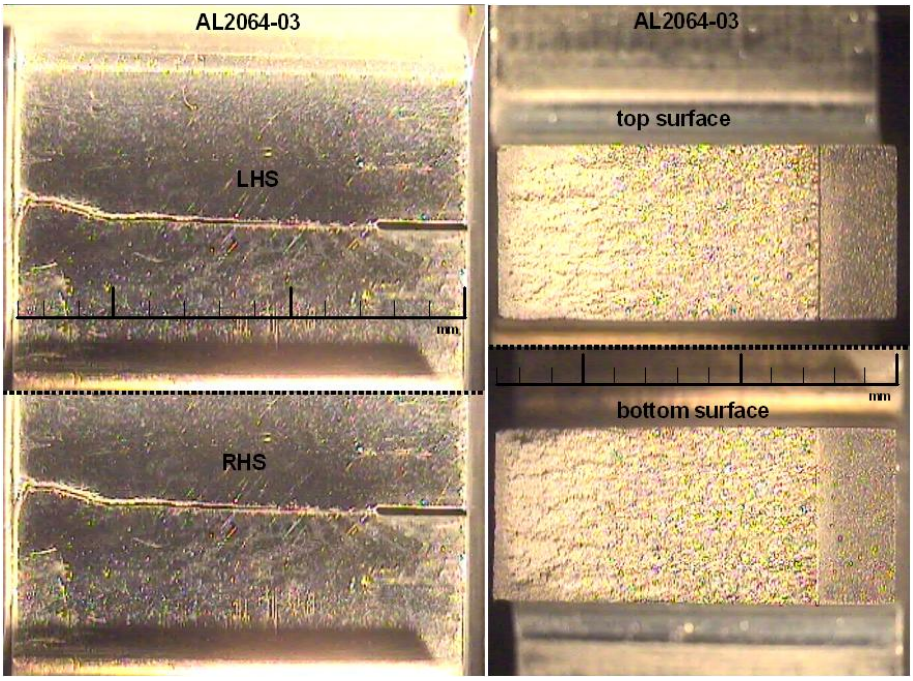

Figure G.9
AL2064-03 Fracture Surfaces

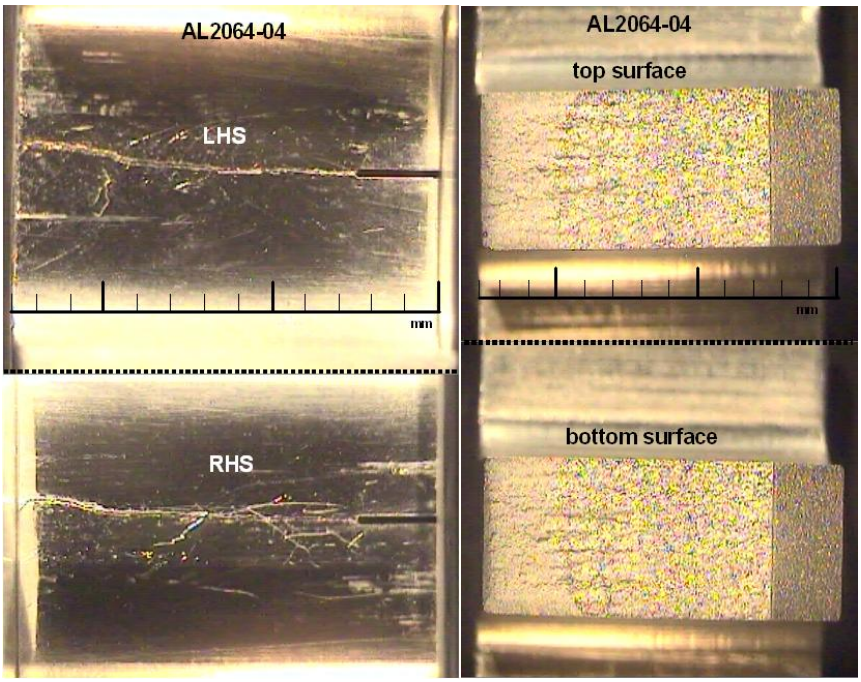

Figure G.10
AL2064-04 Fracture Surfaces

APPENDIX G

FRACTURE SURFACES

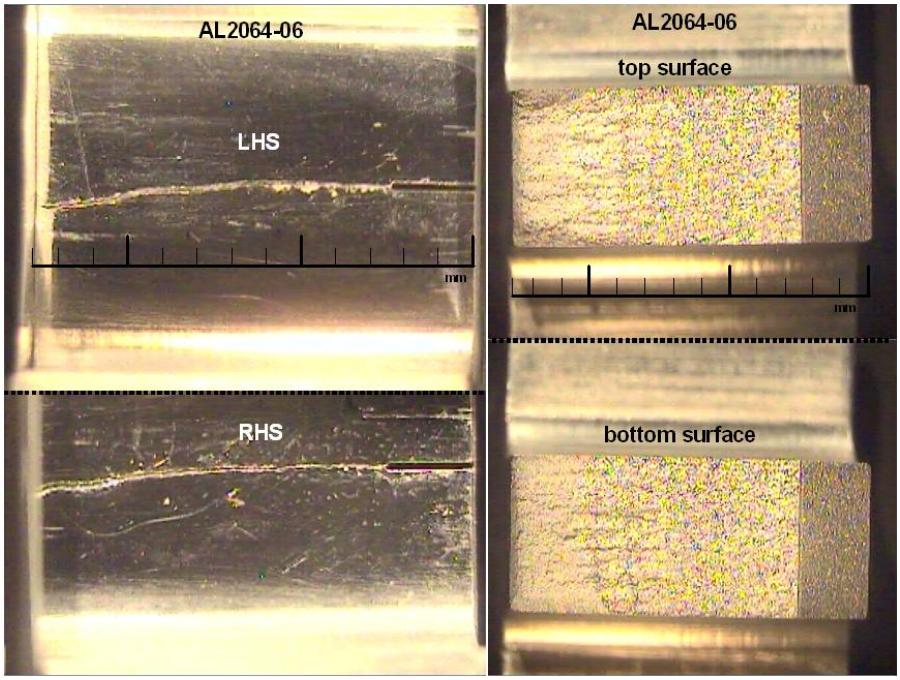

Figure G.11
AL2064-06 Fracture Surfaces

APPENDIX H

COMPARISON PLOTS

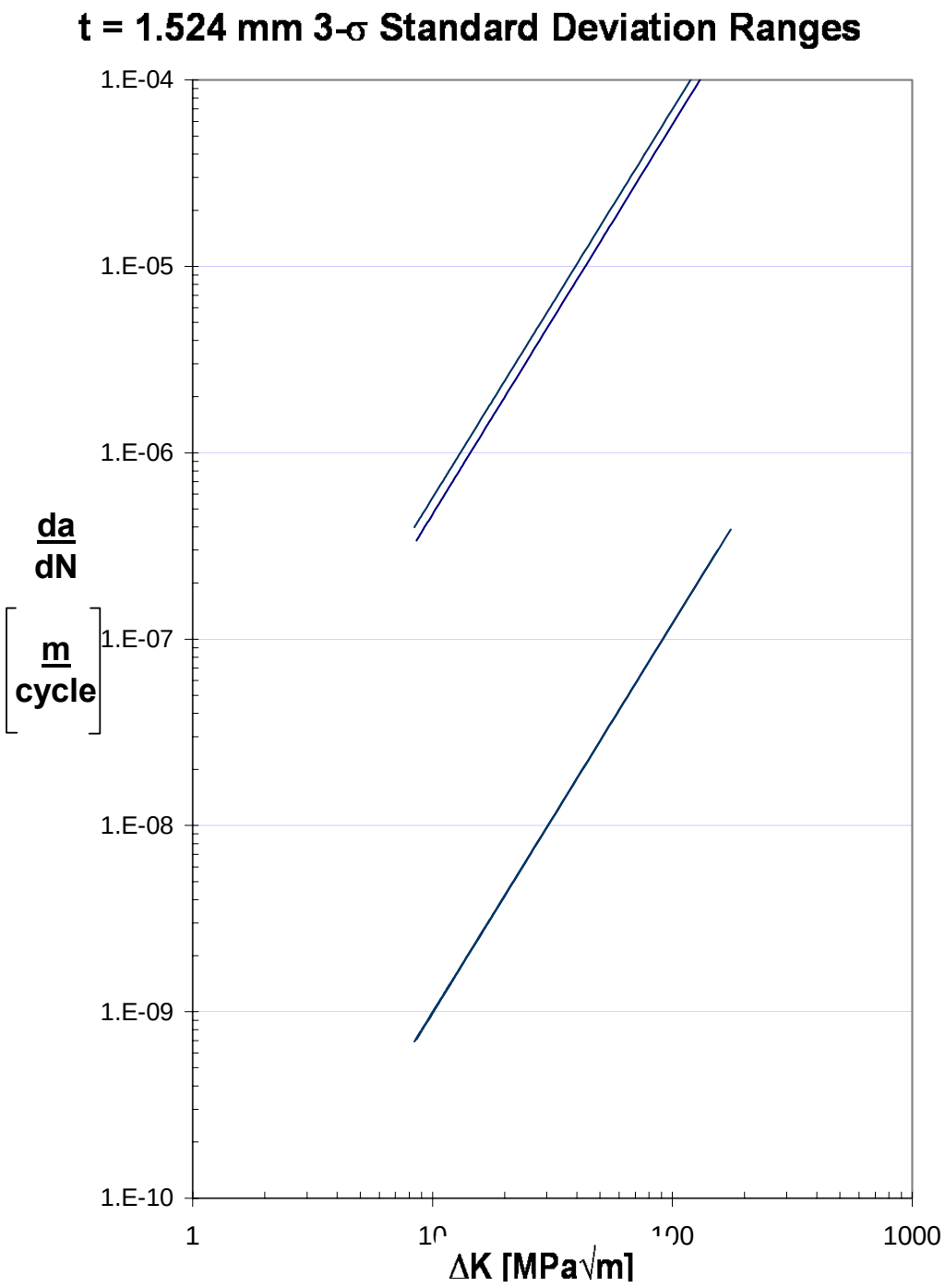

Figure H.1
1.254 mm CGR Standard Deviation

APPENDIX H

COMPARISON PLOTS

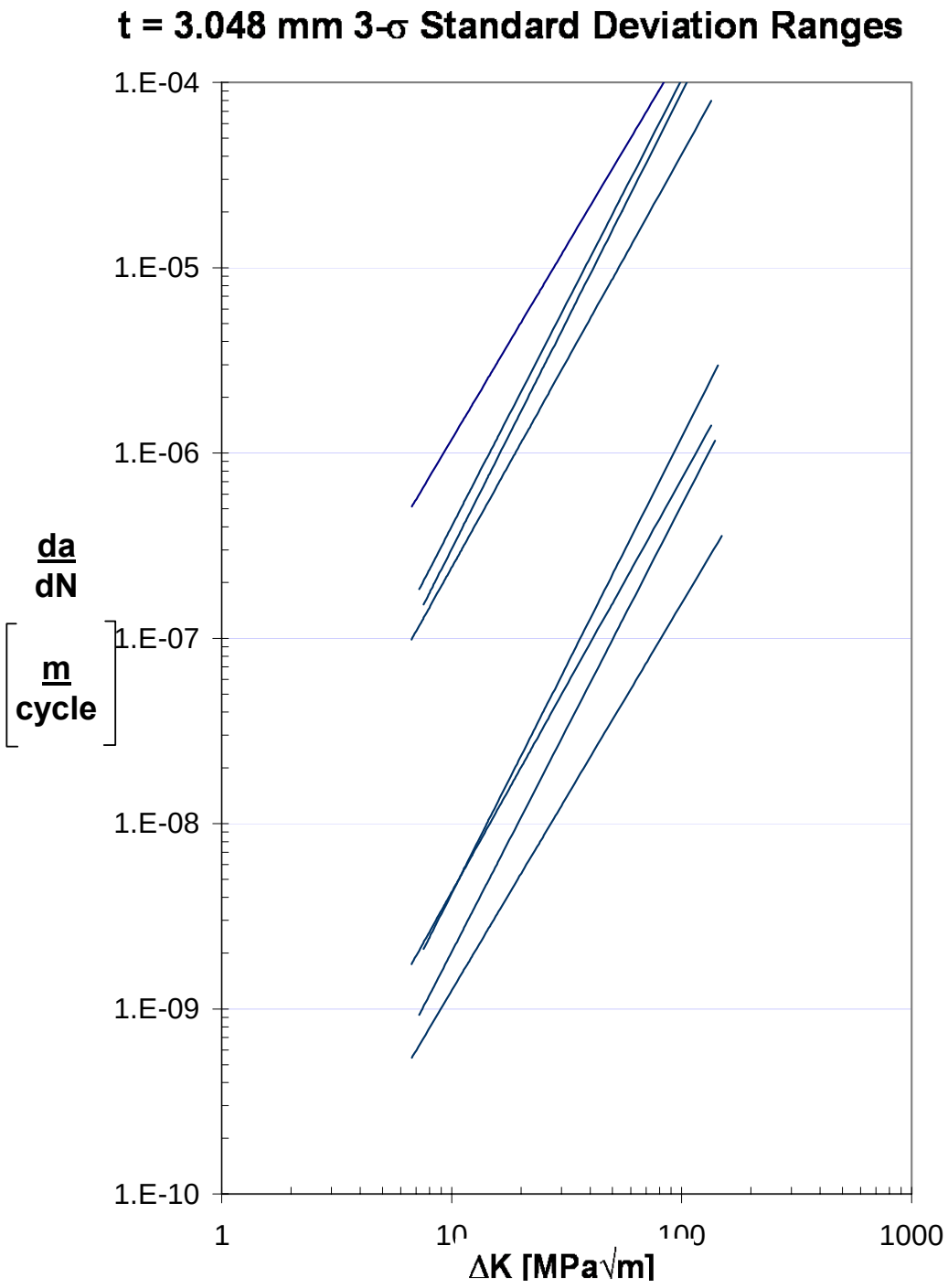

Figure H.2
3.048mm CGR Standard Deviation

APPENDIX H

COMPARISON PLOTS

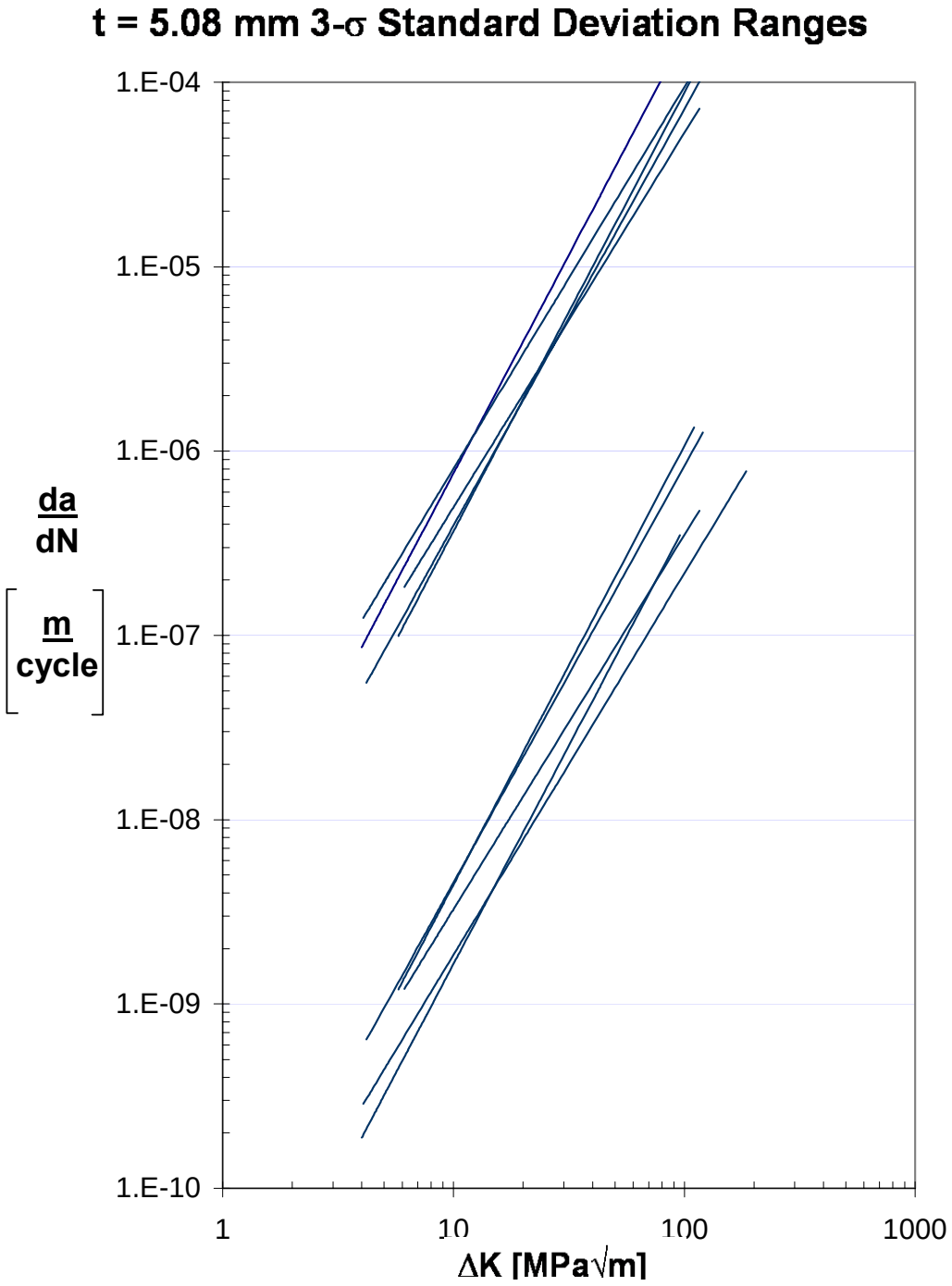

Figure H.3
5.08 mm CGR Standard Deviation

APPENDIX H

COMPARISON PLOTS

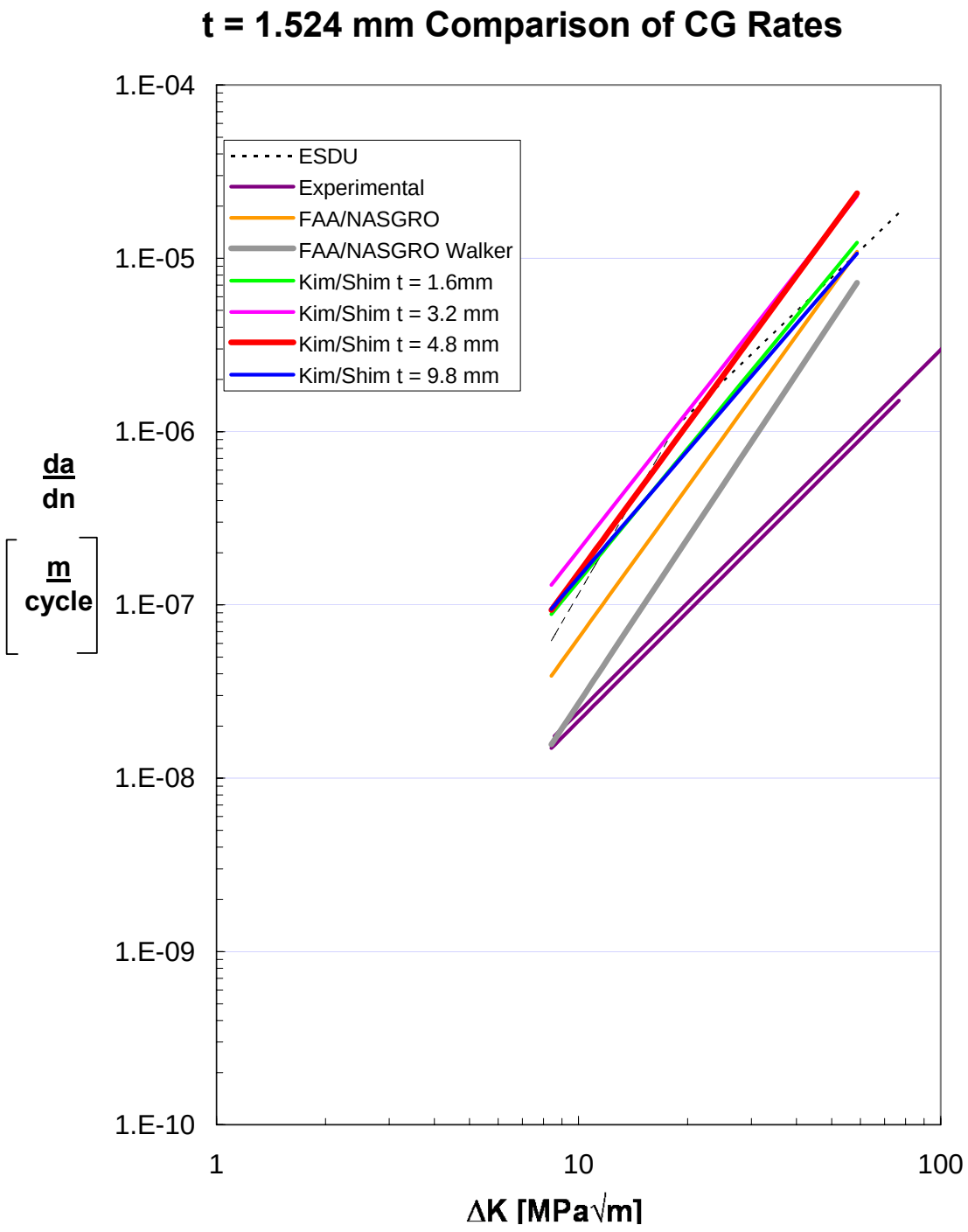

Figure H.4
1.524 mm CGR Comparison

APPENDIX H

COMPARISON PLOTS

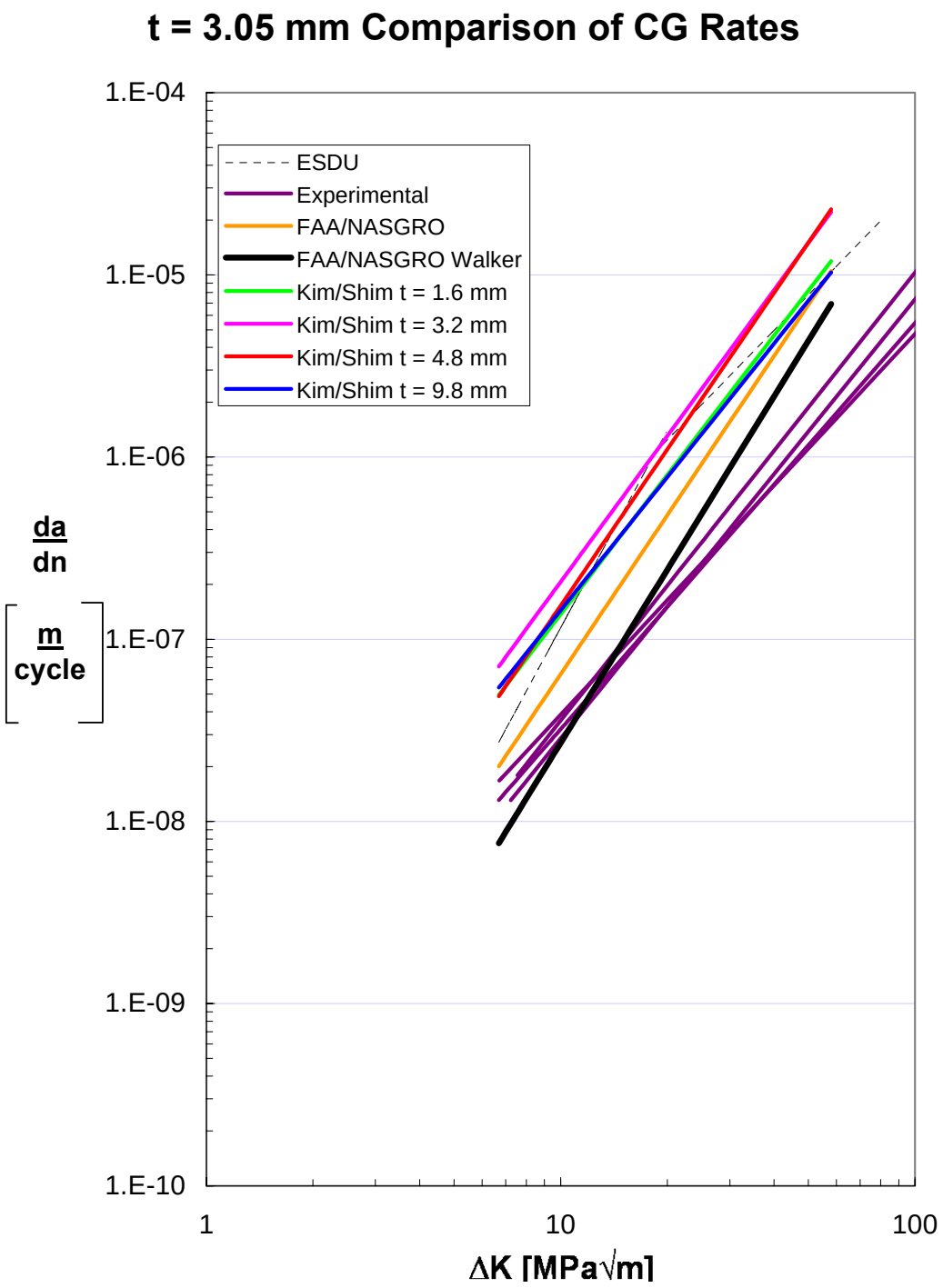

Figure H.5
3.048 mm CGR Comparison

APPENDIX H

COMPARISON PLOTS

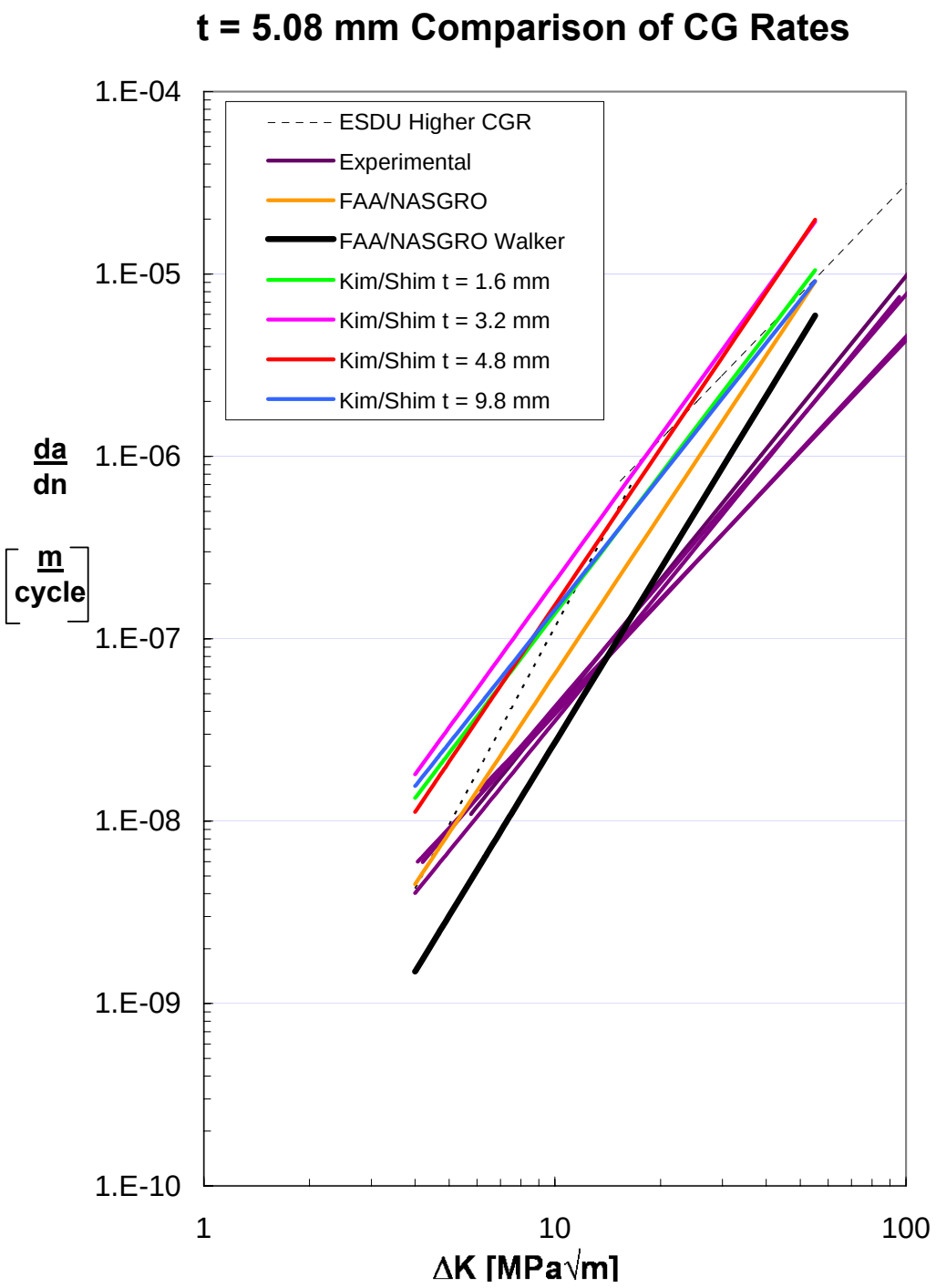

Figure H.6
5.08 mm CGR Comparison

APPENDIX I

INDIVIDUAL PLOTS

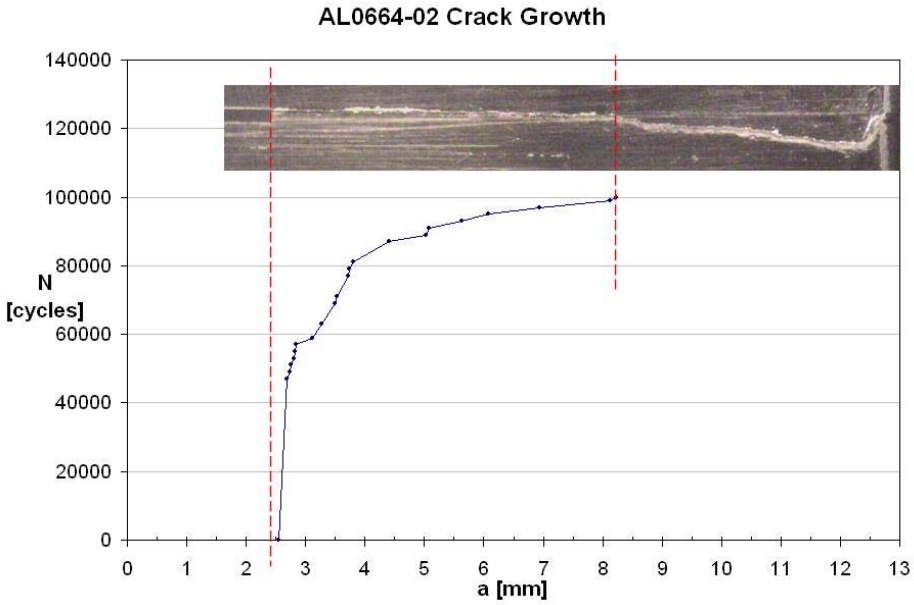

Figure I.1
AL0664-02 Crack Growth

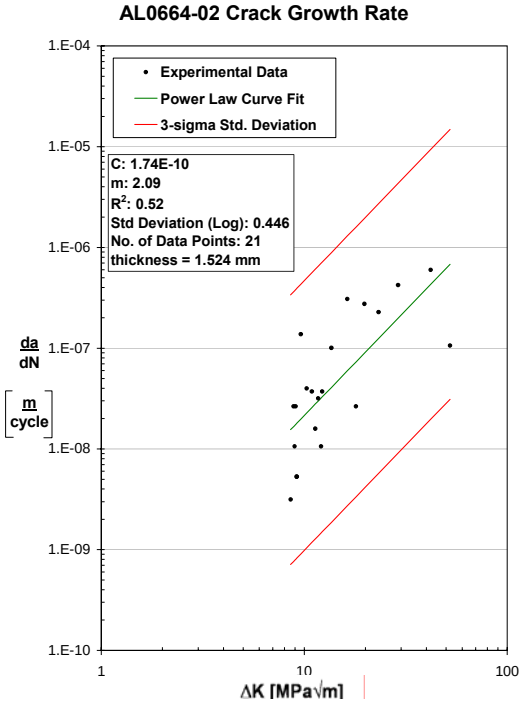

Figure I.2
AL0664-02 Crack Growth Rate

APPENDIX I

INDIVIDUAL PLOTS

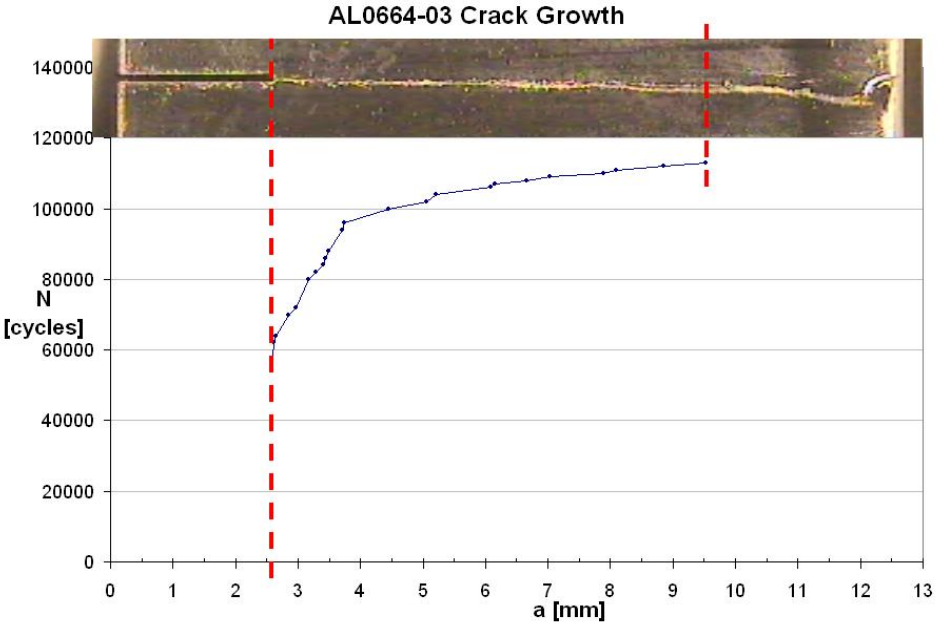

Figure I.3
AL0664-03 Crack Growth

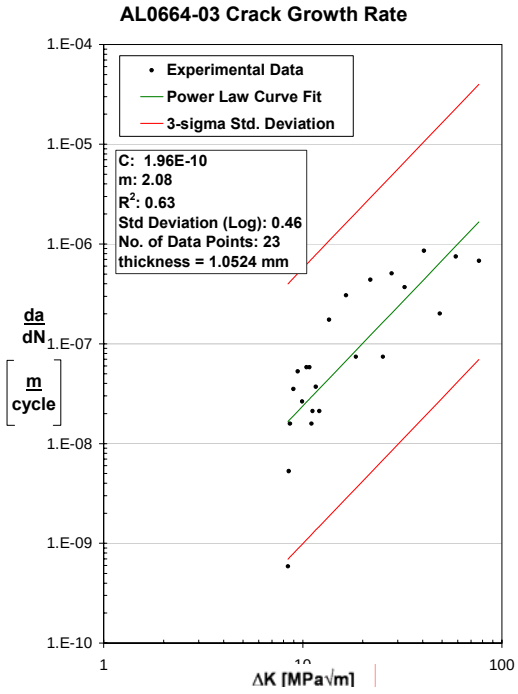

Figure I.4
AL0664-03 Crack Growth Rate

APPENDIX I

INDIVIDUAL PLOTS

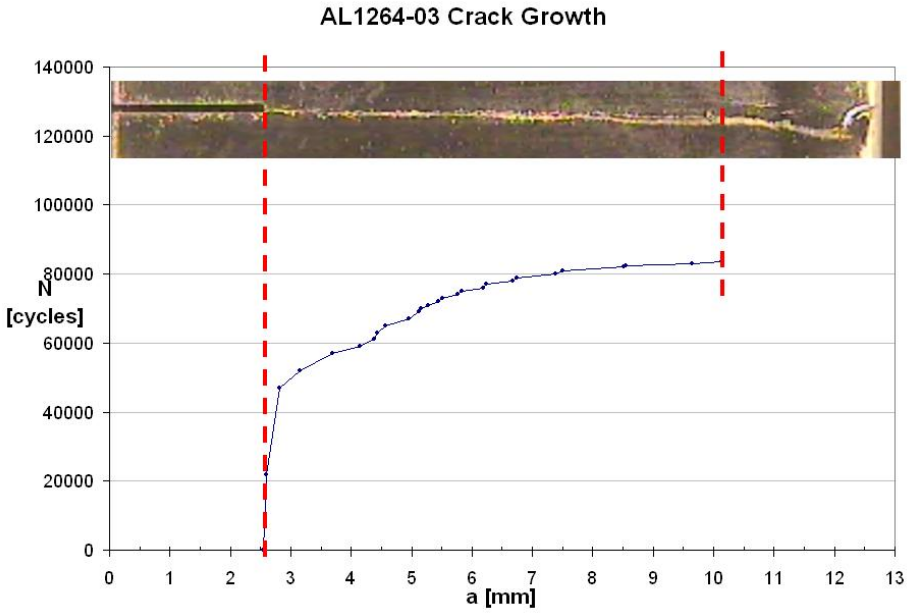

Figure I.5
AL1264-03 Crack Growth

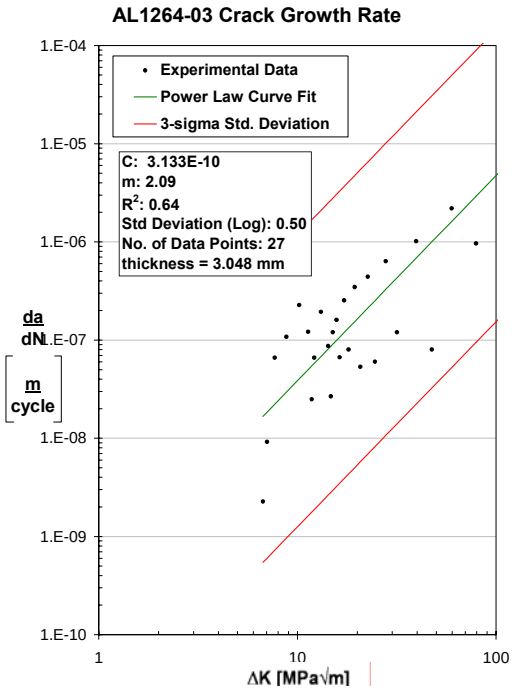

Figure I.6
AL1264-03 Crack Growth Rate

APPENDIX I

INDIVIDUAL PLOTS

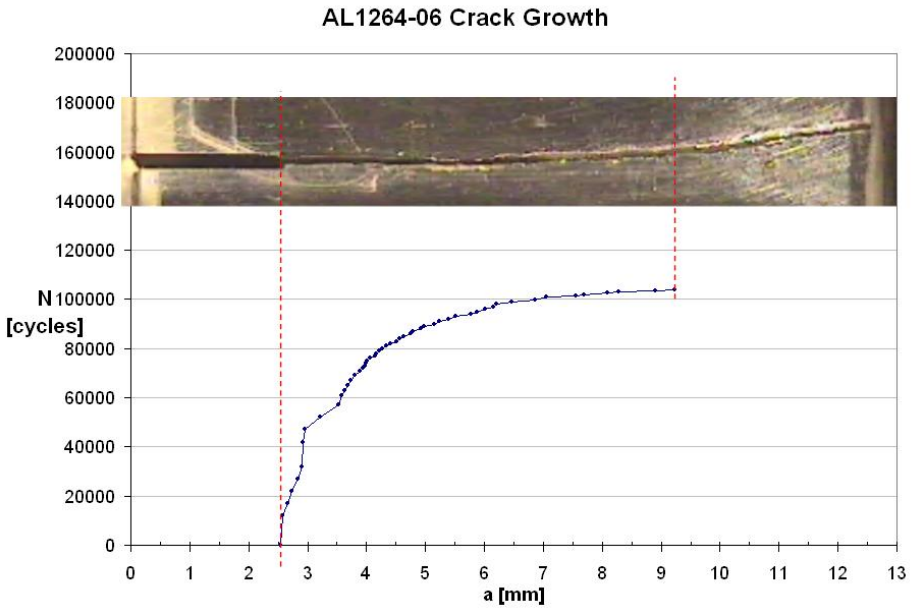

Figure I.7
AL1264-06 Crack Growth

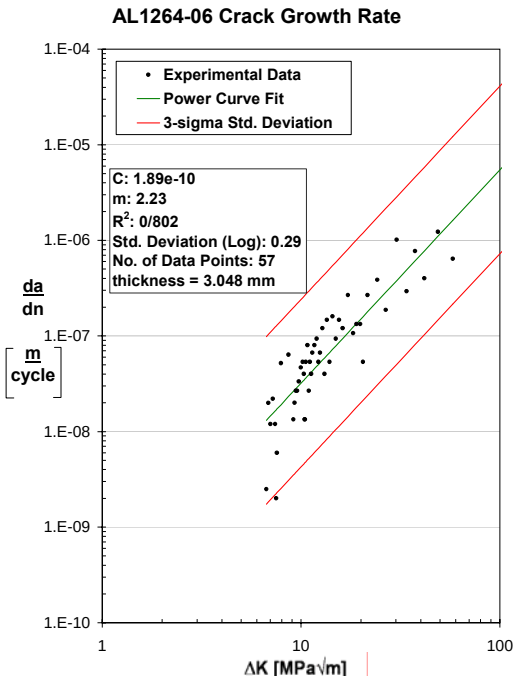

Figure I.8
AL1264-06 Crack Growth Rate

APPENDIX I

INDIVIDUAL PLOTS

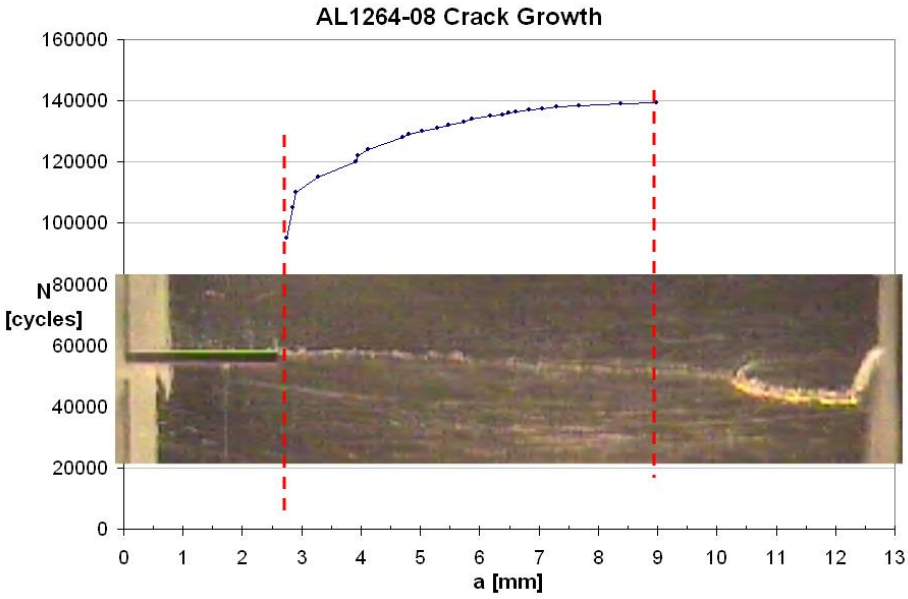

Figure I.9
AL1264-08 Crack Growth

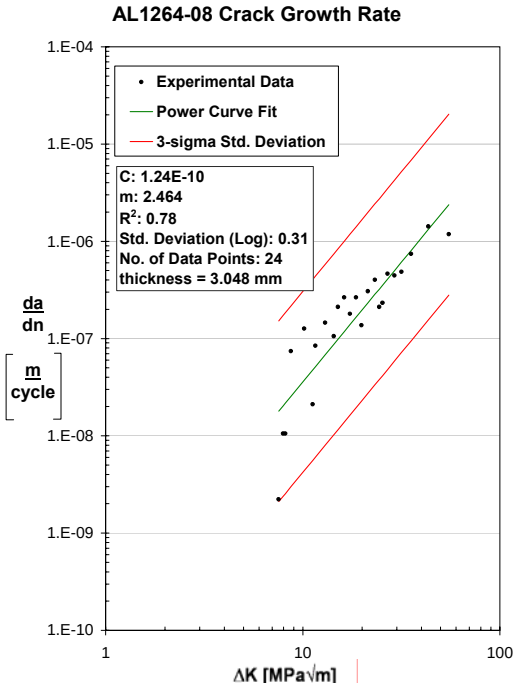

Figure I.10
AL1264-08 Crack Growth Rate

APPENDIX I

INDIVIDUAL PLOTS

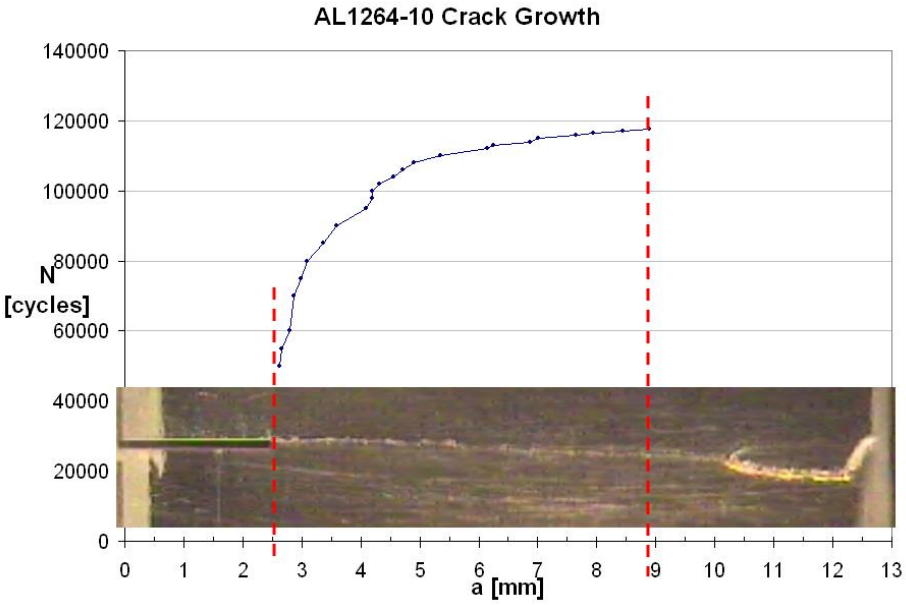

Figure I.11
AL1264-10 Crack Growth

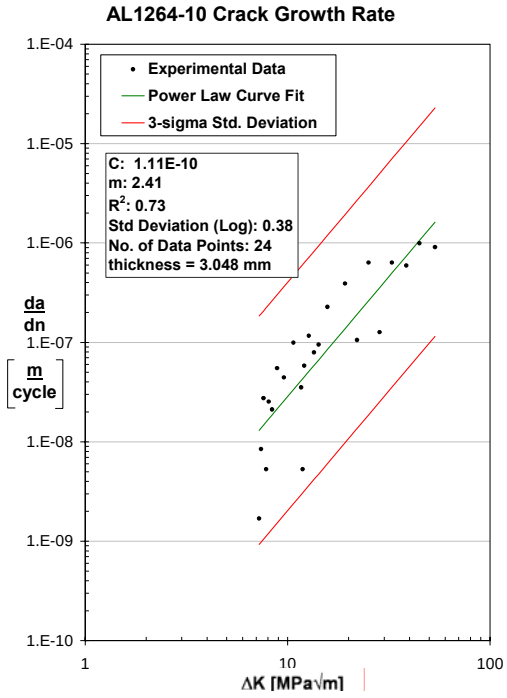

Figure I.12
AL1264-10 Crack Growth Rate

APPENDIX I

INDIVIDUAL PLOTS

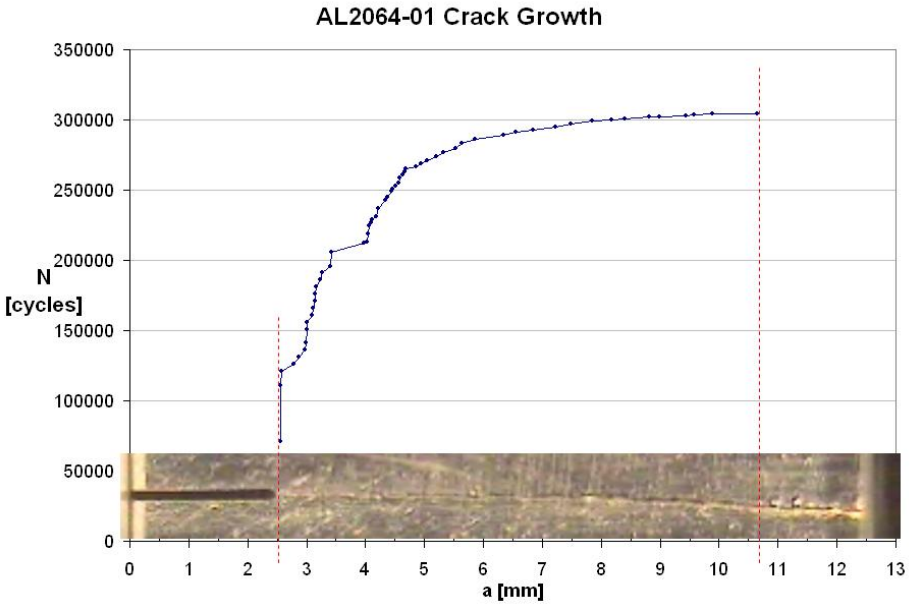

Figure I.13
AL2064-01 Crack Growth

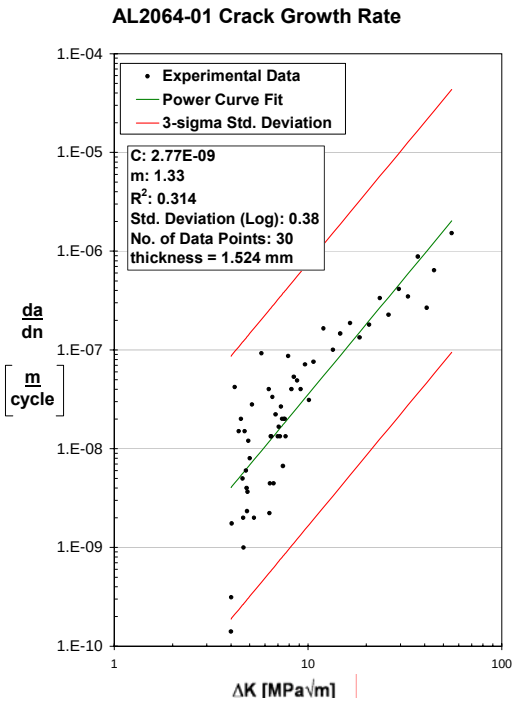

Figure I.14
AL2064-01 Crack Growth Rate

APPENDIX I

INDIVIDUAL PLOTS

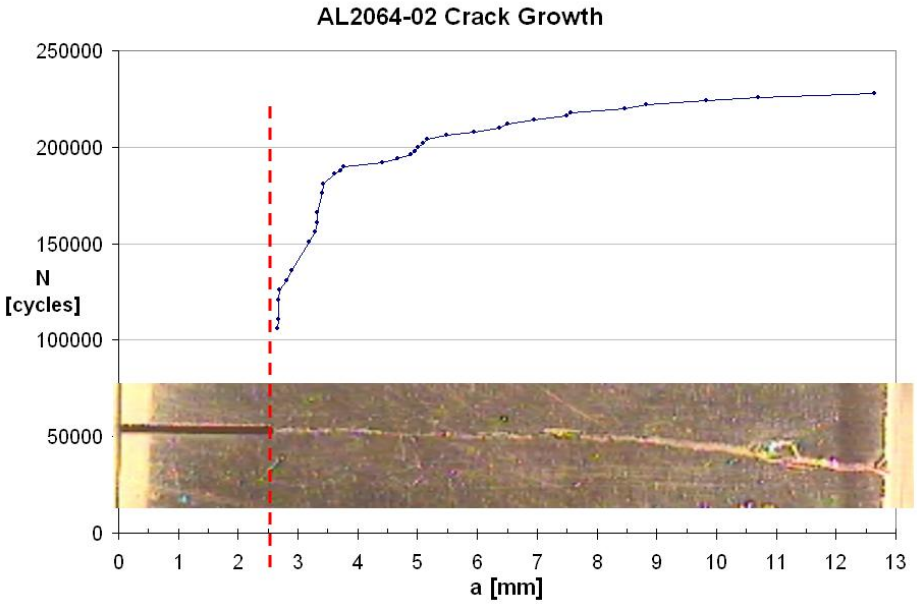

Figure I.15
AL2064-02 Crack Growth

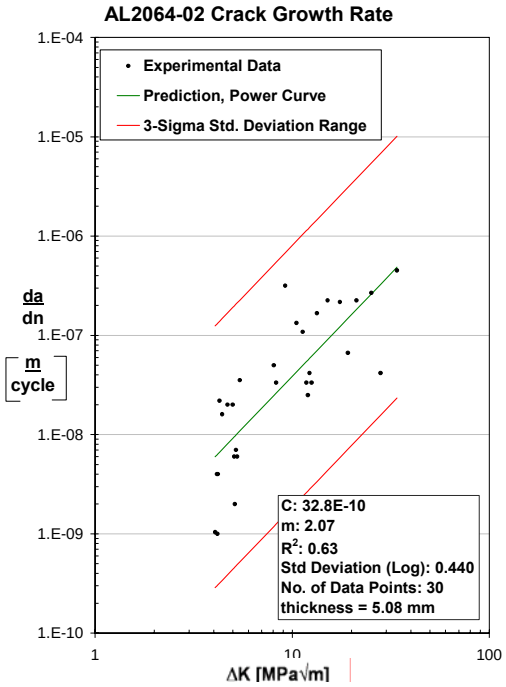

Figure I.16
AL2064-02 Crack Growth Rate

APPENDIX I

INDIVIDUAL PLOTS

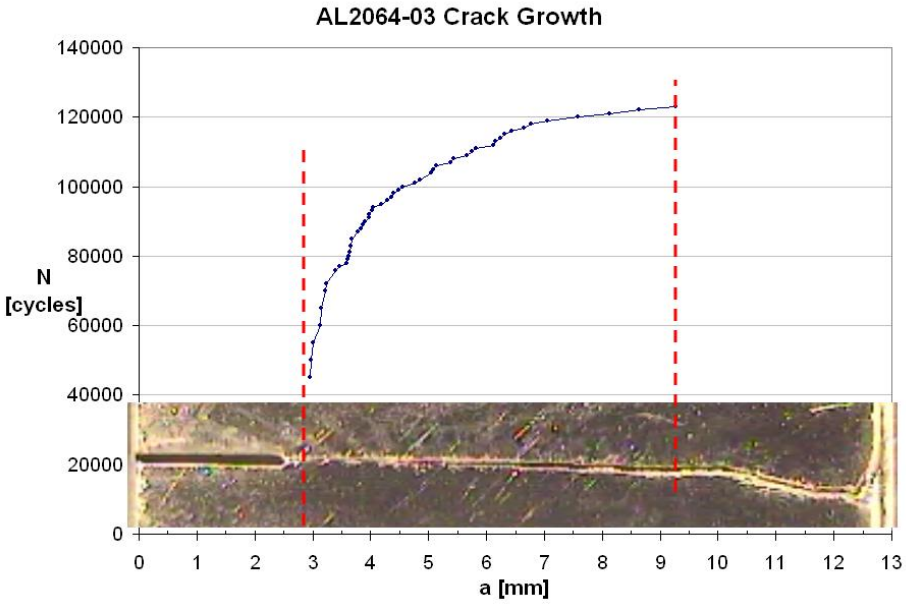

Figure I.17
AL2064-03 Crack Growth

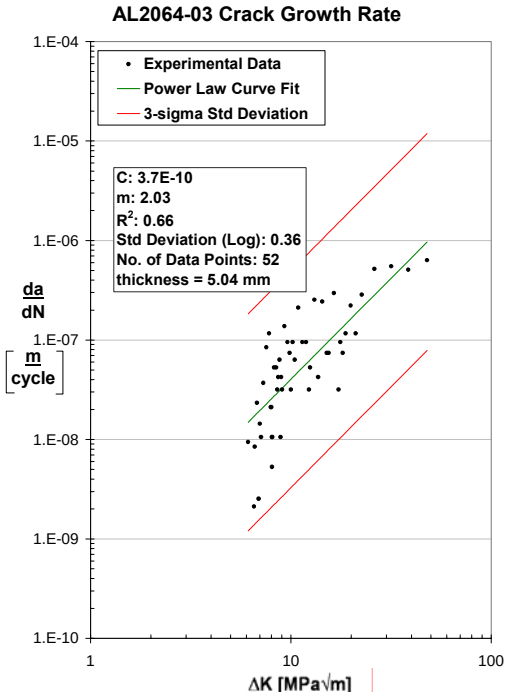

Figure I.18
AL2064-03 Crack Growth Rate

APPENDIX I

INDIVIDUAL PLOTS

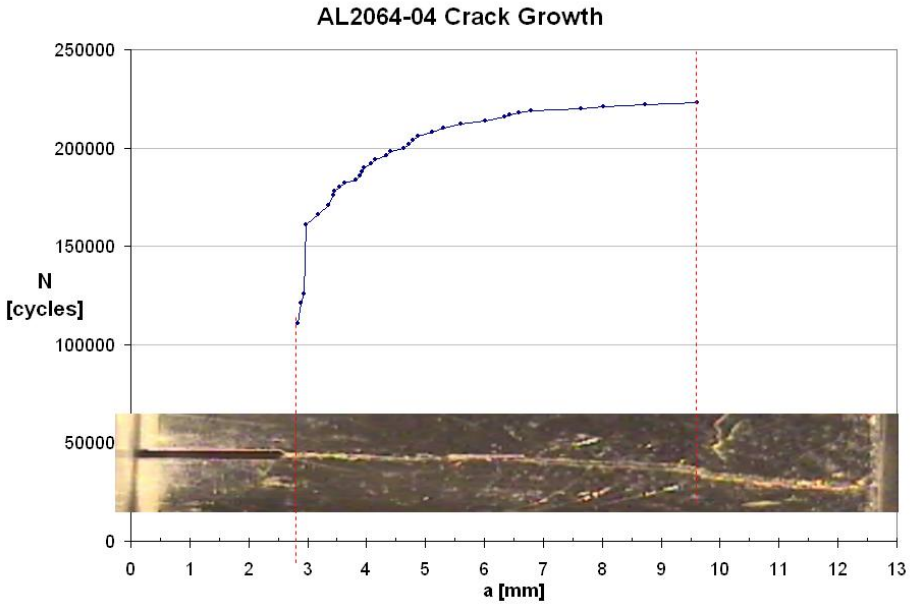

Figure I.19
AL2064-04 Crack Growth

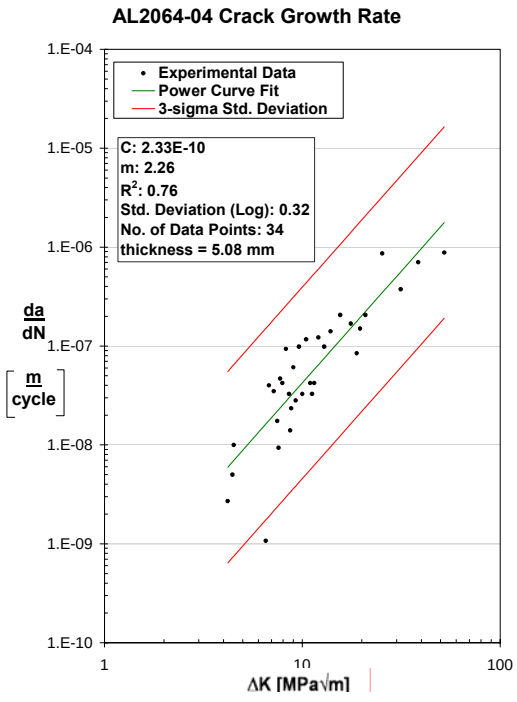

Figure I.20
AL2064-04 Crack Growth Rate

APPENDIX I

INDIVIDUAL PLOTS

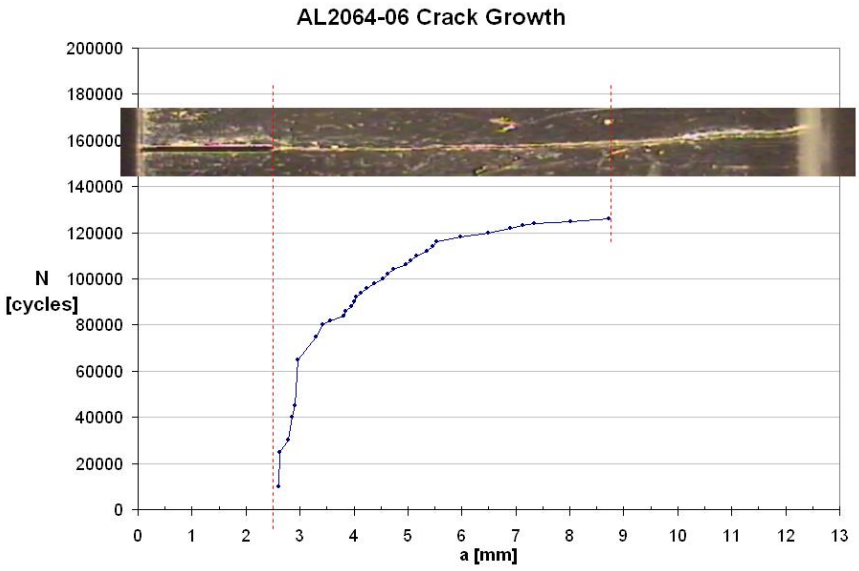

Figure I.21
AL2064-06 Crack Growth

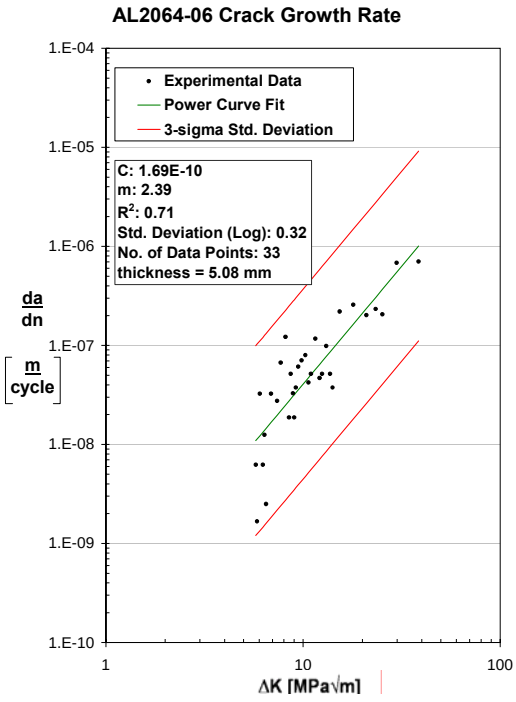

Figure I.22
AL2064-06 Crack Growth Rate

APPENDIX J

STRESS CONCENTRATION FACTOR ANALYSIS

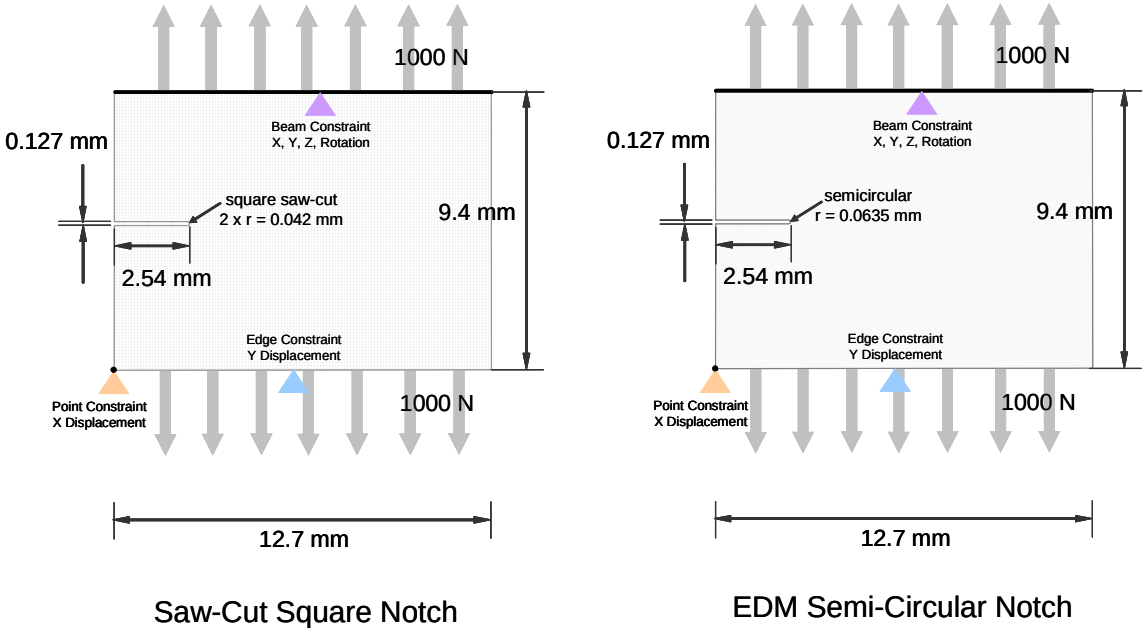

Figure J.1
Mechanica Software Inputs

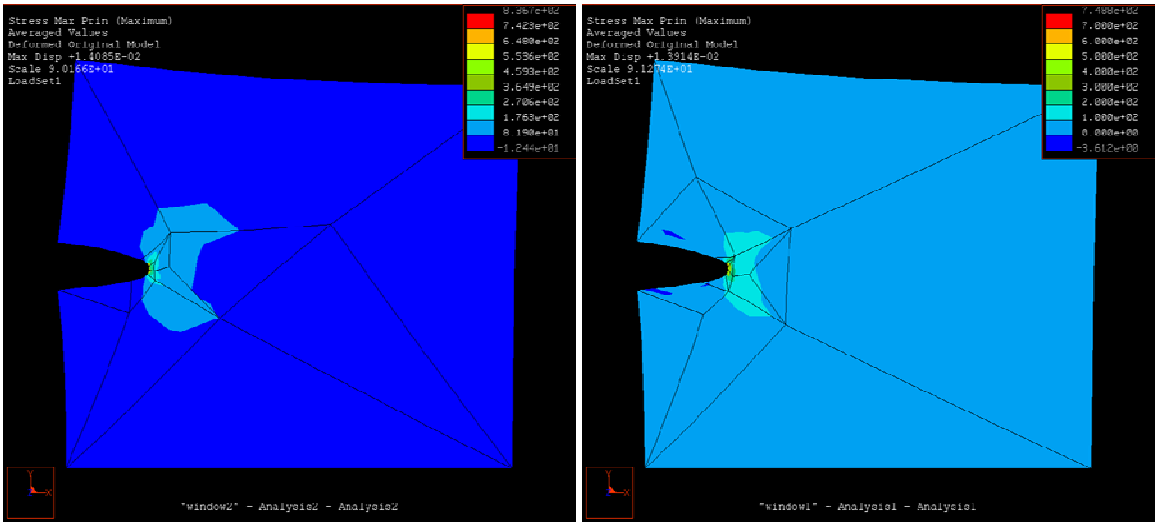

Figure J.2
Mechanica Software Results for Notch Geometries

APPENDIX K

RAW DATA

Table K.1
AL0664-02 Original Experimental Data

AL0664-02	aL [mm]	aR [mm]	Max Stress [MPa]
0	0.0000	0.0000	65.1
1000	0.0000	0.0000	65.1
3000	0.0000	0.0000	65.1
5000	0.0000	0.0000	65.1
7000	0.0000	0.0000	65.1
9000	0.0000	0.0000	65.1
11000	0.0000	0.0000	65.1
13000	0.0000	0.0000	65.1
15000	0.0000	0.0000	65.1
17000	0.0000	0.0000	65.1
19000	0.0000	0.0000	65.1
21000	0.0000	0.0000	65.1
23000	0.0000	0.0000	65.1
25000	0.0000	0.0000	65.1
27000	0.0000	0.0000	65.1
29000	0.0000	0.0000	68.2
31000	0.0000	0.0000	68.2
33000	0.0000	0.0000	68.2
35000	0.0000	0.0000	68.2
37000	0.0000	0.0000	68.2
39000	0.0000	0.0000	68.2
41000	0.0000	0.0000	68.2
43000	0.0000	0.0000	68.2
45000	0.0000	0.0000	68.2
47000	0.1693	0.1270	68.2
49000	0.2328	0.1693	68.2
51000	0.2540	0.1905	68.2
53000	0.3598	0.1905	68.2
55000	0.3810	0.1905	68.2
57000	0.4022	0.1905	68.2
59000	0.5503	0.5927	68.2
61000	0.5503	0.5927	68.2
63000	0.7832	0.6773	68.2
65000	0.7832	0.6773	68.2
67000	0.7832	0.6773	68.2
69000	0.9525	0.9525	68.2
71000	1.0160	0.9525	68.2
73000	1.0160	0.9525	68.2
75000	1.0160	0.9525	68.2
77000	1.2277	1.1218	68.2
79000	1.2700	1.1218	68.2
81000	1.2700	1.2700	68.2
83000	1.2700	1.2700	68.2
85000	1.2700	1.2700	68.2
87000	2.0108	1.7357	68.2
89000	2.5400	2.4342	68.2
91000	2.6458	2.4342	68.2
93000	3.1115	3.0692	68.2
95000	3.5983	3.4925	68.2
97000	4.4450	4.3392	68.2
99000	5.5880	5.5880	68.2
100000	5.7150	5.6727	1320

APPENDIX K

RAW DATA

Table K.2
AL0664-03 Original Experimental Data

AL0664-03	aL [mm]	aR [mm]	Max Stress [MPa]	AL0664-03	aL [mm]	aR [mm]	Max Stress [MPa]
0	0.000	0.000	68.2	104000	2.646	2.688	68.2
2000	0.000	0.000	68.2	106000	3.493	3.598	68.2
4000	0.000	0.000	68.2	107000	3.598	3.641	68.2
6000	0.000	0.000	68.2	108000	4.128	4.128	68.2
8000	0.000	0.000	68.2	109000	4.445	4.551	68.2
10000	0.000	0.000	68.2	110000	5.292	5.419	68.2
12000	0.000	0.000	68.2	111000	5.609	5.503	68.2
14000	0.000	0.000	68.2	112000	6.477	6.138	68.2
16000	0.000	0.000	68.2	113000	6.985	6.985	68.2
18000	0.000	0.000	68.2	114000	0.000	0.000	68.2
20000	0.000	0.000	68.2				
22000	0.000	0.000	68.2				
24000	0.000	0.000	68.2				
26000	0.000	0.000	68.2				
28000	0.000	0.000	68.2				
30000	0.000	0.000	68.2				
32000	0.000	0.000	68.2				
34000	0.000	0.000	68.2				
36000	0.000	0.000	68.2				
38000	0.000	0.000	68.2				
40000	0.000	0.000	68.2				
42000	0.000	0.000	68.2				
44000	0.000	0.000	68.2				
46000	0.000	0.000	68.2				
48000	0.000	0.000	68.2				
50000	0.000	0.000	68.2				
52000	0.000	0.000	68.2				
54000	0.000	0.064	68.2				
56000	0.000	0.064	68.2				
58000	0.000	0.064	68.2				
60000	0.000	0.064	68.2				
62000	0.000	0.148	68.2				
64000	0.000	0.212	68.2				
66000	0.000	0.212	68.2				
68000	0.000	0.212	68.2				
70000	0.254	0.381	68.2				
72000	0.381	0.466	68.2				
74000	0.381	0.466	68.2				
76000	0.381	0.466	68.2				
78000	0.381	0.466	68.2				
80000	0.529	0.741	68.2				
82000	0.656	0.847	68.2				
84000	0.847	0.889	68.2				
86000	0.847	0.953	68.2				
88000	0.889	0.995	68.2				
90000	0.889	0.995	68.2				
92000	0.889	0.995	68.2				
94000	1.058	1.270	68.2				
96000	1.101	1.312	68.2				
98000	1.101	1.312	68.2				
100000	1.799	2.011	68.2				
102000	2.498	2.540	68.2				

APPENDIX K

RAW DATA

Table K.3
AL1264-03 Original Experimental Data

AL1264-03	aL [mm]	aR [mm]	Max Stress [MPa]
0	0.0000	0.0000	54.3
2000	0.0000	0.0000	54.3
7000	0.0000	0.0000	54.3
12000	0.0000	0.0000	54.3
17000	0.0000	0.0000	54.3
22000	0.1000	0.0000	54.3
27000	0.0000	0.0000	54.3
32000	0.0000	0.0000	54.3
37000	0.0000	0.0000	54.3
42000	0.0000	0.0000	54.3
47000	0.3200	0.2400	54.3
52000	0.6200	0.6000	54.3
57000	1.0000	1.3000	54.3
59000	1.463	1.750	54.3
61000	1.950	1.750	54.3
63000	2.200	1.800	54.3
65000	2.139	1.925	54.3
67000	2.487	2.353	54.3
68000	2.487	2.353	54.3
69000	2.727	2.460	54.3
70000	2.727	2.513	54.3
71000	2.754	2.727	54.3
72000	2.941	2.861	54.3
73000	2.995	2.941	54.3
74000	3.262	3.182	54.3
75000	3.262	3.342	54.3
76000	3.663	3.636	54.3
77000	3.690	3.716	54.3
78000	4.144	4.144	54.3
79000	4.198	4.211	54.3
80000	4.759	4.920	54.3
81000	4.920	5.000	54.3
82000	6.069	5.882	54.3
82500	6.069	5.962	54.3
83000	7.165	7.059	54.3
83500	7.353	7.834	54.3

APPENDIX K

RAW DATA

Table K.4
AL1264-06 Original Experimental Data

AL1264-06	aL [mm]	aR [mm]	Max Stress [MPa]	AL1264-06	aL [mm]	aR [mm]	Max Stress [MPa]
0	0.00	0.00	54.3	102000	5.347	4.973	54.3
2000	0.00	0.00	54.3	102500	5.615	5.481	54.3
7000	0.00	0.00	54.3	103000	6.016	5.481	54.3
12000	0.00	0.06	54.3	103500	6.417	6.310	54.3
17000	0.12	0.14	54.3	104000	6.952	6.417	54.3
22000	0.12	0.26	54.3				
27000	0.30	0.30	54.3				
32000	0.36	0.36	54.3				
37000	0.30	0.40	54.3				
42000	0.36	0.40	54.3				
47000	0.38	0.44	54.3				
52000	0.54	0.80	54.3				
57000	1.123	0.856	54.3				
58000	1.123	0.856	54.3				
59000	1.123	0.856	54.3				
61000	1.176	0.909	54.3				
63000	1.203	0.963	54.3				
65000	1.203	1.069	54.3				
67000	1.310	1.069	54.3				
69000	1.310	1.203	54.3				
71000	1.471	1.230	54.3				
72000	1.471	1.337	54.3				
73000	1.524	1.364	54.3				
74000	1.551	1.364	54.3				
75000	1.551	1.390	54.3				
76000	1.551	1.497	54.3				
77000	1.604	1.604	54.3				
78000	1.631	1.631	54.3				
79000	1.711	1.658	54.3				
80000	1.711	1.738	54.3				
81000	1.818	1.765	54.3				
82000	1.818	1.925	54.3				
83000	2.005	1.925	54.3				
84000	2.005	2.032	54.3				
85000	2.139	2.032	54.3				
86000	2.219	2.192	54.3				
87000	2.299	2.192	54.3				
88000	2.380	2.406	54.3				
89000	2.487	2.406	54.3				
90000	2.540	2.674	54.3				
91000	2.727	2.674	54.3				
92000	2.807	2.888	54.3				
93000	2.995	2.941	54.3				
94000	3.262	3.208	54.3				
95000	3.422	3.262	54.3				
96000	3.476	3.476	54.3				
97000	3.743	3.476	54.3				
98000	3.797	3.529	54.3				
99000	4.144	3.716	54.3				
100000	4.358	4.278	54.3				
101000	4.706	4.305	54.3				
101500	5.080	4.946	54.3				

APPENDIX K

RAW DATA

Table K.5
AL1264-08 Original Experimental Data

Al1264-08	aL [mm]	aR [mm]	Max Stress [MPa]
0	0.000	0.000	54.3
1000	0.000	0.000	54.3
2000	0.000	0.000	54.3
3000	0.000	0.000	54.3
4000	0.000	0.000	54.3
6000	0.000	0.000	54.3
8000	0.000	0.000	54.3
10000	0.000	0.000	54.3
15000	0.000	0.000	54.3
20000	0.000	0.000	54.3
25000	0.000	0.000	54.3
30000	0.000	0.000	54.3
35000	0.000	0.000	54.3
40000	0.000	0.000	54.3
45000	0.000	0.000	54.3
50000	0.000	0.000	54.3
55000	0.000	0.000	54.3
60000	0.000	0.000	54.3
65000	0.000	0.000	54.3
70000	0.000	0.000	54.3
75000	0.000	0.000	54.3
80000	0.000	0.000	59.4
85000	0.000	0.000	59.4
90000	0.000	0.000	59.4
95000	0.318	0.106	59.4
98000	0.318	0.106	59.4
100000	0.318	0.106	59.4
105000	0.529	0.106	59.4
110000	0.635	0.106	59.4
115000	1.101	0.381	59.4
120000	1.693	1.058	59.4
122000	1.778	1.058	59.4
124000	1.799	1.376	59.4
126000	1.799	1.376	59.4
128000	2.328	2.011	59.4
129000	2.540	2.011	59.4
130000	2.646	2.328	59.4
131000	2.963	2.540	59.4
132000	2.963	2.900	59.4
133000	3.493	2.900	59.4
134000	3.493	3.175	59.4
135000	3.747	3.535	59.4
135500	3.916	3.768	59.4
136000	4.043	3.852	59.4
136500	4.233	3.895	59.4
137000	4.424	4.170	59.4
137500	4.551	4.487	59.4
138000	4.932	4.593	59.4
138500	5.186	5.080	59.4
139000	5.927	5.757	59.4
139500	6.414	6.456	59.4

APPENDIX K

RAW DATA

Table K.6
AL1264-10 Original Experimental Data

AL1264-10	aL [mm]	aR [mm]	Max Stress [MPa]
0	0.000	0.000	58.1
2000	0.000	0.000	58.1
4000	0.000	0.000	58.1
6000	0.000	0.000	58.1
10000	0.000	0.000	58.1
15000	0.000	0.000	58.1
20000	0.000	0.000	58.1
25000	0.000	0.000	58.1
30000	0.000	0.000	58.1
35000	0.000	0.000	58.1
40000	0.000	0.000	58.1
45000	0.000	0.000	58.1
50000	0.127	0.042	58.1
55000	0.212	0.042	58.1
60000	0.423	0.106	58.1
65000	0.423	0.106	58.1
70000	0.529	0.106	58.1
75000	0.677	0.212	58.1
80000	0.889	0.212	58.1
85000	0.889	0.762	58.1
90000	1.291	0.804	58.1
95000	1.693	1.397	58.1
98000	1.820	1.482	58.1
100000	1.842	1.482	58.1
102000	2.074	1.482	58.1
104000	2.223	1.799	58.1
106000	2.434	1.905	58.1
108000	2.646	2.074	58.1
110000	3.133	2.498	58.1
112000	3.704	3.493	58.1
113000	3.916	3.493	58.1
114000	4.487	4.191	58.1
115000	4.657	4.276	58.1
116000	5.059	5.144	58.1
116500	5.503	5.292	58.1
117000	5.863	5.927	58.1
117500	6.414	6.287	58.1

APPENDIX K

RAW DATA

Table K.7
AL2064-01 Original Experimental Data

AL2064-01	aL [mm]	aR [mm]	Max Stress [MPa]	AL2064-01	aL [mm]	aR [mm]	Max Stress [MPa]
0	0.000	0.000	32.6	223100	1.604	1.390	35.7
2000	0.000	0.000	32.6	225100	1.631	1.417	35.7
4000	0.000	0.000	32.6	227100	1.631	1.471	35.7
6000	0.000	0.000	32.6	229100	1.684	1.471	35.7
11000	0.000	0.000	32.6	231100	1.684	1.604	35.7
16000	0.000	0.000	32.6	233100	1.684	1.604	35.7
21000	0.000	0.000	32.6	235100	1.684	1.604	35.7
26000	0.000	0.000	32.6	237100	1.684	1.658	35.7
31000	0.000	0.000	32.6	239100	1.684	1.658	35.7
36000	0.000	0.000	32.6	241100	1.684	1.658	35.7
41000	0.000	0.000	32.6	243100	1.738	1.872	35.7
46000	0.000	0.000	32.6	245100	1.791	1.872	35.7
51000	0.000	0.000	32.6	247100	1.791	1.872	35.7
56000	0.000	0.000	32.6	249100	1.791	2.005	35.7
61000	0.000	0.000	32.6	251100	1.791	2.059	35.7
66000	0.000	0.000	32.6	253100	1.872	2.085	35.7
71000	0.020	0.000	32.6	255100	1.872	2.166	35.7
76000	0.000	0.000	32.6	257100	1.872	2.166	35.7
81000	0.000	0.020	32.6	259100	1.925	2.166	35.7
86000	0.000	0.000	32.6	261100	2.005	2.166	35.7
91000	0.000	0.000	32.6	263100	2.005	2.246	35.7
96000	0.000	0.000	32.6	265100	2.005	2.299	35.7
101000	0.000	0.000	32.6	267100	2.139	2.513	35.7
106000	0.000	0.020	32.6	269100	2.273	2.540	35.7
111000	0.020	0.025	32.6	271100	2.326	2.700	35.7
116000	0.000	0.025	32.6	274100	2.593	2.727	35.7
121000	0.040	0.040	32.6	277100	2.620	2.941	35.7
126000	0.300	0.200	32.6	280100	2.941	3.048	35.7
131000	0.350	0.300	32.6	283100	2.968	3.208	35.7
136000	0.350	0.500	32.6	286100	3.235	3.396	35.7
141000	0.400	0.500	32.6	289100	3.609	4.011	35.7
146000	0.500	0.500	32.6	291100	3.877	4.144	35.7
151000	0.440	0.500	32.6	293100	4.064	4.545	35.7
156000	0.500	0.450	32.6	295100	4.679	4.679	35.7
161000	0.500	0.600	32.6	297100	4.813	5.080	35.7
166000	0.560	0.600	32.6	299100	5.321	5.294	35.7
171000	0.560	0.640	32.6	300100	5.535	5.748	35.7
176000	0.560	0.640	32.6	301100	5.855	5.882	35.7
181000	0.560	0.700	32.6	302100	6.256	6.310	35.7
186000	0.640	0.740	32.6	302600	6.497	6.417	35.7
191000	0.720	0.740	32.6	303100	6.818	6.978	35.7
196000	0.860	0.880	32.6	303600	6.978	7.085	35.7
201000	0.860	0.880	32.6	304100	7.353	7.353	35.7
206000	0.880	0.900	32.6				
211100	0.880	0.900	32.6				
212100	1.577	1.310	35.7				
213100	1.604	1.364	35.7				
214100	1.604	1.364	35.7				
215100	1.604	1.364	35.7				
217100	1.604	1.364	35.7				
219100	1.604	1.390	35.7				
221100	1.604	1.390	35.7				

APPENDIX K

RAW DATA

Table K.8
AL2064-02 Original Experimental Data

AL2064-02	aL [mm]	aR [mm]	Max Stress [MPa]	AL2064-02	aL [mm]	aR [mm]	Max Stress [MPa]
0	0.000	0.000	32.6	212000	4.033	3.900	46.5
2000	0.000	0.000	32.6	214000	4.500	4.333	46.5
6000	0.000	0.000	32.6	216000	4.933	4.967	46.5
11000	0.000	0.000	32.6	218000	5.067	5.000	46.5
16000	0.000	0.000	32.6	220000	5.833	6.033	46.5
21000	0.000	0.000	32.6	222000	5.900	6.667	46.5
26000	0.000	0.000	32.6	224000	7.167	7.400	46.5
31000	0.000	0.000	32.6	226000	8.167	8.167	46.5
36000	0.000	0.000	32.6	228000	10.167	10.500	46.5
41000	0.000	0.000	32.6				
46000	0.000	0.000	32.6				
51000	0.000	0.000	32.6				
56000	0.000	0.000	32.6				
61000	0.000	0.000	32.6				
66000	0.000	0.000	32.6				
71000	0.000	0.000	32.6				
76000	0.000	0.000	32.6				
81000	0.000	0.000	32.6				
86000	0.000	0.000	32.6				
91000	0.000	0.000	32.6				
96000	0.000	0.000	32.6				
101000	0.000	0.000	32.6				
106000	0.120	0.100	32.6				
111000	0.120	0.140	32.6				
116000	0.120	0.140	32.6				
121000	0.140	0.140	32.6				
126000	0.180	0.140	32.6				
131000	0.300	0.240	32.6				
136000	0.340	0.360	32.6				
141000	0.340	0.360	32.6				
146000	0.340	0.360	32.6				
151000	0.800	0.500	32.6				
156000	0.800	0.700	32.6				
161000	0.860	0.700	32.6				
166000	0.860	0.720	32.6				
171000	0.860	0.720	32.6				
176000	0.880	0.840	32.6				
181000	0.880	0.900	32.6				
186000	1.000	1.000	32.6				
186000	1.067	1.067	46.5				
188000	1.267	1.067	46.5				
190000	1.267	1.200	46.5				
192000	2.067	1.667	46.5				
194000	2.433	1.833	46.5				
196000	2.700	2.000	46.5				
198000	2.700	2.133	46.5				
200000	2.767	2.167	46.5				
202000	2.767	2.333	46.5				
204000	2.833	2.400	46.5				
206000	2.900	3.000	46.5				
208000	3.400	3.400	46.5				
210000	3.833	3.833	46.5				

APPENDIX K

RAW DATA

Table K.9
AL2064-03 Original Experimental Data

AL2064-03	aL[mm]	aR[mm]	Max Stress [MPa]	AL2064-03	aL[mm]	aR[mm]	Max Stress [MPa]
0	0.0000	0.0000	46.5	111000	3.2597	3.3020	46.5
5000	0.0000	0.0000	46.5	112000	3.5983	3.5560	46.5
10000	0.0000	0.0039	46.5	113000	3.5983	3.6195	46.5
15000	0.0000	0.0000	46.5	114000	3.7042	3.7042	46.5
20000	0.0000	0.0000	46.5	115000	3.7465	3.8100	46.5
25000	0.0000	0.0000	46.5	116000	3.8947	3.8947	46.5
30000	0.0018	0.0000	46.5	117000	4.0005	4.2333	46.5
35000	0.0000	0.0000	46.5	118000	4.2122	4.2545	46.5
40000	0.0000	0.0000	46.5	119000	4.3815	4.6567	46.5
45000	0.32	0.53	46.5	120000	5.1012	4.9742	46.5
50000	0.37	0.50	46.5	121000	5.6727	5.5033	46.5
55000	0.42	0.53	46.5	122000	6.1595	6.0325	46.5
60000	0.64	0.55	46.5	123000	6.7945	6.6675	46.5
65000	0.66	0.55	46.5				
70000	0.68	0.68	46.5				
72000	0.70	0.70	46.5				
74000	0.70	0.70	46.5				
76000	0.83	0.87	46.5				
77000	0.89	0.97	46.5				
78000	1.08	1.02	46.5				
79000	1.12	1.02	46.5				
80000	1.16	1.02	46.5				
81000	1.19	1.02	46.5				
82000	1.19	1.02	46.5				
83000	1.19	1.04	46.5				
84000	1.19	1.04	46.5				
85000	1.23	1.04	46.5				
86000	1.23	1.04	46.5				
87000	1.38	1.10	46.5				
88000	1.42	1.16	46.5				
89000	1.48	1.16	46.5				
90000	1.4817	1.25	46.5				
91000	1.5240	1.33	46.5				
92000	1.5452	1.3335	46.5				
93000	1.5875	1.3758	46.5				
94000	1.5875	1.4393	46.5				
95000	1.7145	1.5875	46.5				
96000	1.7357	1.7568	46.5				
97000	1.8627	1.7780	46.5				
98000	1.9050	1.7992	46.5				
99000	1.9685	1.9262	46.5				
100000	1.9685	2.0532	46.5				
101000	2.2437	2.2013	46.5				
102000	2.3072	2.3283	46.5				
103000	2.3072	2.3283	46.5				
104000	2.4342	2.5823	46.5				
105000	2.4977	2.5823	46.5				
106000	2.4977	2.6882	46.5				
107000	2.8152	2.8787	46.5				
108000	2.8152	2.9633	46.5				
109000	3.1750	3.0903	46.5				
110000	3.1962	3.2173	46.5				

APPENDIX K

RAW DATA

Table K.10
AL2064-04 Original Experimental Data

AL2064-04	aL [mm]	aR [mm]	Max Stress [MPa]	AL2064-04	aL [mm]	aR [mm]	Max Stress [MPa]
0	0.000	0.000	32.6	214000	3.206	3.731	46.5
2000	0.000	0.000	32.6	216000	3.788	3.825	46.5
4000	0.000	0.000	32.6	217000	3.844	3.938	46.5
6000	0.000	0.000	32.6	218000	3.938	4.144	46.5
11000	0.000	0.000	32.6	219000	4.313	4.181	46.5
16000	0.000	0.000	32.6	220000	5.344	4.875	46.5
21000	0.000	0.000	32.6	221000	5.531	5.438	46.5
26000	0.000	0.000	32.6	222000	6.750	5.625	46.5
31000	0.000	0.000	32.6	223000	6.788	7.350	46.5
36000	0.000	0.000	32.6				
41000	0.000	0.000	32.6				
46000	0.000	0.000	32.6				
51000	0.000	0.000	32.6				
56000	0.000	0.000	32.6				
61000	0.000	0.000	32.6				
66000	0.000	0.000	32.6				
71000	0.000	0.000	32.6				
76000	0.000	0.000	32.6				
81000	0.000	0.000	32.6				
86000	0.000	0.000	32.6				
91000	0.000	0.000	32.6				
96000	0.000	0.000	32.6				
101000	0.000	0.000	32.6				
106000	0.000	0.000	32.6				
111000	0.200	0.400	32.6				
121000	0.200	0.500	32.6				
126000	0.300	0.500	32.6				
131000	0.300	0.500	32.6				
136000	0.340	0.625	32.6				
156000	0.275	0.450	46.5				
161000	0.300	0.575	46.5				
166000	0.625	0.650	46.5				
171000	0.700	0.925	46.5				
176000	0.806	0.994	46.5				
178000	0.825	1.013	46.5				
180000	0.975	1.050	46.5				
182000	1.088	1.106	46.5				
184000	1.350	1.219	46.5				
186000	1.388	1.313	46.5				
188000	1.406	1.350	46.5				
190000	1.444	1.406	46.5				
192000	1.594	1.500	46.5				
194000	1.613	1.594	46.5				
196000	1.838	1.763	46.5				
198000	1.856	1.875	46.5				
200000	2.138	2.063	46.5				
202000	2.194	2.175	46.5				
204000	2.288	2.213	46.5				
206000	2.325	2.344	46.5				
208000	2.494	2.663	46.5				
210000	2.719	2.831	46.5				
212000	3.094	3.019	46.5				

APPENDIX K

RAW DATA

Table K.11
AL2064-06 Original Experimental Data

AL2064-06	aL [mm]	aR[mm]	Max Stress [MPa]
0	0.000	0.000	46.5
5000	0.000	0.000	46.5
10000	0.000	0.125	46.5
15000	0.000	0.125	46.5
20000	0.000	0.125	46.5
25000	0.050	0.125	46.5
30000	0.375	0.125	46.5
35000	0.375	0.125	46.5
40000	0.500	0.125	46.5
45000	0.500	0.250	46.5
50000	0.500	0.250	46.5
55000	0.500	0.250	46.5
60000	0.500	0.250	46.5
65000	0.600	0.250	46.5
70000	0.600	0.250	46.5
75000	0.875	0.625	46.5
80000	0.900	0.875	46.5
82000	0.900	1.144	46.5
84000	1.350	1.181	46.5
86000	1.369	1.238	46.5
88000	1.500	1.313	46.5
90000	1.556	1.388	46.5
92000	1.594	1.425	46.5
94000	1.650	1.519	46.5
96000	1.875	1.538	46.5
98000	1.913	1.781	46.5
100000	2.194	1.819	46.5
102000	2.213	1.969	46.5
104000	2.363	2.025	46.5
106000	2.531	2.325	46.5
108000	2.663	2.381	46.5
110000	2.719	2.531	46.5
112000	2.963	2.681	46.5
114000	3.038	2.813	46.5
116000	3.094	2.906	46.5
118000	3.563	3.319	46.5
120000	4.200	3.713	46.5
122000	4.313	4.407	46.5
123000	4.650	4.538	46.5
124000	4.819	4.781	46.5
125000	5.625	5.344	46.5
126000	6.225	6.150	46.5

APPENDIX L

CALIBRATION RAW DATA

Table L.1
Calibration Raw Data

Trial	Date	Channel 1 Wire Color	Channel 1 ε [μstrain]	Channel 2 ε [μstrain]	Ch1 Pre-ld Zero ε [μstrain]	Ch2 Pre-ld Zero ε [μstrain]	Ch1 Post-ld Zero ε [μstrain]	Ch2 Post-ld Zero ε [μstrain]	$\varepsilon_{average}$ [μstrain]	$\varepsilon_{calculated}$ [μstrain]	ε_{FEM} [μstrain]	Channel 1 $\sigma_{calculate}$ [MPa]	Channel 2 $\sigma_{calculate}$ [MPa]
1	6/3/2006	Orange	725	647	4	6	0	0	686	756	772	145	129
2	6/3/2006	Orange	726	648	0	0	5	10	687	756	772	145	130
3	6/6/2006	Orange	855	582	-1	1	4	-6	719	756	772	171	116
4	6/6/2006	Orange	812	636	-1	1	-7	7	724	756	772	162	127
5	6/6/2006	Orange	825	596	0	0	27	-20	711	756	772	165	119
6	6/6/2006	Orange	802	643	1	0	2	1	723	756	772	160	129
7	6/6/2006	Yellow	686	665	-1	0	-5	0	676	756	772	137	133
8	6/6/2006	Yellow	690	675	-1	-1	-1	-2	683	756	772	138	135
9	6/6/2006	Yellow	689	685	-1	-2	-15	20	687	756	772	138	137
10	6/6/2006	Yellow	700	685	-3	-3	-1	-4	693	756	772	140	137
11	6/6/2006	Orange	730	570	1	0	-3	3	650	756	772	146	114
12	6/6/2006	Orange	735	580	-1	1	0	-7	658	756	772	147	116
13	6/6/2006	Orange	755	581	0	0	0	0	668	756	772	151	116
14	6/6/2006	Orange	773	585	0	0	0	0	679	756	772	155	117
15	6/6/2006	Yellow	703	680	-2	0	50	60	692	756	772	141	136
16	6/6/2006	Yellow	720	665	0	-1	5	-5	693	756	772	144	133
17	6/6/2006	Yellow	725	662	5	-5	0	0	694	756	772	145	132
18	6/6/2006	Yellow	732	667	0	0	0	0	700	756	772	146	133

BIBLIOGRAPHY

1. ASTM, *E647: STANDARD TEST METHOD FOR MEASUREMENT OF FATIGUE CRACK GROWTH RATES*, ASTM, EDITOR. 2000, AMERICAN SOCIETY FOR TESTING AND MATERIALS: PHILADELPHIA. P. 1-42.

2. SURESH, S., *FATIGUE OF MATERIALS*. 2ND EDITION ED. 1998, CAMBRIDGE: CAMBRIDGE UNIVERSITY PRESS. 609.

3. NEWMAN, J.A., *EFFECTS OF LOAD RATIO ON THRESHOLD FATIGUE CRACK GROWTH OF ALUMINUM ALLOYS*, IN *ENGINEERING MECHANICS*. 2000, VIRGINIA POLYTECHNICAL UNIVERSITY: BLACKSBURG. P. 1-197.

4. MICROSOFT. *MICROSOFT OFFICE PROFESSIONAL EXCEL 2003 SP2 ASSISTANCE*. 2003 [CITED 2006 05/02/06]; AVAILABLE FROM: HTTP://OFFICE.MICROSOFT.COM/EN-US/ASSISTANCE/DEFAULT.ASPX.

5. HAYTER, A.J., *PROBABILITY AND STATISTICS FOR ENGINEERS AND SCIENTISTS*. 2ND EDITION ED. 2002: DUXBURY THOMPSON LEARNING. 639-642.

6. FAA/DOT, *METALLIC MATERIALS PROPERTIES DEVELOPMENT & STANDARDIZATION*, FAA/DOT, EDITOR. 2003. P. 1-1728.

7. ASM, *ATLAS OF FATIGUE CURVES*, ASM, EDITOR. 1986, AMERICAN SOCIETY OF METALS.

8. FAA/DOT, *FATIGUE CRACK GROWTH DATABASE FOR DAMAGE TOLERANCE ANALYSIS*, FAA/DOT, EDITOR. 2005. P. 1-126.

9. ESDU, *FATIGUE CRACK PROPAGATION RATES & THRESHOLD STRESS INTENSITY FACTOR RANGES FOR AL ALLOY PLATE, EXTRUDED BAR, & FORGINGS*. 1998, EUROPEAN STANDARD DATA UNIT. P. 1-50.

10. FORTH, S.C., NEWMAN, JR., J. C., FORMAN, R. C., *ON GENERATING FATIGUE CRACK GROWTH.* INTERNATIONAL JOURNAL OF FATIGUE, 2003. 25: P. 0009-0015.

11. KIM, J.K., SHIM, D. S., *THE VARIATION IN FATIGUE CRACK GROWTH DUE TO THE THICKNESS EFFECT.* INTERNATIONAL JOURNAL OF FATIGUE, 2000. 22: P. 0611-0618.

12. HARTER, J.A., *AFGROW USERS GUIDE AND TECHNICAL MANUAL*, W.-P.A.F. BASE, EDITOR. 2004. P. 1-279.

13. ASTM, *E8: STANDARD TEST METHOD FOR TENSION TESTING OF METALLIC MATERIALS*, ASTM, EDITOR. 2004, AMERICAN SOCIETY FOR TESTING AND MATERIALS: PHILADELPHIA. P. 1-24.

14. ASTM, *E1820: STANDARD TEST METHOD FOR MEASUREMENT OF FRACTURE TOUGHNESS*, ASTM, EDITOR. 2001, AMERICAN SOCIETY FOR TESTING AND MATERIALS: PHILADELPHIA. P. 1-46.

15. CPS. *COMPOSITES*. 2006 [CITED 2006 4/11/06]; AVAILABLE FROM: HTTP://WWW.ALSIC.COM/INDEX.HTML.

16. CMI. *CORE DESIGNS*. 2006 [CITED 2006 04/10/06]; AVAILABLE FROM: HTTP://WWW.CELLULARMATERIALS.COM/.

17. ASTM, *F606: STANDARD TEST METHOD FOR DETERMINING MECHANICAL PROPERTIES OF EXTERNALLY & INTERNALLY THREADED, FASTENERS, WASHERS, AND RIVETS*, ASTM, EDITOR. 2005, AMERICAN SOCIETY FOR TESTING AND MATERIALS: PHILADELPHIA. P. 1-15.

18. AIA, *FASTENER TEST METHODS*, AIA, EDITOR. 1997, AEROSPACE INDUSTRIES ASSOCIATION. P. 1-46.

19. ASTM, *F543: STANDARD SPECIFICATIONS AND TEST METHOD FOR MECHANICAL METAL BONE SCREWS*, ASTM, EDITOR. 2002, AMERICAN SOCIETY FOR TESTING AND MATERIALS: PHILADELPHIA.

20. EVERETT, J.R.A. *CRACK GROWTH CHARACTERISTICS OF FIXED AND ROTORARY WING AIRCRAFTS*. IN *6TH JOINT FAA/DOD/NASA AGING AIRCRAFT CONFERENCE*. 2002.

21. NEWMAN, J.A., LINDENBURG, R. A., PIASCIK, R. A., *FAILURE ANALYSIS OF HELICOPTER EXTERNAL FUEL TANK*, NASA, EDITOR. 2002. P. 1-11.

22. RITCHIE, R.O., PETERS, J. O., *SMALL FATIGUE CRACKS: MECHANICS, MECHANISMS, AND ENGINEERING APPLICATION.* MATERIAL TRANSACTIONS, 2001. 42(1): P. PP. 0058-0067.

23. MCDOWELL, D.L., *AN ENGINEERING MODEL FOR SMALL CRACKS IN FATIGUE.* ENGINEERING FRACTURE MECHANICS, 1997. 56(03): P. 0357-0377.

24. DEVENPORT, W.J. *EXPERIMENTAL METHODS: FRACTURE TOUGHNESS*. AOE3054 2006 [CITED 2006 06/06/06]; AVAILABLE FROM: HTTP://WWW.AOE.VT.EDU/~DEVENPOR/AOE3054/CLASSES/CLASS%2010%20NOTES%20-%20FRACTURE%20TOUGHNESS.PDF.

25. WRIGHT, D. *DESIGN AND ANALYSIS OF MACHIE ELEMENTS: PLASTICITY*. 2005 [CITED 06-11-06]; AVAILABLE FROM: HTTP://WWW.MECH.UWA.EDU.AU/DANOTES/FRACTURE/PLASTICITY/PLASTICITY.HTML.

26. ASTM, *E399: STANDARD TEST METHOD FOR PLANE STRAIN FRACTURE TOUGHNESS OF METALLIC MATERIALS*, ASTM, EDITOR. 1997, AMERICAN SOCIETY FOR TESTING AND MATERIALS: PHILADELPHIA. P. 1-31.

27. ACI. *MATERIAL PROPERTIES: ALUMINUM ALLOY 7075-T73, -T735X*. 2006 [CITED 2006 06-11-06]; AVAILABLE FROM: HTTP://WWW.MATWEB.COM/.

28. VISHAY MEASUREMENTS GROUP, E.D., *STUDENT MANUAL FOR STRAIN GAGE TECHNOLOGY*. 1983, VISHAY MEASUREMENT GROUP, EDUCATION DIVISION. P. 1-45.

29. NDTRC. *NDT RESOURCE CENTER: EDUCATIONAL RESOURCES: MATERIALS & PROCESSES: FRACTURE TOUGHNESS*. 2001 [CITED 2006 6-11-06]; AVAILABLE FROM: HTTP://WWW.NDE-ED.ORG/EDUCATIONRESOURCES/COMMUNITYCOLLEGE/MATERIALS/MECHANICAL/FRACTURETOUGHNESS.HTM.

30. STANZL-TSCHEGG, S.E., PLASSER, O., TSCHEGG, E. K., VASUDEVAN, A. K. , *INFLUENCE OF MICROSTRUCTURE AND LOAD RATIO ON FATIGUE THRESHOLD BEHAVIOR IN 7075 ALUMINUM ALLOY.* INTERNATIONAL JOURNAL OF FATIGUE, 1999. 21: P. PPS255-S262.